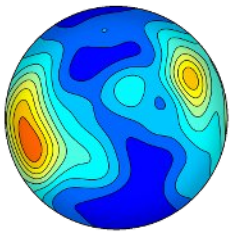

ORIENT

Orient 3.4.2
Spherical Projection and Orientation Data Analysis Software User Manual

Contents

Legal

License

Citation

Orient is the result of countless hours of work over three decades. It is released for free in the hope that it will be useful for scientific and educational purposes. Commercial institutions should contact the author with details of the intended use. In return for free use, any significant use of the software in analyzing data or preparing diagrams must be cited in publications, presentations, reports, or other works. One or more of the following should be cited as appropriate:

Citation for the modified Kamb contouring method (automatic Kamb contouring on a sphere):

Vollmer, F.W., 1995. C program for automatic contouring of spherical orientation data using a modified Kamb method: Computers & Geosciences, v. 21, p. 31-49.

Citation for the triangular orientation plot or automated structural domain analysis:

Vollmer, F.W., 1990. An application of eigenvalue methods to structural domain analysis. Geological Society of America Bulletin, v. 102, p. 786-791.

Citation for use of the Orient software:

Vollmer, F.W., 2015. Orient 3: a new integrated software program for orientation data analysis, kinematic analysis, spherical projections, and Schmidt plots. Geological Society of America Abstracts with Programs, v. 47, n. 7, p. 49.

Citation for Orient 3 software:

Vollmer, F.W., 2016. Orient 3: Spherical projection and orientation data analysis software. www.frederickvollmer.com.

Citation for the Orient 3 User Manual (this document):

Vollmer, F.W., 2016. Orient 3: Spherical projection and orientation data analysis software user manual www.frederickvollmer.com. 96 p.

An acknowledgement such as, “I thank Frederick W. Vollmer for the use of his Orient software”, “Frederick W. Vollmer's Orient software was used to prepare figures”, or even “Orient was used to prepare figures”, is greatly appreciated.

Registration

Please consider registering the software, registration is free. This helps determine usage, and justify the time spent in it's upkeep. To register, send an email to vollmerf@gmail.com with your user name, affiliation, and usage. You will not be placed on any mailing list or contacted again, other than my response with a thank you. For example, send me an email with something like:

User:	Dr. Frederick Vollmer
Affiliation:	SUNY New Paltz, Geology Department
Usage:	Research on joint orientation analysis, Catskill Mountains, NY; fault kinematics in the Hudson Valley fold and thrust belt. Teaching an undergraduate structural geology course with approximately 35 students per year.

If you are specific about the type of project, this can help me in developing future releases. If you are using Orient in a teaching environment, I am interested to know the course and approximate number of students.

Installation

Orient is compiled, tested, and debugged on Macintosh OS X, Windows, and Linux Ubuntu. Macintosh OS X 10.5 to 10.10, Windows XP, 7 to 10, and Linux distributions should all run without problem.

On Macintosh OS X, double click the disk image file (.dmg), and drag the Orient application on to the Applications folder icon, or to any other desired location. If you get the App Can't Be Opened message when double clicking on the Orient icon, right-click on the icon and choose Open from the popup menu.

Gatekeeper in OS X 10.7 to 10.10 must be set to allow applications other than from the Mac App Store to be opened. To do so, open the System Preferences and the Security & Privacy option. Under General select Allow apps downloaded from: Anywhere.

On Windows, unzip the zip file (.zip) using the Extract All option, and drag the Orient application (Orient.exe) to any desired location. Do not try to run the Orient application folder from inside the zip file, this is the most common installation problem.

On Linux unpack the gzip file (.tgz), and copy the Orient application (orient) to any desired location.

The Example Data folder should also be copied for use in the tutorials. After installing a new version, you may wish to reset the preferences using the Restore Defaults command in the Help menu. This will clear any options that may have changed and set them to default values. The preferences are stored in the file Orient3.xml, which is located in the folder Orient in your operating system's application preferences folder. To deinstall simply delete the Orient application folder, and optionally delete the preference folder. No other files are installed on your computer. No administrative permissions are required to install Orient, and it is possible to keep a copy on a thumb drive to run on any computer.

1. Introduction

1.1 Overview

Orient is a fast, professional, easy to use spherical projection and directional data analysis program. In 1986 Orient implemented modified Kamb contouring (automatic contouring on the sphere, Figure 1.1), triangular orientation plots, orientation fields, and automated structural domain analysis (Vollmer, 1988, 1989, 1990, 1993, 1995). Orient 3 brings a new level of accuracy and speed, with many new tools, including interactive data analysis, coordinate conversions, digitizing, and file integration with applications such as Microsoft Excel, LibreOffice, Adobe Illustrator, InkScape, CorelDRAW, and Google Earth.

Orient is for plotting and analyzing *directional data*, data that can be described by the orientation of an axis or vector in space or, equivalently, by a position on a sphere or circle. Examples of data that are represented by unit vectors (directed) or axes (undirected) include geologic bedding planes, fault planes, fault slip directions, fold axes, paleomagnetic vectors, glacial striations, current flow directions, crystallographic axes, earthquake epicenters, cosmic ray arrival directions, comet orbital planes, positions of galaxies, whale migration paths, and the locations of objects on the Earth. Orient has been written to apply to a wide variety data types, however many examples come from structural geology, which requires extensive manipulation and analysis of directional data.

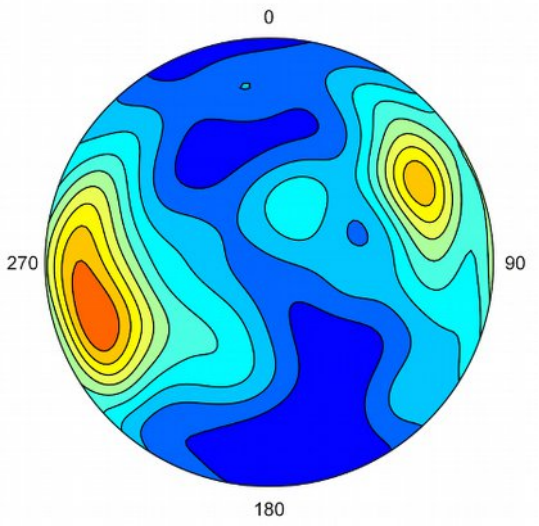

Figure 1.1 Lower hemisphere equal-area modified Kamb contour plot of ice crystallographic axes with contours at 10% density, an example of undirected axial data (data from Kamb, 1959).

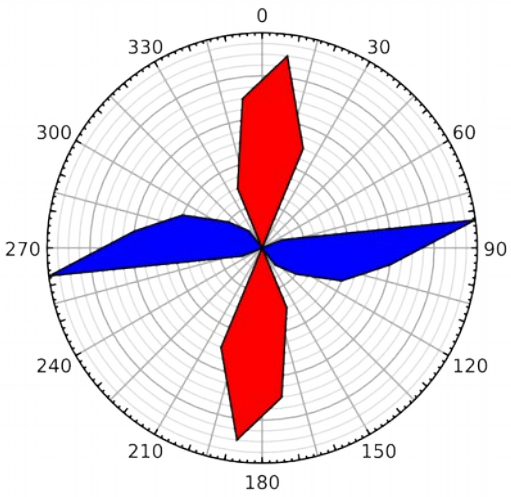

Figure 1.2 Circular frequency polygon plot of the means of two joint sets from each of 24 counties in central New York, plotted as undirected strikes (data from Parker, 1942).

Spherical projections (Figure 1.1) are used to display three dimensional directional data by projecting the surface of a sphere, or hemisphere, onto a plane. Lines and planes in space are considered to pass through the center of a unit sphere, so lines are represented by two diametrically opposed piercing points. Planes are represented by the great circle generated by their intersection with the sphere or, more compactly, by their normal.

Spherical projections include equal-area (used for creating Schmidt nets), stereographic (used for creating Wulff nets or stereonets), and orthographic projections, these can be plotted on either upper or lower hemispheres. Point distributions are analyzed by contouring and by computing eigenvectors of undirected data from orientation matrixes, or vector means of directed data. Figure 1.3 is an example of directed data plotted on both upper and lower hemispheres. Data sets and projections can be rotated about any axis in space, or to principal axes. For two-dimensional data, such as wind or current directions, circular plots and circular histograms, including equal-area and frequency polygon diagrams, can be prepared (Figure 1.2).

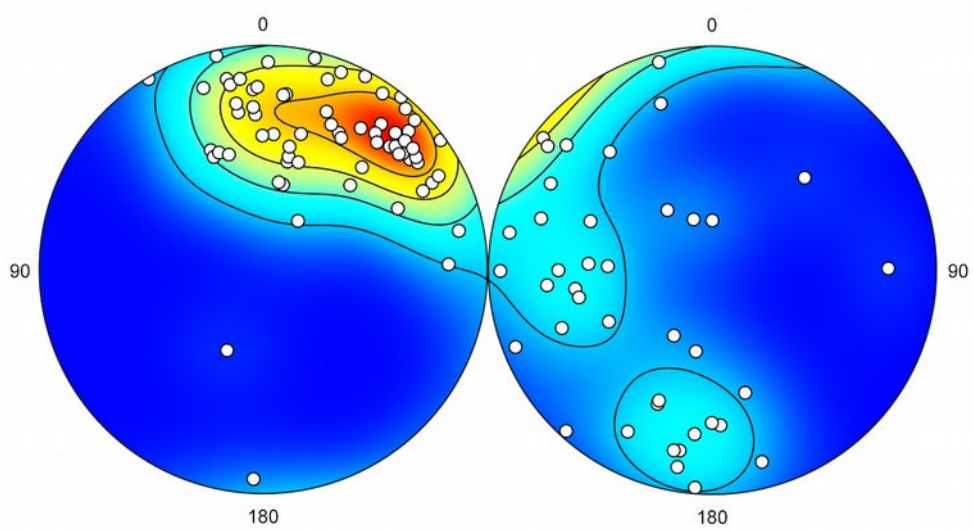

Figure 1.3 Schmidt plot of directed data, magnetic remanence directions from Precambrian volcanics, with modified Kamb contours at 20% density (data from Schmidt and Embleton, 1985, in Fisher, et al., 1987). Projection on left is inverted to display upward directed data.

Data can be input as spherical coordinates, longitude and latitude, azimuth and altitude, declination and inclination, trend and plunge, strike and dip, or other measurements. Orient does kinematic analysis of fault data, which is represented by a plane and the direction of slip within that plane, by generating P and T kinematic axes, tangent line diagrams (Figure 1.4), and beachball plots (Figure 1.5).

Spherical projections represent data *directions*, but not spacial *locations*. Orient therefore includes orientation maps to analyze spacial distributions of orientation data, such as the location of domains of cylindrical folding in polydeformed regions (Figures 1.6 and 1.7). Orient can plot the distribution of data globally (Figure 1.8), and integrates with internet maps, like Google Maps, and with Google Earth.

Additional features include statistical confidence cones, bootstrap analysis, plotting of conical data, small circle fitting with confidence regions, and projection and data rotations. Figure 1.9, for example, is a projection of poles to bedding in graywacke rotated to display fold a cylindrical axis.

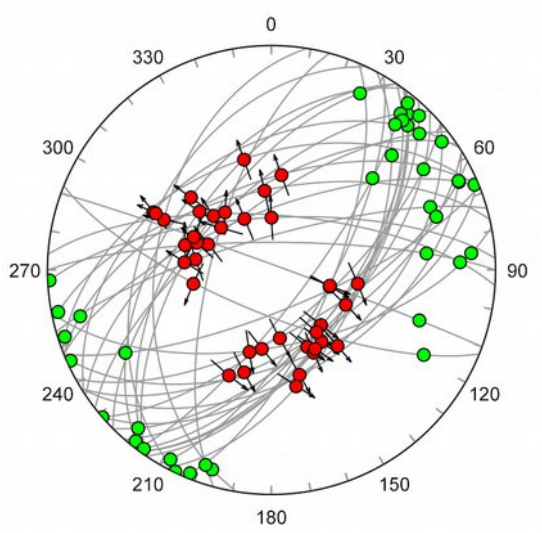

Figure 1.4 Lower hemisphere equal-area slip tangent plot of 38 normal faults from Crete, Greece. Each data point is defined by both a plane and a directed line (data from Angilier, 1979).

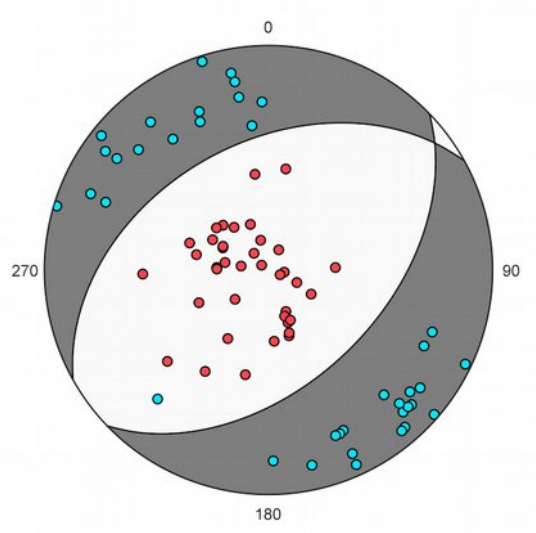

Figure 1.5 Lower hemisphere equal-area beachball diagram of data in Figure 1.4 showing quadrants of P shortening (red) and T extension (cyan) kinematic axes.

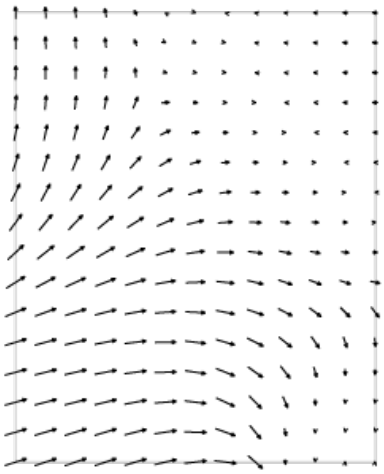

Figure 1.6 An axial orientation field of eigenfoliation dip lines derived from 625 foliation planes, Dovrefjell mountains, Norway (data from Vollmer, 1990).

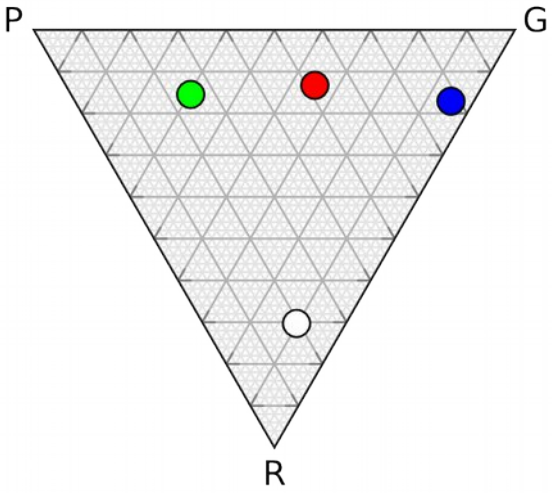

Figure 1.7 Triangular orientation diagram (Point Girdle Random) diagram showing the variations in orientation data symmetry and scatter among structural domains defined from the data in Figure 1.6.

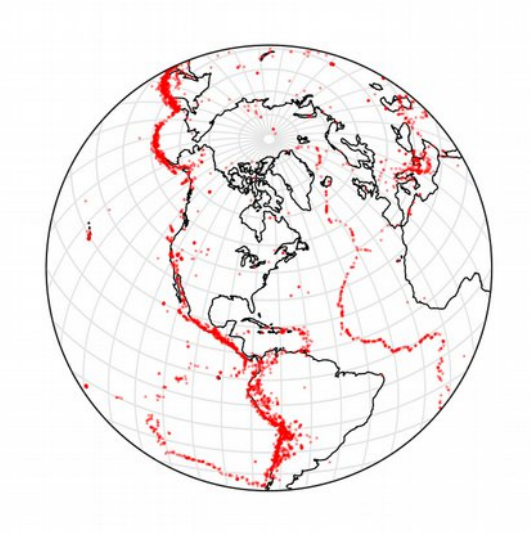

Figure 1.8 Upper hemisphere equal-area projection of 14,229 earthquake epicenters (1980-1990), an example of directed data plotted by latitude and longitude (data from NOAA).

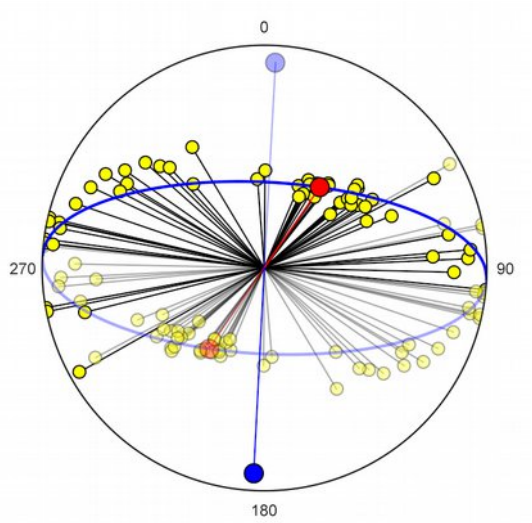

Figure 1.9 Lower hemisphere orthographic projection of 56 poles to bedding in graywacke, Albany County, New York rotated to display fold axis (data from Vollmer, 1981).

1.2 Tutorial 1 – Quick Start

Open the Orient application to display the data entry spreadsheet, the main data display area (Figure 1.9). By default, columns for ID, Station, Strike, Dip, Trend, and Plunge are displayed. The *ID* is an integer that should be unique for each measurement, Station is any alphanumeric string to identify the measurement (to see all available columns, select the menu command View Data Columns, these additional columns will be covered later). Measurements for *planes* should be entered in the strike and dip columns, and *lines* in the trend and plunge columns (these can be changed, for example, if you prefer dip direction over strike).

Use the mouse to examine the icons in the toolbar, from left to right these are Open, Save As, Spherical Projection, Circular Histogram, PGR Plot, Orientation Map, and Preferences. Most of the controls in Orient have *tooltips*, or help hints displayed when the mouse is over the control. Click on the Spherical Projection icon to display the default *Schmidt net* (Figure 1.10). The toolbar icons in the spherical projection window are Export Image As, Find, Zoom In, Zoom Out, Zoom Fit, and Preferences. Export Image As will save the image to a graphics file in various raster (Adobe Photoshop and GIMP compatible) and vector (Adobe Illustrator and Inkscape compatible).

Begin entering numbers into the strike and dip columns, and the spherical projection will automatically update to display them. The ID number is automatically incremented, although a different number can be entered. To identify individual measurements, click on the Find icon in the spherical projection window. In this mode any selected data point will be highlighted in the other window, a colored bar in the spreadsheet, and a selection icon in the spherical projection window (Figure 1.11).

To *only* display data items selected in the spreadsheet, turn on the Plot Selected option in the Graph menu. In this case *only* the selected data will be displayed on the spherical projection. Turn this off before continuing the tutorial.

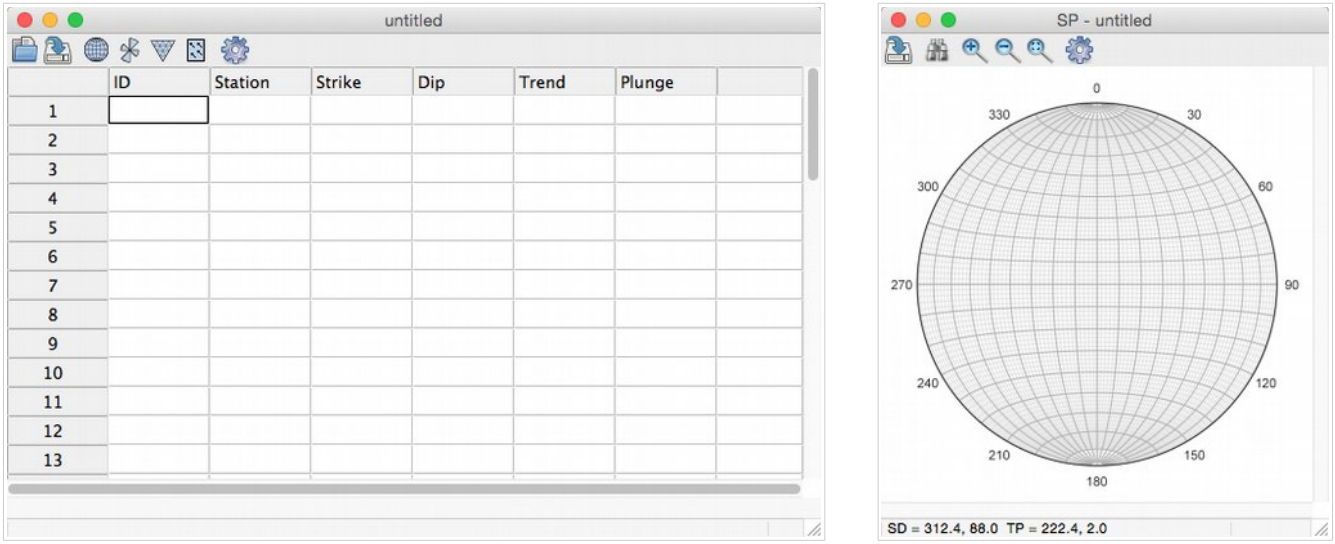

Figure 1.10 The Orient *Data w*indow with the spreadsheet for data entry and display, and a *Spherical Projection* displaying the default Schmidt net.

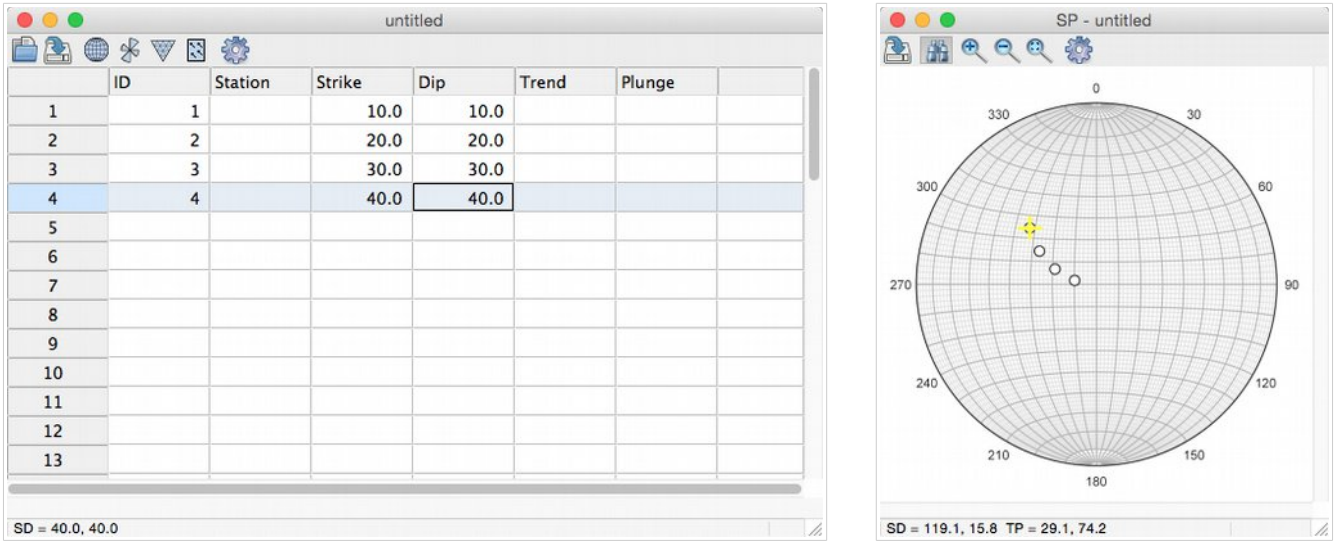

Figure 1.11 Display of data in spreadsheet and spherical projection. The data point can be selected in either window, and will be highlighted in the other window.

Next, open the Preferences dialog by clicking its icon. Select the Spherical Projection option from the pulldown menu, and the Data Symbols panel. Check the Great Circle checkbox (Figure 1.12), and press OK. The projection will update to show great circle arcs for each of the data points (Figure 1.13).

A common calculation required for geologic data analysis is to determine the intersection between two planes, such as bedding and cleavage, or of multiple bedding planes to find a fold axis. To do this in Orient, select the planes, the result is displayed in the status bar and plotted on the spherical projection. The result is displayed in the status bar as the calculated maximum and minimum eigenvectors, and also displayed on the spherical projection (Figure 1.14). The maximum (Max) is a mean value, and the minimum (Min) is the intersection (see Section 4.7 for details).

Finally, click on the Circular Histogram icon to display a circular histogram, or rose diagram, of the data (Figure 1.15). By default the data is displayed as undirected data, and planes are displayed by their strikes.

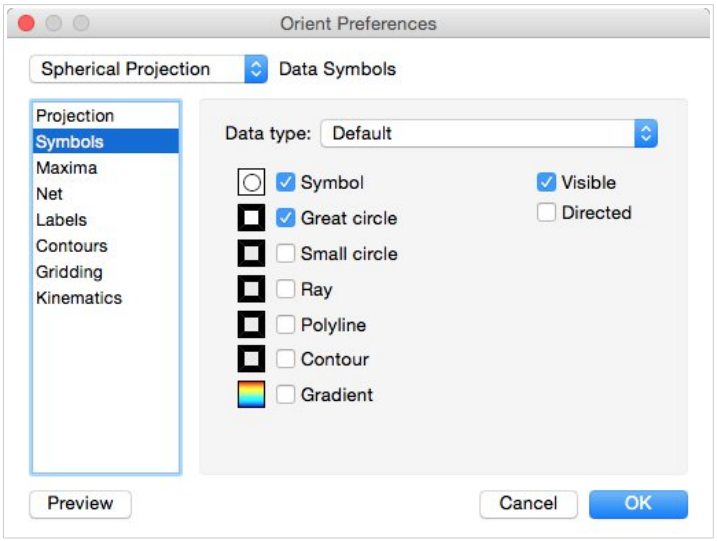

Figure 1.12 The Orient *Preferences* dialog showing spherical projection data symbol options.

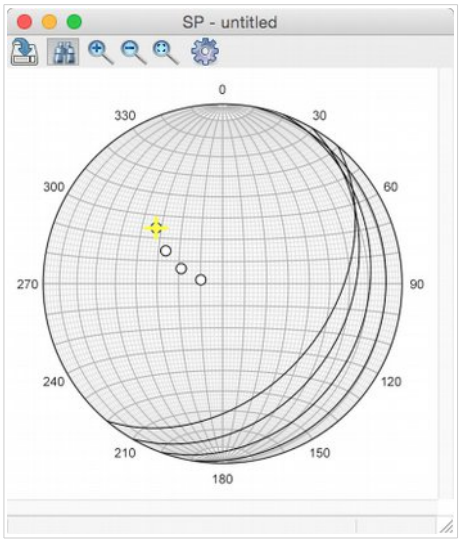

Figure 1.13 The projection after checking the *Great circle* option.

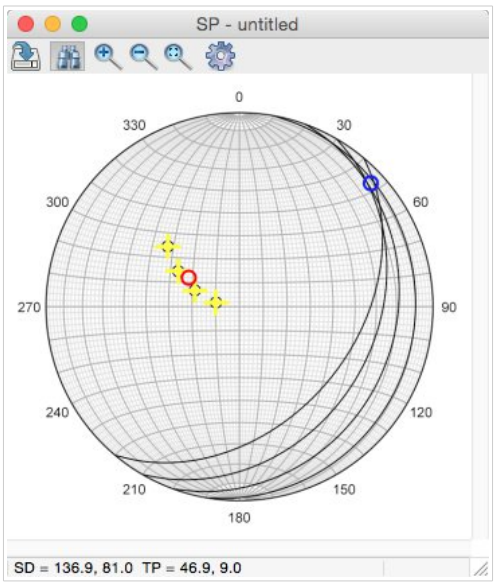

Figure 1.14 The projection after selecting all data points, the minimum (blue) and maximum (red) eigenvectors are displayed.

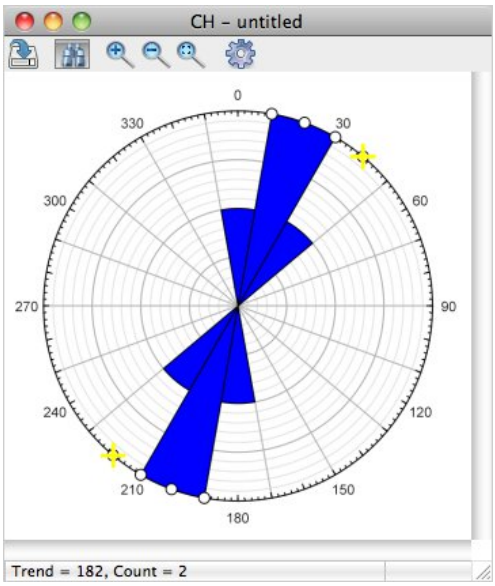

Figure 1.15 Circular histogram of the data displayed in Figure 1.7, showing the *strikes* of the data.

1.3 Graphics Output

Graphics output of plots and diagrams is to bitmap (raster) and vector graphics files. Bitmap files are compatible with photo editing programs such as Adobe Photoshop and GNU Image Manipulation

Program (GIMP, free), and can be imported into most word processing programs. Formats include Portable Networks Graphics (png), Windows Bitmap (bmp), Tagged Image File Format (tiff or tif) and Joint Photographic Experts Group (jpeg or jpg). The default format is *png*, is a widely supported optimally compressed non-lossy format. bmp and tiff files are also non-lossy and widely supported. The *jpg* file format was designed mainly for photographic images, and is less suitable for plots and illustrations.

Vector graphics files allow editing in programs such as Adobe Illustrator, InkScape (free), and Computer Aided Design (CAD) programs such as AutoDesk AutoCAD and QCAD (free). Orient supports Scaled Vector Graphics (svg), Encapsulated PostScript (eps), and AutoCAD Drawing Exchange (dxf) formats.

The default svg format is an open source vector graphics format that is widely supported, including by Adobe Illustrator, InkScape, CorelDRAW, and most web browsers. Some versions of Adobe Illustrator, however, contain bugs that prevent opening *svg* files. For example, on Macintosh, Illustrator 5 can import *svg* files, but Illustrator 6 can not. On Windows, Illustrator 5 can *not* open svg files, but Illustrator 6 *can*. As a work around, try opening the *svg* in another program, such as InkScape or Macintosh Preview, and saving it in another format, such as pdf. Alternatively, save the plot as an eps file which Illustrator should be able to open.

The vector graphics file formats vary in their support of drawing features. svg is the most complete, and Orient saves plot elements as nested *groups*. svg does not support layers, but grouped elements can be moved to layers once opened in a vector graphics editing program. eps format is a widely supported PostScript vector format, but does not support layers, groups, or transparency. The dxf format does support layers, but not transparency, only simple polygon fills are supported, and line styles, text, and colors may vary from other formats.

Note that none of the vector file formats supports bitmaps, such as the gradient contour fills in Orient. To use these in a vector graphics editing program, save the background only, turning off data, label, and net display, and save as a bitmap file. The resulting background can be imported into a vector graphics editing program with the vector graphics overlain.

Format	**Extension**	**Format**	**Comment**
Portable Networks Graphics	png	Bitmap	Best choice for bitmap output
Tagged Image File Format	tiff	Bitmap	Good choice
Windows Bitmap	bmp	Bitmap	Good choice
Joint Photographic Experts Group	jpg	Bitmap	Poor choice for bitmap output, lossy
Scaled Vector Graphics	svg	Vector	Best choice for vector output
Encapsulated PostScript	eps	Vector	Good choice, Adobe format
AutoCAD Drawing Exchange	dxf	Vector	Standard for CAD software

Table 1.1 Summary of graphics output formats supported by Orient.

2. Data and Coordinate Systems

2.1 Introduction

This chapter defines the data types that Orient can analyze, including specification of the angles and coordinates used to describe them. There are numerous ways of describing a direction, including latitude, longitude, trend, inclination, strike, and others. There are also many possible coordinate reference frames, the basics are described here with more detail for those needing it in Section 4.8.

The main goal of this chapter, however, is to get the user quickly started by explaining how to enter data. Often it is simplest to enter the data directly into Orient's spreadsheet, however Orient can read and write files compatible with spreadsheet software such as Microsoft Excel and LibreOffice, and, for many workers, this is a better option. Finally, Section 2.4 explains how data can be digitized from scanned images of spherical projections or maps.

2.2 Data Types

The orientations of lines, axes, and planes in two or three dimensional space are a common data type in the earth sciences, and are referred to as *orientation data* (Watson, 1966; Howarth, 1999; Borradaile, 2003). However, *directional data* and *directional statistics* (Mardia, 1972; Mardia and Jupp, 2000), more specifically refer to lines, axes, and planes, while *orientation statistics* deals with the full spacial orientations of rigid objects in space, including orthonormal frames such as foliation-lineation pairs (Downs, 1972; Mardia and Jupp, 2000; Davis et al., 2015).

Directional data are either unit vectors, *directed* data, or unit axes, *axial* or *undirected* data. Current flow directions, for example, are directed, while fold axes are undirected. Plotting, contouring, and statistical analysis of these data types is different. Geometrically, data represents either lines or planes. On spherical projections planes and lines are considered to pass though the center of a unit sphere. Planes are represented by either their great circle, the intersection of the plane with the unit sphere, or by their *normal* (often referred to as the plane's *pole*).

Unit vectors or axes in three dimensions can be specified by their coordinates on the surface of the unit sphere, or *direction cosines*. However, it is more common to specify two independent angles, a horizontal angle (such as strike, trend, or azimuth) and a vertical angle (such as dip, plunge or inclination). Two dimensional data require a horizontal angle only. Available angular measures and their definitions are listed in Table 1, and discussed in Section 2.2. Orient has separate columns for lines and for planes, this allows data that contains both, such as kinematic orientation data (Chapter 5), to be entered as well. Unused columns can be hidden if desired by opening the *Data Columns Dialog* from the *View Menu*.

Angle units can be specified as either degrees (0 to 360 degrees), gradians (0 to 400 gradians), or radians (0 to 2π radians). Orient stores all numbers internally as radians, which are transparently converted to user units. This is a global preference that sets how angles are read from files and user input, and stored in files. There is no mechanism to determine this from file input, so this should only be done if all files share the same format, or to convert files from one format to another. Degrees is the default value, and will not normally need to be changed.

2.3 Coordinate Systems

Orient is designed to be used with all types of directional measurements and coordinate systems, and converts to and from user coordinates for data entry and output. The user does not normally need to be concerned about the underlying coordinate system, except in the case of rotations or selecting different geographic coordinates (Section 4.8). Orient uses a standard right-handed spherical coordinate system defined with default axes X, Y, Z = Right, Top, Up. In geologic usage these normally correspond to East, North, Up, which conforms to map coordinate systems using Easting, Northing, Elevation. Section 4.8 explains how the default coordinates can be changed to any other orientation, such as global geographic (Orient has 13 standard coordinate systems, which can be modified by rotations about any axis).

Spherical coordinates are specified by two angles, θ (theta) and ϕ (phi). The standard mathematical definitions are that θ is the longitude, or the counterclockwise angle from X in the XY plane, and that ϕ is the colatitude, the angle from Z. However, there are numerous ways to specify the same information with two angles, typically specified by the scientific discipline, such as geology, geography, or astronomy (e.g., Fisher et al, 1987; Mardia and Jupp, 2000). Planes are represented by their normal, or pole. Alternatively, coordinates can be specified by three direction cosines in this coordinate system, which are the coordinates of points on a unit sphere. In Orient the user can specify θ and ϕ for lines and planes according to their data or discipline (Table 2.1).

Geographic data are generally given using longitude as the horizontal angle, the vertical angle is commonly latitude or colatitude, azimuth and altitude are used in astronomy. Geologic data, however, are typically specified using azimuths for horizontal angles, measured clockwise from North (Y), and dips or plunges for vertical angles, measured down from horizontal (the XY plane). Geologic angles are typically strike and dip for planes, or trend and plunge for lines. Orient supports all common conventions (Table 2.1), and converts among them.

To convert between units or to set the default units for data entry, open the *Data Orientation Units Dialog* from the *Data Menu*. This will set the data units entered in the spreadsheet, and will convert any preexisting values to the new format. For example, a common conversion is from strike and dip, to dip and dip direction. The data will be saved in the new format. Note that data files contain the format, opening a saved file will always have the format as saved.

Due to the standard use of geographic locations, typically from GPS (Global Positioning System) positioning, of data points in geology, Orient requires a distinction between two usages of *latitude* and *longitude* for data input. A geologist typically records data locations expressed as Cartesian coordinates, such as UTM (Universal Transverse Mercator), or as latitude and longitude pairs, as well as collecting directional data at that location. Therefore it is necessary to determine whether a *latitude, longitude* pair is meant as the *location* of a data point, or if it is the data point itself. The convention adopted here is that *latitude, longitude* (or *lat, long*) refer to a data point location, and that *latitude sphere, longitude sphere* (or *lats, longs*) refer to the data point to be plotted on a spherical projection.

Column Header	Abbreviation	Notes
Plane θ		Horizontal angle of plane
Strike		Clockwise from North (Y), dip is to right along strike
Strike left	strikel	Clockwise from North (Y), dip is to left along strike
Dip direction	dipdir	Azimuth of dip line
Plane ϕ		Vertical angle of plane
Dip		Angle from XY plane down toward -Z
Line θ		Horizontal angle of line
Azimuth	az	Clockwise angle from North (Y)
Declination	dec	Equal to azimuth
Longitude Sphere	longs	Counterclockwise angle from X
Trend		Equal to azimuth
Line ϕ		Vertical angle of line
Altitude	alt	Equal to latitude
Colatitude	colat	Angle from Z down toward XY plane
Inclination	inc	Angle from XY plane down toward -Z
Latitude Sphere	lats	Angle from XY plane up toward Z
Nadir		Angle from -Z up toward XY plane
Plunge		Equal to inclination
Zenith		Equal to colatitude

Table 2.1 Column headers used to specify data formats in Orient. The header or its abbreviation is used in data files to identify a column of data. A plane requires two header, such as strike and dip. A line also requires two header, such as trend and plunge.

There are, unfortunately, more than one convention for *strike* and *dip*, including two contradictory ones both called the *right-hand rule* (e.g., Ragan, 2009). A distinction must be made, so by default, Orient uses the convention that the dip is to the right looking along the strike (e.g., Pollard and Fletcher, 2005; Twiss and Moores, 2007). A second convention, where the dip is to the left, the thumb of the right hand points down the dip (e.g., Barnes, 1995), is referred to in Orient as s*trike left* (or *strikel*). This convention can be selected using the Data Orientation Units command. A third convention, using a dip octant (N, NE, E, SE, etc.) is automatically converted to one of the above as described in Section 2.4. Finally, dip and dip direction are another common way of giving the orientation of a plane, which is also supported.

2.4 Data Entry

Each data point must include a pair of angles specifying its orientation in space. The first angle is measured in a horizontal plane (θ), and the second in a vertical plane (ϕ). For typical geologic data, these are strike and dip for planes, and trend and plunge for lines. However, all common units are supported (Table 2.1). Two dimensional data require horizontal angles only.

Before entering data, select the desired data format using the Data Orientation Units command. You may also wish to hide or show appropriate columns using the View Data Columns command. Separate columns are used for planes and for lines, so make sure the required columns are visible. The Type column can contain any alphanumeric identifier, for example S0 and S1 are often used in geology to designate bedding and cleavage. This is optional, but is required if multiple *data types* are entered in a

single file. All settings, such as symbol sizes and color, are saved for each type. Additional data attributes include station identifiers, location coordinates, domains, and comments (Table 2.2).

Orient does several automatic data conversions. If data is entered as a bearing with compass quadrants it is automatically converted to a numerical azimuth. Bearings are given as degrees east or west of north or south, for example, N30W will be converted to 330. A conversion is also done for planes in strike and dip, or strike left and dip, formats if a dip octant (N, NE, E, SE, S, SW, W, or NW) is given. The strike (or strike left) will be corrected if necessary. For example a strike, dip pair entered as 10, 30W will be converted to 190, 30.

Normally only one plane or line is entered on a row, however kinematic analysis requires the entry of plane-line pairs, which introduces some complexity. Data entry for this type of data is covered in Section 5.2.

Each data point may be individually weighted by entering a value into the Weight column. The default weight is 1, enter 0 to discount the point, or a positive value to increase its weight, This can be used, for example, to weight count joint or fault data by length or surface area. See Section 7.4 for an example of weighting applied to fitting a small circle. Weighting applies to all calculations except bootstrap confidence cones, which require the resampling of equally weighted points.

2.5 Hidden Data Display

Directed data (vectors) intersect the sphere at only one point, which may occur in either hemisphere. Consequently, some of the data point symbols may be hidden from view. One option is to plot both hemispheres separately (e.g., Figure 1.3), however it may also be useful to plot the data points on the hidden hemisphere on the same plot using a different symbol. In the Preferences dialog Spherical Projection pane, the Directed option can be selected to plot hidden contours, confidence cones, and symbols at 10% to 90% opacity, so they appear semitransparent (e.g., Figure 1.9). Alternatively, symbols on the hidden hemisphere may be plotted as Unfilled.

Undirected data (axes) intersect the sphere at two diametrically opposed points, by convention usually only one is plotted. For example, the one in the lower hemisphere is normally plotted in structural geology, and the one in the upper hemisphere in mineralogy. However, it is sometimes useful to plot both symbols on the same plot, which can be dome using the Undirected option, which similarly allows plotting of hidden contours, confidence cones, and symbols.

When learning the properties of spherical projections, it is instructive to plot one or more data points with both the Symbol and Ray options on, and Directed and Undirected set to 50% opacity. With a spherical projection displayed, use the Rotate Projection command discussed in Section 5.4 to sequentially rotate the projection until the points change hemispheres. Try this for both undirected and directed data, by using the Preferences dialog Symbols Pane Directed checkbox. See Section 5.6 for a Tutorial on this method.

2.6 Spreadsheet Integration

Data entered into the Orient spreadsheet can be saved in several spreadsheet formats: tab separated values (tsv), comma separated values (csv), OpenDocument spreadsheet (ods), Microsoft Excel (xls), and Excel Open Office XLM (xlsx). These are all compatible with most spreadsheet programs, including Microsoft Excel and LibreOffice (Table 2.2).

Orient can also read all of these formats, allowing users to enter data files into Microsoft Excel, LibreOffice, or other spreadsheet software. The only requirements are that the data have a *header* row, consisting of headers listed in Tables 2.1 and 2.3, and that any initial comment lines start with two slashes (//). Table 2.4 gives a simple example, and Table 2.5 gives a more complete example. The simplest possible file would be a list of horizontal angles, such as trends or azimuths, for two dimensional analysis. Three dimensional analysis also requires vertical angles, such as dips or plunges.

The included folder Example Data has numerous examples of compatible files. Open them in Excel or LibreOffice to examine them, they are used in the following tutorials.

Format	**Extension**	**Comment**
Excel XML Spreadsheet	xlsx	Microsoft Excel 2007 and later
Excel Spreadsheet	xls	Microsoft Excel pre-2007
OpenDocument XML Spreadsheet	ods	LibreOffice/OpenOffice, free open source software
Tab Separated Value	tsv	Simple text format with values separated by tabs
Comma Separated Value	csv	Simple text format with values separated by commas

Table 2.2 Summary of spreadsheet formats supported by Orient for opening and saving.

Column Header	Abbreviation	Notes
ID	N	Integer identification number for data point
Station		Alphanumeric station identifier
Zone		Alphanumeric zone, such as UTM grid zone
Easting	East, X	X or easting coordinate of data location
Northing	North, Y	Y or northing coordinate of data location
Elevation	Z	Elevation of data location
Latitude	lat	Latitude of data location (D°, D°M', or D°M'S”)
Longitude	long	Longitude of data location (D°, D°M', or D°M'S”)
Plane θ		Horizontal angle of plane from Table 2.1
Plane ϕ		Vertical angle of plane from Table 2.1
Line θ		Horizontal angle of line from Table 2.1
Line ϕ		Vertical angle of line from Table 2.1
Rake		Rake of line in plane
Sense		Kinematic movement sense, Normal or Reverse
Error		Angular error of line in plane
Alpha		Half apex angle of cone
Weight		Data point weight, default is 1
Type		Alphanumeric data type, as S0 or S1
Label		Alphanumeric label
Domain		Integer identification number for domain
Comment		Alphanumeric comment

Table 2.3 Column headers used to specify data attributes in Orient. The header or its abbreviation is used in data files to identify a column of data. See Table 2.2 for data angles.

Strike	Dip					
230	24					
018	54					
141	15					

Table 2.4 Example of a simple data file as displayed in a spreadsheet, such as Microsoft Excel or LibreOffice, with strikes and dips of planes. See Table 2.1 and 2.2 for other possible column headers.

// Example of an Orient 3 data file in a spreadsheet, this is a file comment, 2015-05-04							
Easting	Northing	Strike	Dip	Trend	Plunge	Type	Comment
8452.05	12885.05	230	24			S0	approximate
8456.03	12825.03	018	54			S0	overturned
8432.12	12922.30	141	15			S1	spaced
8466.08	12865.40			138	02	L	S0/S1
8492.01	12872.00			140	09	L	mineral

Table 2.5 Example of a more complex data file as displayed in a spreadsheet, such as Microsoft Excel or LibreOffice, with an initial file comment, data locations, multiple data types, and data comments. See Tables 2.1 and 2.3 for other possible column headers.

While a number of data files formats are supported (Table 2.2), *tab separated value* (tsv) files are recommended for long term storage and archiving data. The format is a simple text file that can be read by virtually any text editor, word processor, or spreadsheet program. While the *comma separated value* (csv) format is also simple, the fact that text often contains commas requires additional processing.

2.7 Project Files

Orient stores all system settings in an XML *project file* (extension oprx) that is by default stored in the Application Support folder for your system (e.g., on a Macintosh, it is in Users/yourname/Library Support/Orient). Most of the settings, for example the symbol styles and colors, are stored by Type, and will remain in effect for any files that use that data type.

It is also possible, however, to save the project file in another directory. The project file contains links to all the files in the project, as well as all of the settings. The data is not stored in the project file, and remains untouched in your spreadsheet files. When reopening the project file, if the data files are moved or renamed, Orient will report them missing. If so, simply reopen them. When a project is open, the project name is prefaced to the file name in the caption of the spreadsheet data window.

The oprx project file is an XML (Extensible Markup Language) Unicode UTF-8 encoded file that conforms to the W3C XML 1.0 specification, a free open standard format widely used for data files (e.g., Microsoft Office, LibreOffice). It consists of ordered key-value pairs stored in recursively nested dictionaries. XML files are designed to be both human-readable and machine-readable, and can be viewed in text editors and internet browsers.

2.8 *Tutorial 2 – Plotting Spreadsheet Data*

Open a spreadsheet program, such as LibreOffice or Microsoft Excel, and enter the data shown in Table 2.5. Then save the file using a standard format (see Table 2.2).

// My data file				
Strike	Dip	Trend	Plunge	Type
060	65			S0
10	45			S0
40	60			S0
310	60			S0
280	70			S0
		90	40	FH
330	55			S1

Table 2.5 Example of a data file. Enter this into a spreadsheet such as LibreOffice or Microsoft Excel.

Open the file in Orient using the File Open command. Click on the Spherical Projection icon, to get a plot as in Figure 2.1. If you have previously modified settings, however, they will still be in effect. The Help Restore Defaults command can be used to reset all settings to default.

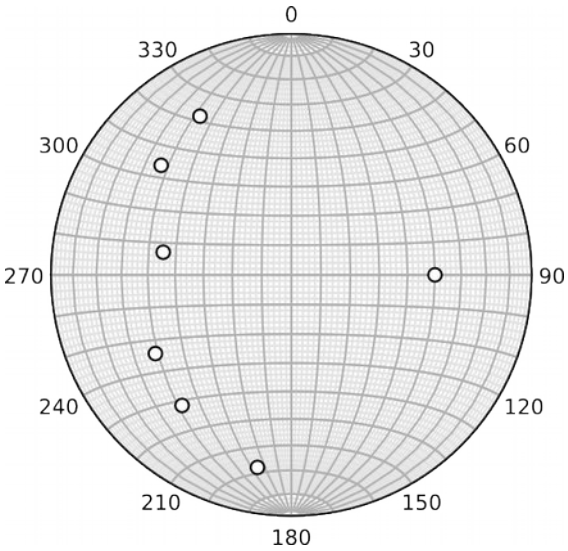

Figure 2.1 Lower hemisphere equal-area projection of data from Table 2.5.

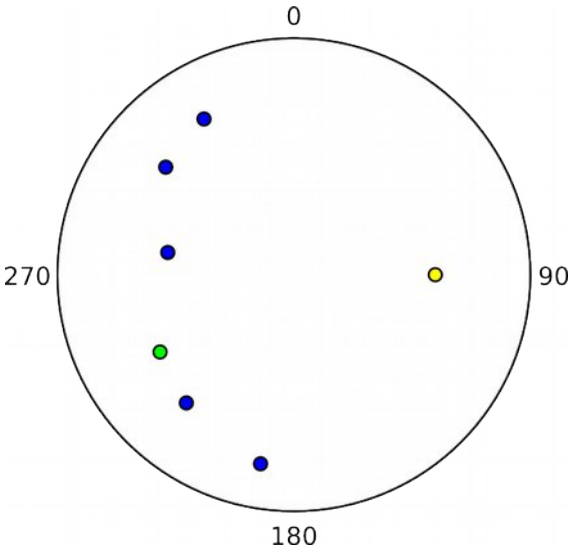

Figure 2.2 Equal-area scatter plot as in Figure 2.1 after removing the Schmidt net, and assigning colors to the data symbols.

To prepare the plot for presentation, it is good to simplify it and focus on the data, so change some of the settings as follows. From the spherical projection window, press the Preferences icon. Under Spherical Projection in the Net pane, turn off both Net and Axes. Click on Preview to see the result. In the Labels pane, set the Increment to -90, Offset to 14, and Size to 12.

Next, assign different colors to the data types. In the Symbols pane select data type S0 (bedding), click on the data symbol icon, and assign the Fill Color blue. Select data type S1 (cleavage) and assign its fill color to green, and FH (a fold hinge) yellow. Press Preview, and the plot should be as shown in Figure 2.2.

Now add great circles to represent the planes. In the *Symbols* pane select data type S0 again and check the Great Circle checkbox. Then select data type S1, check the Great Circle checkbox, and set the Stroke Color to green (Figure 2.3). A plot of planes represented by their great circles is a *β (beta) diagram.* With a lot of data this type of diagram becomes crowded, and loses any statistical significance, but for a small number of points it can help with visualization. A plot with planes represented by their poles is a *π (pi) diagram,* or *S-pole diagram*, and is preferred over a β diagram as a better statistical representation.

Finally, add the S0 maxima. In the Maxima pane select the S0 data type, and check Visible. For this plot just add the Minimum Eigenvector, which gives us a best-fit fold axis. Uncheck the Symbol for both the Maximum and Intermediate Eigenvectors. For the Minimum Eigenvector check the Symbol and Great Circle checkboxes, and set their colors to red (Figure 2.4).

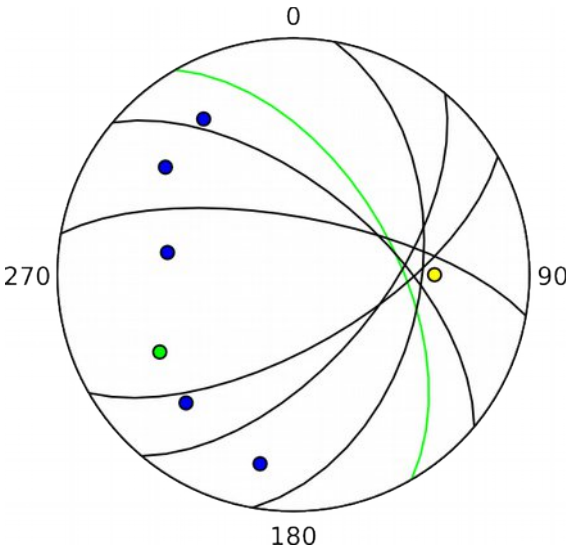

Figure 2.3 Equal-area plot as in Figure 2.2 with planes represented as great circles.

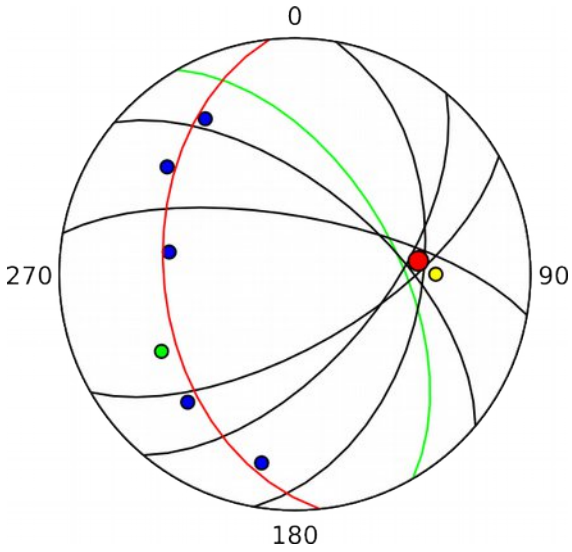

Figure 2.4 Equal-area plot as in Figure 2.3 with best-fit great circle and pole given by the minimum eigenvector of S0 (bedding).

2.9 Digitizing Data

When digital data files or text listings of directional data are not available, data can be digitized from scanned images of spherical projections or maps. To digitize a spherical projection from a suitable source image, insure that the image is undistorted, that is circular, and that the north point is unrotated. An image editing program such as Adobe Photoshop or GIMP can remove distortion and rotate the image if necessary.

Open the image in Orient using the File Open Image command, which will display the Digitizing window (Figure 2.5). Click on the Digitize icon to display the Digitize dialog (Figure 2.6). Select the correct options for the spherical projection, the projection options are stereographic, equal-area, or orthographic, in either upper- or lower-hemisphere (one hopes that the original author correctly specified these). Select the data type, line or plane, and press OK.

A prompt will ask for three points on the perimeter of the projection, after entering these, a circle will be drawn over the projection. If the circle is a reasonable fit, proceed to digitize the points, which will appear in the Data window spreadsheet. If not, the circle can be reinitialized, or distortion of the image

may need to be removed. Spurious data points can be deleted in the spreadsheet as necessary. If digitizing needs to be interrupted, save the file and reopen the file and image later to resume. To change data type, lines or planes, reopen the Digitize dialog, select the desired one, press enter, and continue digitizing.

Digitizing directional data from a map is similar. Make sure the image is undistorted, and that the X and Y directions are orthogonal with north to the top. The X and Y coordinate scales do not need to be equal, but they must each be scaled linearly within the map area. If necessary, remove any distortion using an image editor. Select Map as the source, the correct element, line or plane, and press OK. There will be a prompt for two points with known coordinates to define the area and coordinates. If the result is satisfactory, begin digitizing the elements by clicking on a start point and then an end point. The coordinates entered into the spreadsheet will be the center point between the two points.

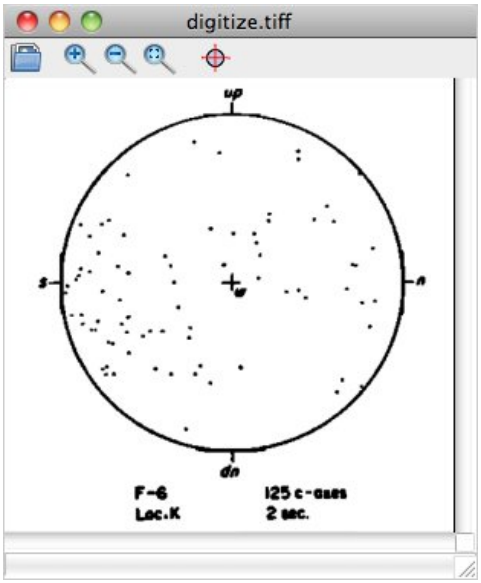

Figure 2.5 An image of a spherical projection opened in the *Digitize Window*.

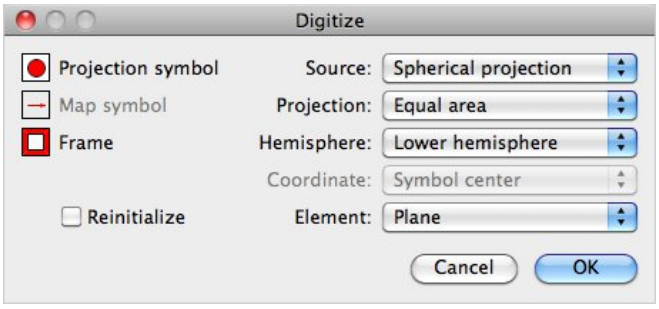

Figure 2.6 The *Digitize Dialog* showing options for digitizing orientation data from images.

3. Circular Plots

3.1 Introduction

Circular plots for two dimensional directional data include scatter plots, circular histograms, and circular frequency polygons (Davis 1985; Fisher et al. 1987; Cheeney, 1983; Howarth, 1999; Mardia and Jupp, 2000). Circular plots can also be used to display the horizontal angles of lines and planes, such as lineation trends. For planes it is possible to plot the strike direction, dip direction, or the azimuth of the plane normal. The data may be directed or undirected. Undirected data plots two points at 180°, or can be plotted on a double angle, modulo 180°, plot. The settings for these plots are in the Preferences dialog using the Circular Histogram selection.

3.2 Circular Scatter Plots

A simple circular scatter plot shows the data distribution on a circular plot, normally the perimeter of a unit circle (Cheeney, 1983; Mardia and Jupp, 2000). Directional rays may be drawn from the circle center, or symbols plotted on the perimeter. The vector mean, for directed or undirected data (Section 3.4), can also be displayed. There are many variations on scatter plots, Orient implements ray plots with lines drawn from the center, and with symbols on the perimeter (Figures 3.1 and 3.2).

Figure 3.1 is a circular scatter plot of the travel directions of 76 turtles after laying eggs (data from Gould cited in Mardia and Jupp, 2000), an example of directed circular directional data. In order to better visualize overlapping data points, the opacity of the data point symbols is set to 50%. Figure 3.2 is a plot of the means of two joint sets from each of 24 counties in central New York (data from Parker, 1942). This data is plotted as strike azimuths, an example of undirected data.

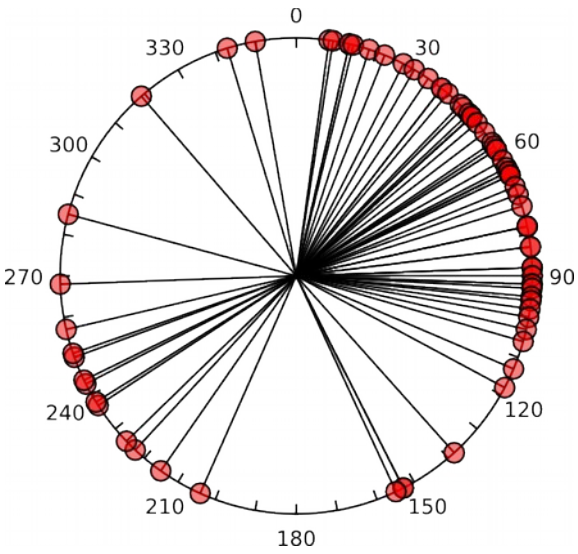

Figure 3.1 Circular scatter plot of the orientations of 76 turtles after laying eggs (Gould's data from Mardia and Jupp, 2000).

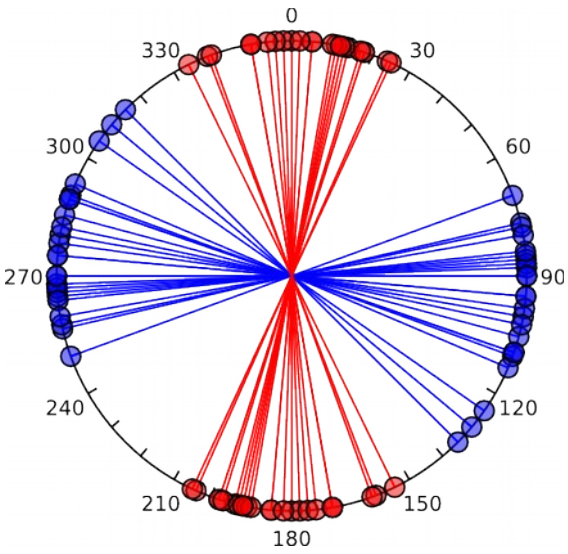

Figure 3.2 Circular scatter plot of the means of two joint sets from each of 24 counties in central New York (data from Parker, 1942).

3.3 Circular Histograms

Two dimensional directional data is commonly displayed as a *circular frequency histogram*, where the data count is tallied for bins or sectors of a set angular width. A commonly used graph is a *rose diagram* constructed with sector *radii* proportional to class frequency, an *equidistance* rose diagram. Figure 3.3 shows an example for directed data. Unfortunately, such a diagram is biased, and not a true histogram, because the area displayed for a single count increases with the radius. An unbiased plot is an equal-area circular histogram where each count has an equal area, and the sector *area* is proportional to class frequency (Cheeney, 1983; Mardia and Jupp, 2000; Figure 3.4). Figures 3.5 and 3.6 are examples for *undirected* data.

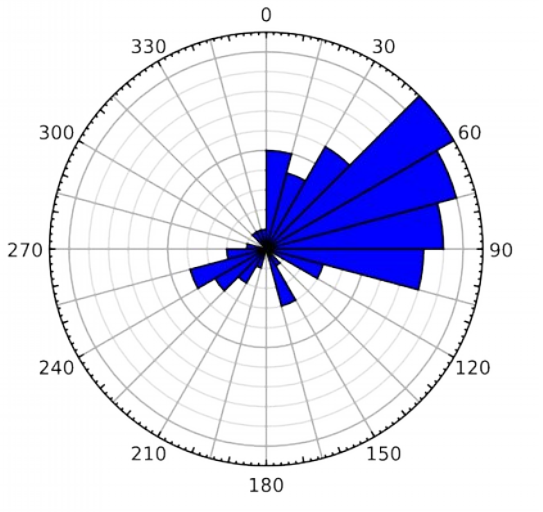

Figure 3.3 Equidistance rose diagram of the directed turtle data shown in Figure 3.1. The increasing area for larger bin counts results in an area bias, so this is not a true histogram.

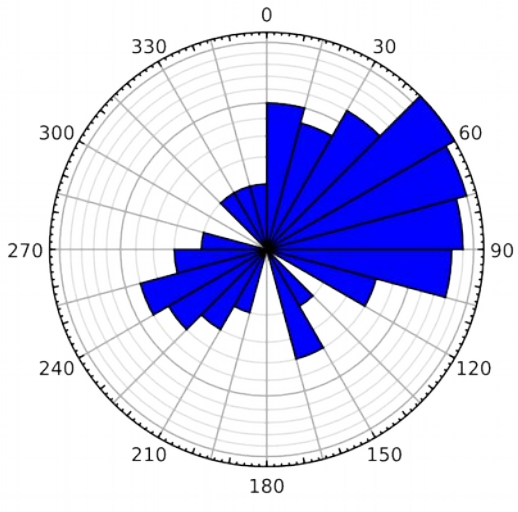

Figure 3.4 Equal-area circular histogram, or rose diagram, of the directed turtle data shown in Figure 3.1. Each count has an equal area, removing area bias.

Each of these plots is drawn with 24 bins, or 15° sectors. The selection of bin size will change the appearance of the diagram, an example is shown for circular frequency polygons in Section 3.3.

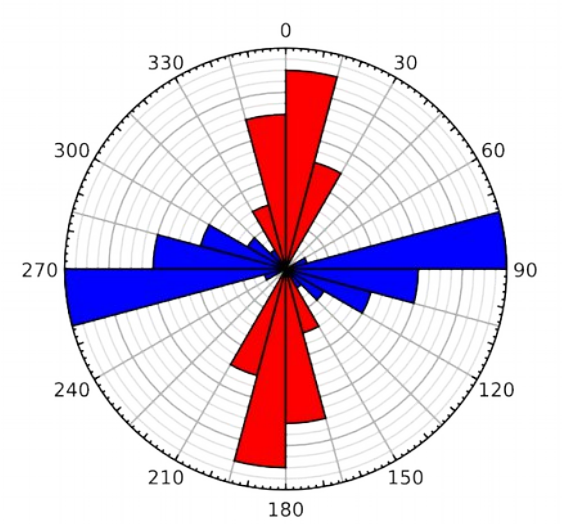

Figure 3.5 Equidistance rose diagram of the undirected joint data shown in Figure 3.2. The increasing area for larger bin counts results in an area bias, so this is not a true histogram.

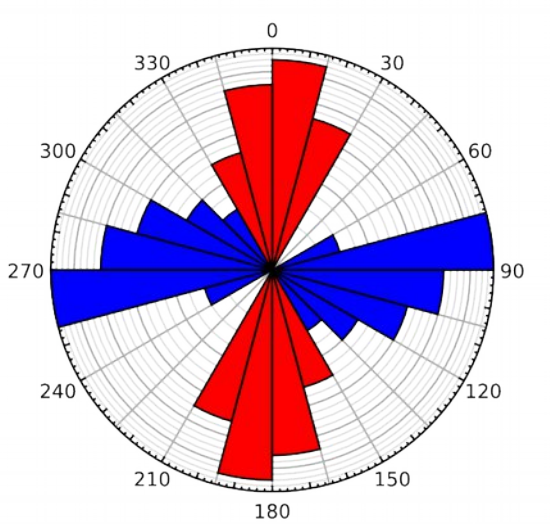

Figure 3.6 Equal-area circular histogram of the undirected joint data shown in Figure 3.2. Each count has an equal area, removing area bias.

3.4 Circular Frequency Polygons

A circular frequency polygon (Haughton, 1864, in Howarth, 1999), or kite diagram (Davis, 1986; Swan and Sandilands, 1995), is an alternative graph for displaying the circular directional data. In a circular frequency polygon diagram the bin sector centers are connected by straight lines to form a polygon. Figure 3.5 is a circular frequency polygon diagram of the directed turtle data (Figure 3.1) using 24 15° bin sectors, the same size as in Figures 3.3 to 3.6.

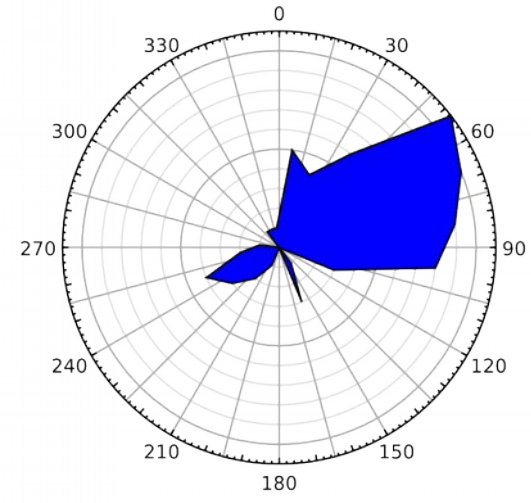

Figure 3. 7 Circular frequency polygon plot, or kite diagram, of the directed turtle data shown in Figure 3.1, using 24 15°

Figure 3.8 is an example of an undirected circular frequency polygon using the joint data (Figure 3.2), also using 24 15° bins. To illustrate the effect of bin size on circular histograms, Figure 3.8 is the same data plotted using 12 30° bins.

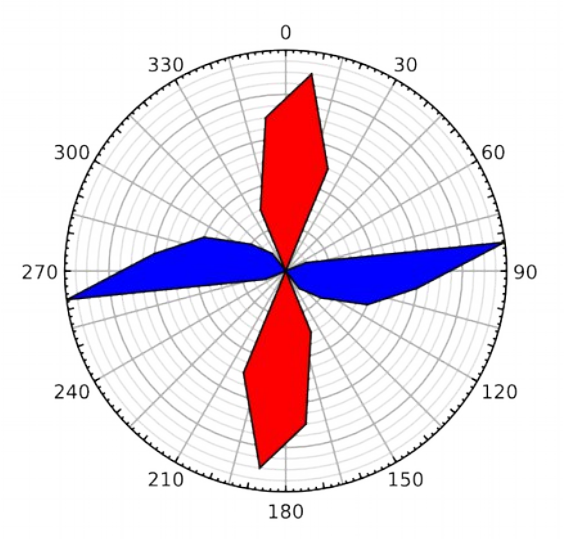

Figure 3.8 Circular frequency polygon plot, or kite diagram, of the undirected joint data shown in Figure 3.2, using 24 15° sector bins.

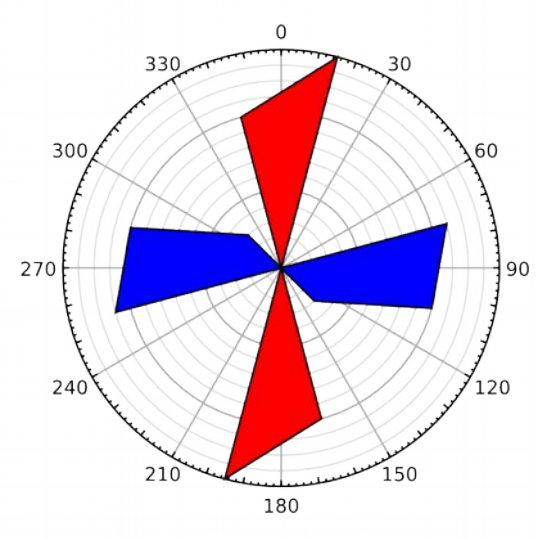

Figure 3.9 Circular frequency polygon diagram of the joint data as in Figure 3.8, but using 12 30° sector bins.

3.5 Circular Mean

A simple measure of location, or best-fit, to circular directional data is the *mean direction*, which is calculated as a vector sum. For directed data the two sums are calculated:

$$\bar{C} = \frac{1}{n}\sum_{i=1}^{n} cos\theta_i$$

$$\bar{S} = \frac{1}{n}\sum_{i=1}^{n} sin\theta_i$$

Then the *mean resultant length* and direction, or center of mass of the coordinates, is calculated as:

$$\bar{R} = \sqrt{(\bar{C}^2 + \bar{S}^2)}$$

$$\bar{\theta} = \arctan(\bar{S}/\bar{C})$$

Since the mean resultant length approaches 1 as directions converge, it is common to cite the *sample circular variance*:

$$V = 1 - \bar{R}$$

which is 0 when all the directions are identical. For undirected data the same calculation is done, however θ is doubled prior to the summation, and the result is halved. For details of statistical measures and tests for circular directional data see Mardia (1972), Cheeney (1983), Davis (1985), Fisher et al. (1987), and Mardia and Jupp (2000).

3.6 *Tutorial 3 – Circular Plots*

Open the file Gould from the Example Data folder (any of the csv, tsv. ods, or xlsx versions) in Orient, and click on the Circular Histogram icon. In the Preferences dialog check Directed in the Circular Histogram Symbols pane. If no settings have been previously modified the projection will look as in Figure 3.4. The Help Restore Defaults command can be used to reset the preferences if desired.

This is an example of *directed* circular data. The default display is an equal-area circular histogram, or rose diagram. In the Symbols pane this data type is displayed as Default, as none was specified in the file. Next, in the Histogram pane, select the Equidistance plot (Figure 3.3), and then the Frequency Polygon (Figure 3.7) to compare plot types. Note how the equal distance plot unequally scales the areas, giving more significance to each additional data point in a bin. This is why it is generally preferable to use an equal area or frequency polygon (kite) plot.

Next, open the file Parker 1942. This is an example of *undirected* circular data. They are treated as circular (instead of spherical) data because, although joints are planar, only the strikes were reported. Note that, because these are planes recorded by strike, the direction plotted should be specified as *Strike,* otherwise the plane's normal would be plotted. Reset the Histogram to Equal-Area.

There are two *data types* in this file, J1 and J2. In the Symbols pane, select J1 and set the Histogram Fill Color to red, and uncheck Symbol for both data types, J1 and J2, and uncheck Directed. The resulting plot should be as in Figure 3.6. Next, in the Histogram pane, select the Equidistant plot (Figure 3.5), and then the Frequency Polygon (Figure 3.8) to compare plot types.

4. Spherical Projections

4.1 Introduction

A primary function of Orient is the creation and manipulation of *spherical projections* of directional data, in particular *azimuthal* spherical projections that project the surface of a sphere onto a plane. This chapter discusses mathematical concepts related to spherical projections, in particular the geometry of several common projections, and the *spherical nets* which are commonly used to display and work with these projections. A final section on nomenclature discuses terminology and common errors that occur in the literature.

4.2 Geometry of Spherical Projections

A *spherical projection* is a mathematical transformation that maps points on the surface of a sphere to points on another surface, commonly a plane. Astronomers, cartographers, geologists, and others have devised numerous such projections over thousands of years, however two, the *stereographic projection* and the *equal-area projection*, are particularly useful for displaying the angular relationships among lines and planes in three-dimensional space. A third projection, the *orthographic projection*, is less commonly used, but is important for some applications, and is easily visualized. These are *azimuthal* spherical projections, projections of a sphere onto a plane that preserve the directions (*azimuths*) of lines passing through the center of the projection. This is an important characteristic as azimuths, or horizontal angles from north (strike, trend, etc.), are standard measurements in structural geology, geophysics, and other scientific disciplines.

The directions of lines and planes in space are fundamental measurements in structural geology. Since planes can be uniquely defined by the orientation of the plane's *pole*, or *normal*, it is sufficient to describe the direction of a line. If only the *direction* of a line, and not it's position, is being considered, it can be described in reference to a unit sphere, of radius, R = 1. A right-handed cartesian coordinate system is defined with zero at the center of the sphere. A standard convention, used here, is to select X, Y, Z = East, North, Up (see Section 4.8 for alternative conventions). A line, L, passing through the center of the sphere, the origin, will pierce the sphere at two diametrically opposed points (Figure 4.1).

If the line represents undirected *axial* data (as opposed to *directed* data), such as a fold axis or the pole to a joint plane, it is allowable to choose either point. In structural geology the convention is to choose the point on the lower hemisphere, P (the opposite convention is used in mineralogy). The three coordinates of point P are known as *direction cosines*, and uniquely define the direction of the line. More commonly, the *trend* (*azimuth* or *declination*) and *plunge* (*inclination*) of the line are given. In Figure 4.1, the trend of the line is 090°, and it's plunge is δ. It is a helpful reminder to designate horizontal angles using three digits, where 000° = north, 090° = east, 180° = south, etc., and to specify vertical angles using two digits, from horizontal, 00°, to vertical, 90°. Note that directed data, such as fault slip directions, may have negative, upward directed, inclinations.

An important tool for plotting line and plane data by hand, and for geometric problem solving, is a *spherical net*. A spherical net is a grid formed by the projection of great and small circles, equivalent to lines of longitude and latitude. Nets are commonly either *meridianal* or *polar*, that is, projected onto a meridian (often the equator) or a pole. The terms *equator* and *pole* (or *axis*) will be used to refer to the equivalent geometric features on the net, it is essential to remember that they do not have an absolute reference frame, that is, the net axis is *not* equivalent to geographic north. When used to plot data by

hand, an overlay with an absolute geographic reference frame (North, East, South, etc.) is used (Ragan 2009).

The projections described here are *spherical projections*, so *equal-area projection* is assumed to mean *equal-area spherical projection.* Other projections are possible, such as *hyperboloidal projections*, which include equal-area and stereographic hyperboloidal projections (Yamaji, 2008; Vollmer, 2011). In these projections the surface of a *hyperboloid* is projected onto a plane. These are used in the context of strain analysis, and are unlikely to be confused with the more common spherical projections.

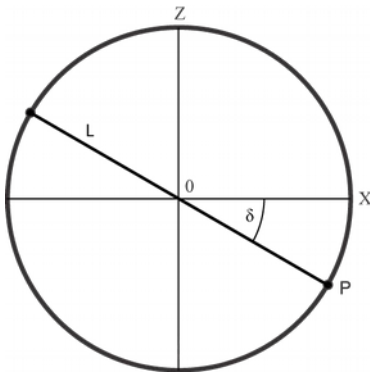

Figure 4.1 Definition of the point, P, on the unit sphere that defines the orientation of the undirected line L. The line is trending toward X (east) and it's plunge is δ. The Y coordinate axis (north) is into the page.

4.3 Orthographic Projection

The orthographic projection is an important projection in which points are projected along parallel rays, as if illuminated by an infinitely distant light source. Figure 4.2 gives the geometric definition of the orthographic spherical projection. A corresponding orthographic polar net is shown in Figure 4.3, and an orthographic meridianal net in Figure 4.4. The projection of point P in the sphere to point P' on the plane is parallel to the Cartesian axis Z, effectively giving a projection following a ray from Z equals positive infinity. This type of projection gives a realistic view of a distant sphere, such as the moon viewed from Earth. It is azimuthal, but angles and area are not generally preserved. When plotting geologic data it is important that area, and therefore data densities, are preserved, so the orthographic projection unsuitable for such purposes. The net does, however, have other uses, such as the construction of block diagrams (e.g., Ragan, 2009).

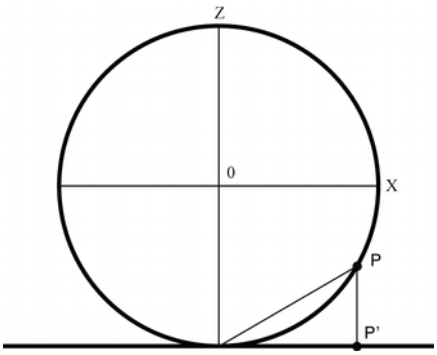

Figure 4.2 Geometric definition of the orthographic spherical projection. Point P on the sphere is projected to point P' on the plane.

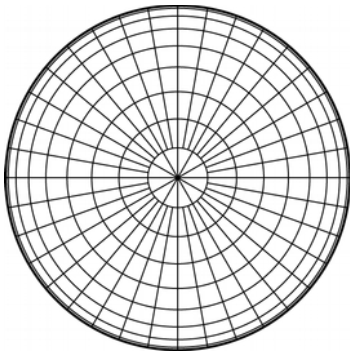

Figure 4.3 Polar orthographic net.

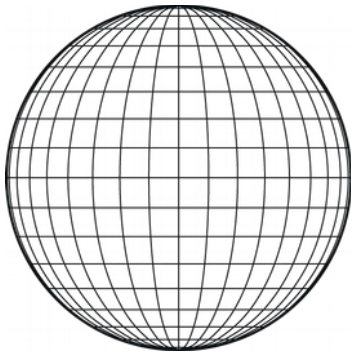

Figure 4.4 Meridianal orthographic net.

4.4 Stereographic Projection

The *stereographic* or *equal-angle* spherical projection is widely used in mineralogy and structural geology. It was known to the Greeks Hipparchus and Ptolemy, and given its present name by François d'Aguilon in 1613 (Snyder, 1987). It is defined geometrically by a ray passing from a point on the sphere (here Z = 1) through a point P on the sphere to the projected point P' on the plane (Figure 4.5).

The corresponding *stereographic nets* are shown in Figures 4.6 and 4.7. Both hemispheres can be represented, however the convention in structural geology is to use the *lower hemisphere*. The meridinal stereographic net is known as a *stereonet* (Bucher, 1944; Billings 1954; Donn and Shimer, 1958; Badgley, 1959), or *Wulff net*, named after the crystallographer G.V. Wulff who published a stereographic net in 1902 (Whitten, 1966), although a much older example was published by François de Aguilón in 1613 (Section 4.15). The stereonet is commonly used in mineralogy, however, the convention is to use the *upper hemisphere*. It is therefore good practice to clearly label all projections, for example *lower-hemisphere stereographic projection.*

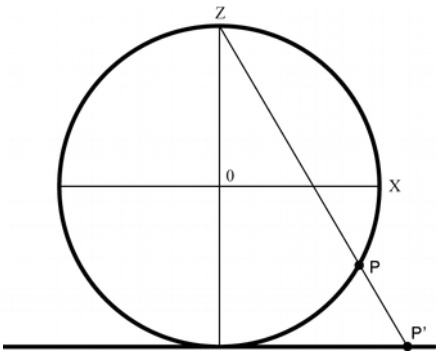

Figure 4.5 Geometric definition of the stereographic projection. Point P on the sphere is projected to point P' on the plane.

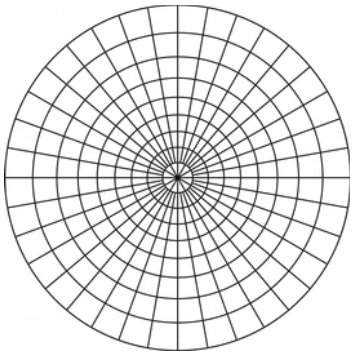

Figure 4.6 Polar stereographic net.

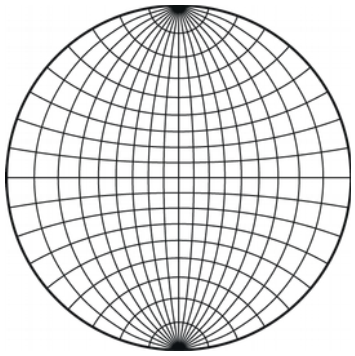

Figure 4.7 Meridianal stereographic net, stereonet or Wulff net.

The projection is *azimuthal*, so lines passing through the center of the projection have true direction, these represent great circles. Note that area in Figures 4.6 and 4.7 is distorted, the projection preserves angles (is *conformal*), but it does not preserve area. An important consequence is that great circles (such as meridians) and small circles project as circular arcs. These properties make it useful for numerous geometric constructions in structural geology (Bucher, 1944; Phillips, 1954; Donn and Shimer, 1958; Badgley, 1959; Lisle and Leyshorn, 2004; Ragan, 2009).

4.5 Equal-Area Projection

The *Lambert azimuthal equal-area spherical projection* was presented by Johann Heinrich Lambert in 1722 as a map projection that preserved area (Lambert, 1722; Snyder, 1987; Section 4.11). It is not conformal, however it *preserves area*, so densities are not distorted. This equal-area projection is used widely in the geologic literature for the presentation of directional data, and is the most likely of these projections to be encountered in literature related to structural geology. Figures 4.8, 4.9, and 4.10 illustrate the geometric definition, polar net, and meridianal net respectively.

In 1925 Walter Schmidt (see Section 4.12) recognized that the equal-area projection should be used for plotting samples of rock fabrics, such as crystallographic axes, this was later extended to bedding planes, joints, and other directional data (Schmidt, 1925; Sander, 1948, 1950, 1970; Phillips, 1954; Badgley, 1959; Turner and Weiss, 1963; Whitten, 1966; Ramsay, 1967; Hobbs et al., 1976; Fisher et al., 1987; Mardia and Jupp, 2000; Van der Pluijm and Marshak, 2004; Pollard and Fletcher, 2005; Twiss and Moores, 2007; Ragan, 2009; Fossen, 2016).

The term *azimuthal* indicates that, like stereographic and orthographic projections, lines passing through the center have true direction, and that it is projected onto a plane. This distinguishes it from other equal-area projections, which include the projection of a sphere onto conical and other surfaces, however, in structural geology, it can usually be referred to simply as an *equal-area projection* without ambiguity. The projection is also known as the Schmidt projection, after Walter Schmidt who first used it in structural geology (Schmidt, 1925; Turner and Weiss, 1963), and the meridianal equal-area net

(Figure 4.10), is known as a *Schmidt net* (Knopf and Ingerson, 1938; Billings, 1942; Sander, 1948, 1950, 1970; Mardia and Jupp, 2000). The polar equal-area net, or Billings net (Figure 4.9), is useful for rapidly plotting measurements by hand.

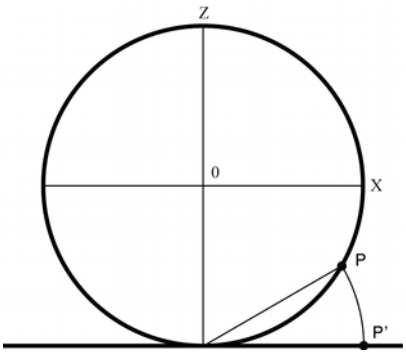

Figure 4.8 Geometric definition of the equal-area projection.

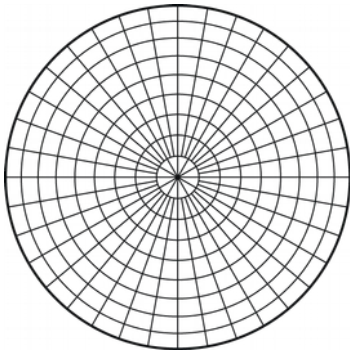

Figure 4.9 Polar equal-area net, or Billings net.

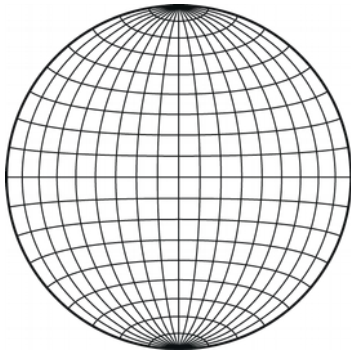

Figure 4.10 Meridianal equal-area net, or Schmidt net.

4.6 Density Distortion

A common requirement is to plot a sample of directional data to evaluate their density distribution, a descriptive statistical procedure intended to identify significant clusters, girdles, or other patterns. In 1925 Walter Schmidt recognized that the distortion of area makes the stereographic projection unsuitable for studying rock fabric data, and proposed the use of the Lambert equal-area projection for such directional data (Figure 4.10; Section 4.11).

To illustrate the effect of density distortion, 2048 directed data points were calculated on a spherical Fibonacci grid (Swinbank and Purser, 2006; command Data Fibonacci Sphere), and plotted using orthographic (Figure 4.11), stereographic (Figure 4.12), and Lambert equal-area (Figure 4.13) projections. The points have equal densities on the sphere (except at the very center), but the densities are highly distorted by the orthographic and stereographic projections.

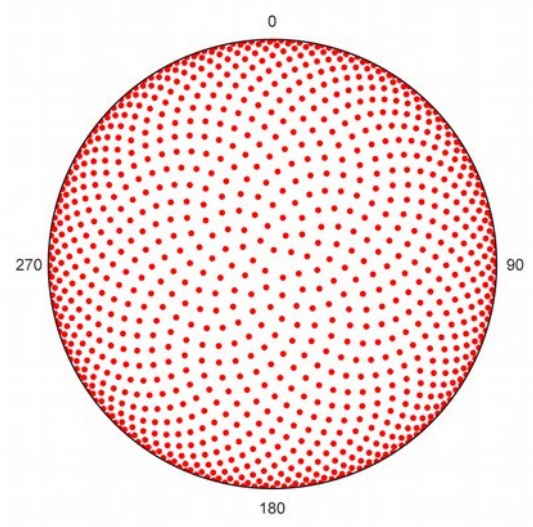

Figure 4.11 Lower-hemisphere *orthographic* projection of 2048 directed data points on a spherical Fibonacci grid to illustrate density distortion. The *Data Fibonacci Sphere* command will generate this distribution.

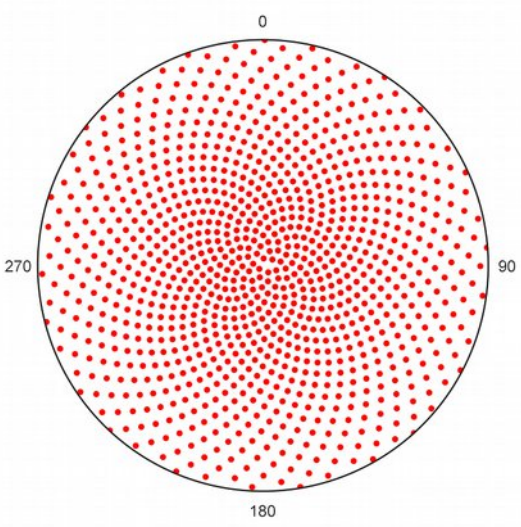

Figure 4.12 Lower-hemisphere *stereographic* projection of data as in Figure 4.11 to illustrate density distortion.

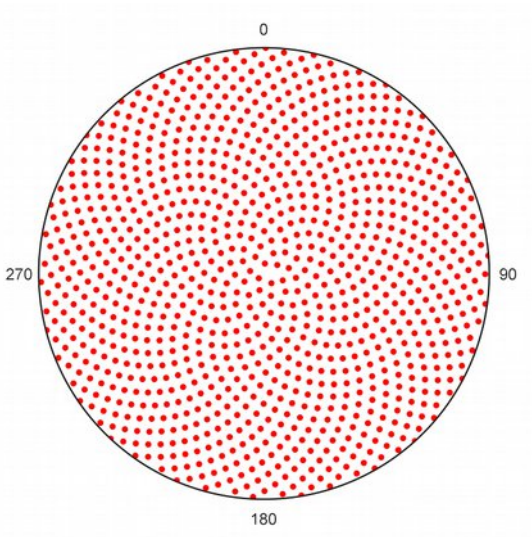

Figure 4.13 Lower hemisphere Lambert *equal-area* projection (*Schmidt plot*) of data as in Figure 4.11 illustrating the lack of density distortion.

The lack of distortion in Figure 4.13 illustrates the advantage of the Lambert equal-area projection for plotting fabric data, and why it is normally used (Schmidt, 1925; Sander, 1948, 1950, 1970; Phillips, 1954; Badgley, 1959; Turner and Weiss, 1963; Whitten, 1966; Ramsay, 1967; Hobbs et al., 1976; Fisher et al., 1987; Mardia and Jupp, 2000; Van der Pluijm and Marshak, 2004; Pollard and Fletcher, 2005; Twiss and Moores, 2007; Ragan, 2009; Fossen, 2016). The term *Schmidt plot* has been proposed for such a plot (Vollmer, 2015; Section 4.12), and is used in subsequent sections.

4.7 Maxima and Eigenvectors

Spherical directional data is characterized by either directed unit vectors or undirected axes in space. The concept of a *mean* value is familiar when dealing with *scalar* values like temperature. Determining such a value for directional data is more complex, averaging trends and plunges separately does *not* work. As with circular data, a useful measure is the *vector mean*, the center of mass for directed data. The procedure for finding the mean is similar to that for directed circular data. A data point on a unit sphere can be represented by three coordinates, which are its direction cosines. If we designate this point as the vector $\mathbf{x} = (x_1, x_2, x_3)$, then the *mean vector* is the averaged sum:

$$\bar{\mathbf{x}} = \frac{1}{n}\sum_{i=1}^{n}\mathbf{x}_i$$

with *mean resultant length*:

$$\bar{R} = \|\bar{\mathbf{x}}\|$$

and *mean direction*, the normalized mean vector:

$$\bar{\mathbf{x}}_0 = \bar{\mathbf{x}}\bar{R}^{-1}$$

Axial data requires the computation of *eigenvectors*, an important concept that gives best-fit values, or moments of inertia, for tensors, such as the *principal stresses* of a stress tensor. In the context of directional data, imagine that each line passing through the center of the unit sphere is represented by a small mass at each of the two points where it pierces the sphere. If the sphere were spinning, it would have a tendency to spin about the axis of minimum density, this is the minimum eigenvector. If it were rolling, it would have a tendency to stop with the maximum density at the bottom, this is the maximum eigenvector, the intermediate eigenvector is exactly 90° from the other two. As an example, Figure 4.14 is a Schmidt plot of bedding plane normals represented by points on the lower hemisphere.

The *orientation tensor*, or scatter matrix (Fisher, Lewis and Emblton, 1987; Mardia and Jupp, 2000), is given by:

$$\bar{\mathbf{T}} = \frac{1}{n}\sum_{i=1}^{n} \mathbf{x}_i \mathbf{x}_i^T$$

the averaged sum of the unit directional vectors times their transpose. The eigenvectors of this matrix are determined and plotted. In Figure 4.15 the maximum eigenvector is plotted as a red circle, and the minimum a blue circle. In cylindrical folds the minimum eigenvector of poles to bedding gives an estimate of a cylindrical *fold axis*, and a great circle normal to the minimum eigenvector gives the best-fit plane through the plane poles (Figure 4.15).

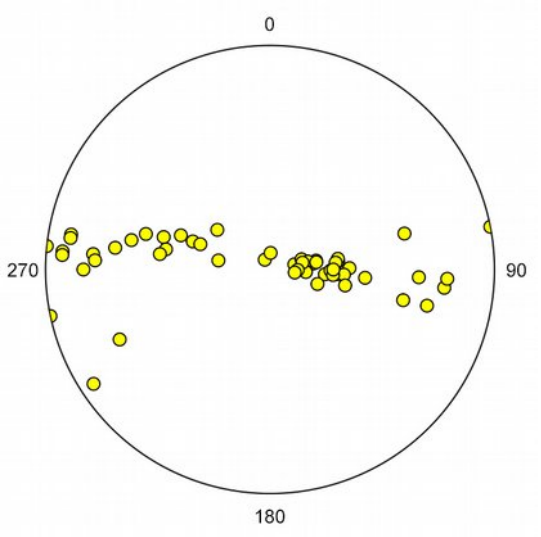

Figure 4.14 Schmidt scatter plot of 56 poles to folded bedding in graywacke, Albany County, New York (data from Vollmer, 1981).

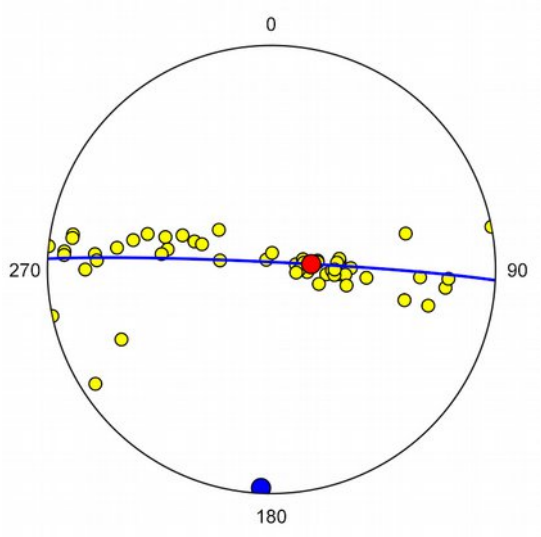

Figure 4.15 Schmidt plot as in Figure 4.14, with maximum (red), minimum (blue) eigenvectors, and the great circle normal to the minimum eigenvector. The minimum eigenvector is an estimate of the *fold axis*.

See Figure 1.9 and Section 5.6 for a visualization of this data. For details of statistical measures and tests for spherical directional data see Mardia (1972), Cheeney (1983), Davis (1985), Fisher et al. (1987), and Mardia and Jupp (2000).

4.8 *Tutorial 4 – Scatter Plots*

Open the file Vollmer 1981a from the Example Data folder (any of the csv, tsv, ods, or xlsx versions) in Orient, and click on the Spherical Projection icon.

If not already done, remove the Schmidt net from the background. Click on the Preferences icon, and locate the Net pane under the Spherical Projection settings. Uncheck both Axes and Net. Next, in the Labels pane, change the Increment to -90, Offset to 14, and the Size to 12.

In the Symbols pane, Data Type S0 should be selected, and the Symbol checkbox checked. Set the Fill Symbol Color to yellow. At this point the plot should look as in Figure 4.14.

To add eigenvector maxima, select the Maxima pane, and check Visible. Under Maximum Eigenvector check Symbol, and under Minimum Eigenvector check Symbol and Great Circle. Set the great circle Stroke Width to 2. The plot should now look as in Figure 4.15. This type of scatter plot gives a simple summary of the data distribution. Section 4.9 shows how to add contouring, and Chapter 6 discusses how to add confidence cones about the maxima.

4.9 Contouring

A simple Schmidt *scatter plot* of data using an equal-area projection (Figure 4.14), or with maxima displayed (Figure 4.15) may suffice for some data sets. However, since the first use of lower hemisphere equal-area projections for displaying directional data (Schmidt, 1925), they have commonly been contoured to bring out underlying patterns such as girdles or point clusters (Figure 4.16).

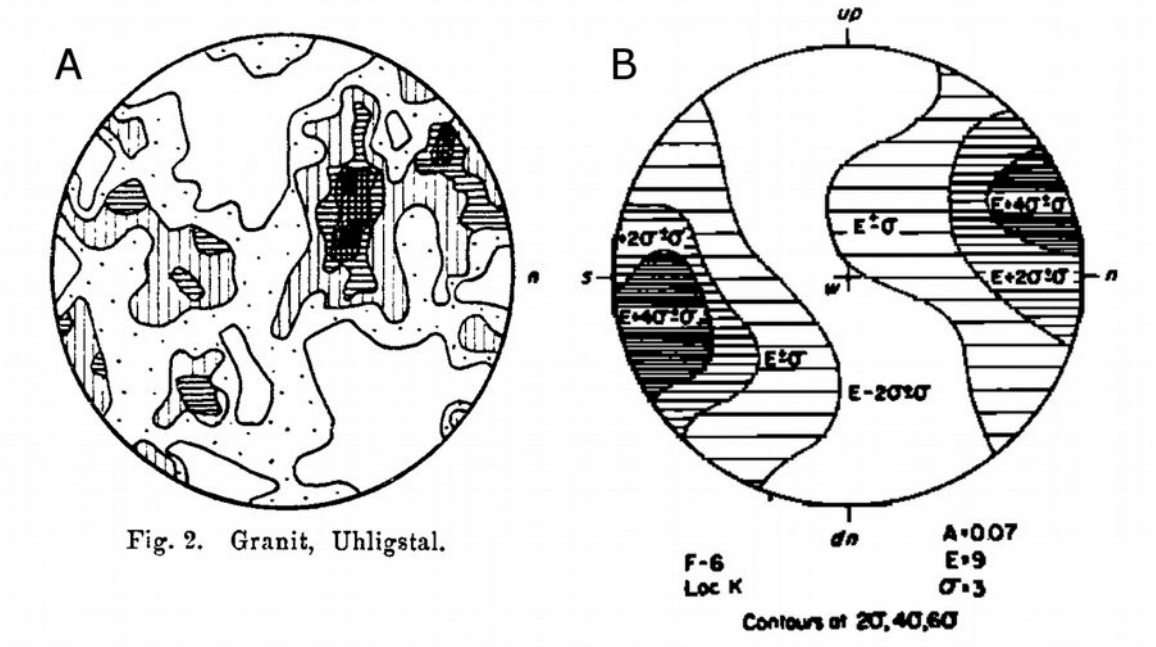

Fig. 2. Granit, Uhligstal.

Figure 4.16 Early examples of contoured lower hemisphere equal-area projections. (A) Crystallographic fabric in a sample of granite (Schmidt, 1925). (B) Crystallographic axes in a sample of ice (Kamb, 1959).

Schmidt (1925) devised a method to hand contour directional data using percentages. This method, or variants of it, is still used (Ragan, 2009), although it is generally superseded by computerized methods (Vollmer, 1995; Ragan, 2009). Schmidt contouring, however, suffers in that it does not correctly take into account the sample size. Kamb (1959) therefore introduced a method using binomial statistics, giving a greater statistical validity to the contours (Kamb, 1959; Vollmer, 1995).

A problem with both the Schmidt and Kamb methods, in addition to being hand-contouring methods, is that the density calculations are done on the projection plane *after* projecting the data points from the sphere, causing distortion. Therefore a *modified Kamb method*, which calculates density directly on the sphere, was introduced in Orient in 1986 (Vollmer, 1988, 1990, 1995). An alternative method, using *probability density* estimation on the sphere, is given by Diggle and Fisher (1985). Orient implements the modified Kamb, modified Schmidt (Vollmer, 1995), and probability density methods.

The settings related to contouring are in the Preferences dialog on the *S*pherical Projection Contours and Gridding panels. Gridding is the first step in contouring, in which the density calculations are done. In this panel select the Method, Modified Kamb or Probability Density (Modified Schmidt is not recommended). Normally Weighting should be left at the default setting Exponential, Sigma at the default 3, and Calculate Kappa checked. Details for these settings can be found in Vollmer (1995) and Diggle and Fisher (1985). The number of nodes, Nodes, sets the number of calculated grid points, the default of 100 gives 10000 calculated nodes. A value of 30 is the approximate minimum for acceptable contours, the default value of 100 generally gives very good resolution.

Once the gridding method is selected, the Contour Settings pane is used to set the number and type of contour lines. Figure 4.17 is a Schmidt scatter plot of crystallographic axes of ice (from Kamb, 1956), which is shown contoured using the 3σ modified Kamb method with a 2σ contour interval in Figure 4.18. This is the data and contour levels that Kamb used to hand-contour Figure 4.16 B. The Contour levels option selected, and an Interval of 2 entered for this plot.

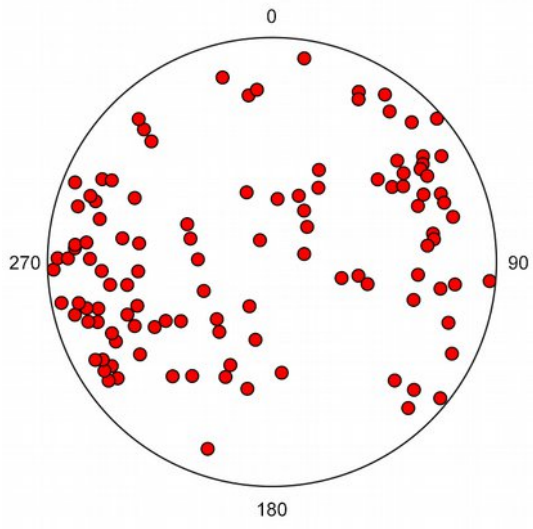

Figure 4.17 Schmidt scatter plot of crystallographic axes of ice (data digitized from Kamb, 1956).

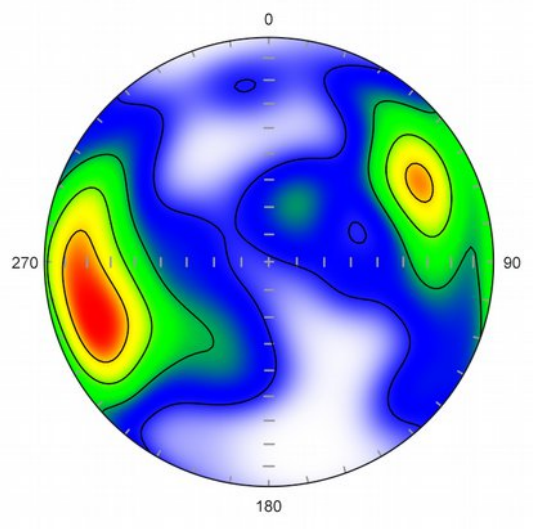

Figure 4.18 Schmidt plot with 3σ modified Kamb contours of the data from Figure 4.17 with contours at 2σ. Compare with Figure 4.16 B. This plot uses a WBGYR Gradient option.

It is also possible to scale the contour levels to *multiples of uniform density*, by checking Uniform density from the Gridding Settings pane. This option is only available for Exponential weighting of the Modified Kamb method, and when Contour interval is selected. This rescales the grid so the contour interval is in multiples of the expected uniform density. A scale bar can also be optionally displayed for the color gradient scale (Figure 4.19).

An alternate, and perhaps preferable, choice for selecting contours is to contour the density distribution at equal levels (Fisher et al., 1987). Figure 4.20 is a 3σ modified Kamb contour plot of this data contoured at 20% density, 5 equally spaced levels over the density distribution. To do this, select Contour levels In the Contour Settings panel, and enter the number of Contour levels, in this case 5 which gives contours at 20% density.

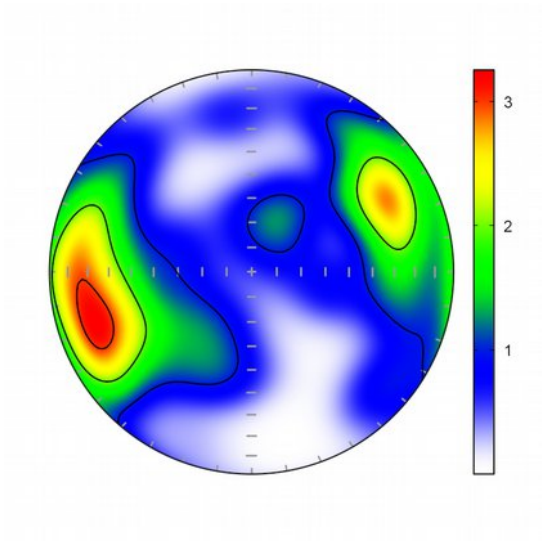

Figure 4.19 Schmidt plot of data in Figure 4.17 with 3σ modified Kamb contours at multiples of uniform density, with scale bar.

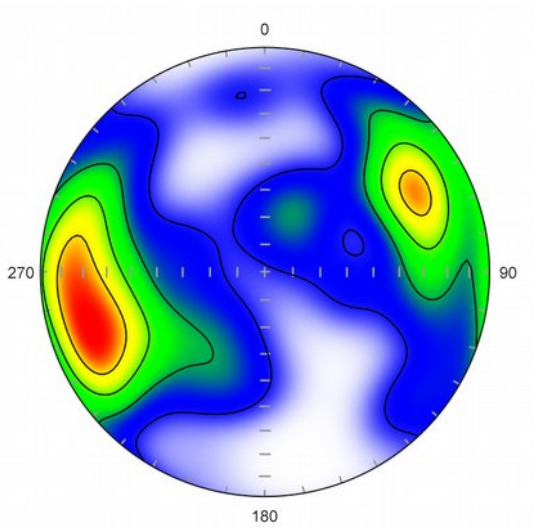

Figure 4.20 Schmidt plot of data in Figure 4.17 with probability density contours at 20% density, 5 equally spaced levels over the density distribution.

Figure 4.21 is an additional example of this data, but contoured at 10% density, using the BCYR gradient. Figure 4.21 is the same plot, but with the Fill contours option selected in the Contour Settings pane.

An additional method that can be used is the probability density method of Diggle and Fisher (1985). An example plot is shown in Figure 4.23. In this case the resulting contours are similar to those given by the 3σ modified Kamb method (Figure 4.21), however this is not the case for all data sets.

Finally, Figure 4.24 is a 3σ modified Kamb contoured Schmidt plot of the folded graywake data from Figure 4.14 for an example of data with a strong girdle disstribution.

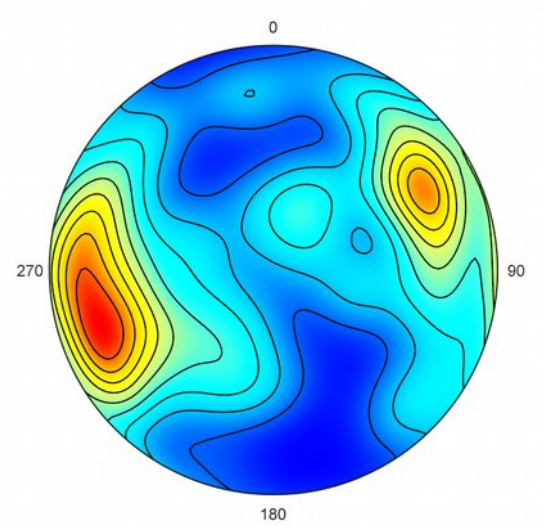

Figure 4.21 Schmidt plot of data in Figure 4.17 with 3σ modified Kamb contours at 10% density. This plot uses the *BCYR Gradient* option.

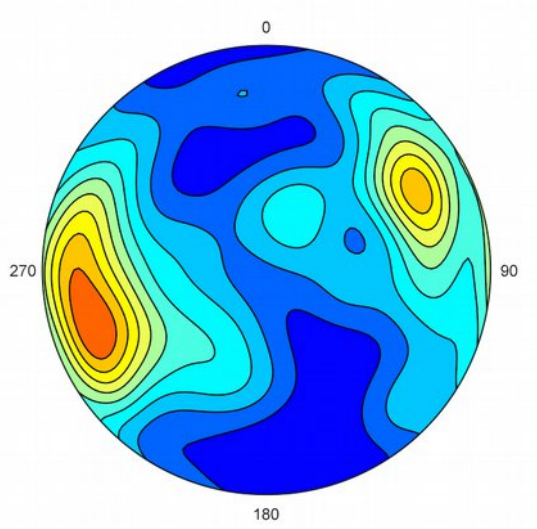

Figure 4.22 Schmidt plot of data in Figure 4.17 with 3σ modified Kamb contours at 10% density, and the *Gradient* and *Fill Contours* options on.

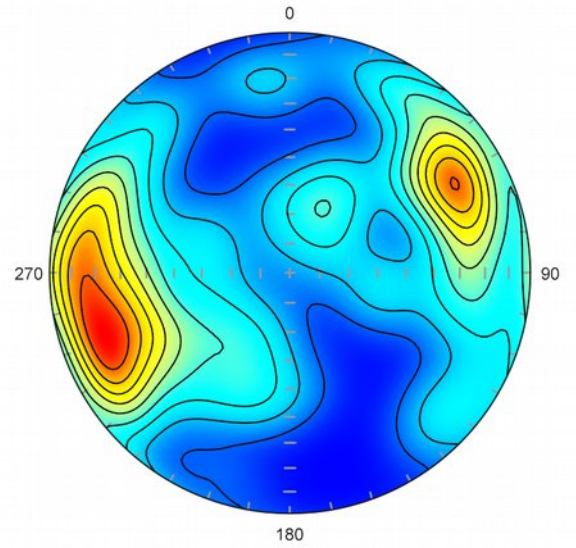

Figure 4.23 Schmidt plot of data in Figure 4.17 with probability density contours at 10% density. In this case, the method gives contours similar to the 3σ modified Kamb method (Figure 4.21).

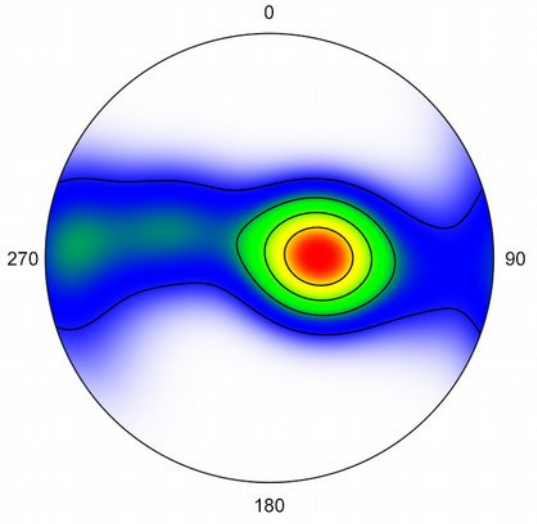

Figure 4.24 Schmidt plot of poles to bedding from Figure 4.14 with modified Kamb contours at 20% density.

4.10 *Tutorial 5 – Contour Plots*

Open the file Vollmer 1981a from the Example Data folder (any of the csv, tsv. ods, or xlsx versions) in Orient, and click on the Spherical Projection icon. Click on the Preferences icon, and locate the Net pane under the Spherical Projection settings. Uncheck both Axes and Net. Next, in the Labels pane, change the Increment to -90, Offset to 14, and Size to 12. If still on from the previous tutorial, turn off eigenvector and confidence cone display in the Maxima panel. The Help Restore Defaults command can be used to reset all preferences if desired.

In the Symbols pane the S0 (bedding) data set should be selected. Uncheck the Symbol option, and check both Contour and Gradient. Click on the gradient paint picker and select the WBGYR (White Blue Green Yellow Red) preset. Finally, in the Contours pane select Contour levels, and set the Levels to 5. This gives modified Kamb contours at 20% density levels, and the plot should appear as in Figure 4.24.

4.11 History and Terminology

Spherical projections have long been used for mapping the terrestrial and celestial spheres. The *stereographic projection* was known to the Greeks Hipparchus and Ptolemy, and was given its present name by François d'Aguilon in 1613 (de Aguilón, 1613; Snyder, 1985; Figures 4.25 and 4.26). The more recent *Lambert azimuthal equal-area projection* was invented by Lambert in 1772 (Lambert, 1772; Snyder, 1985; Figure 4.27).

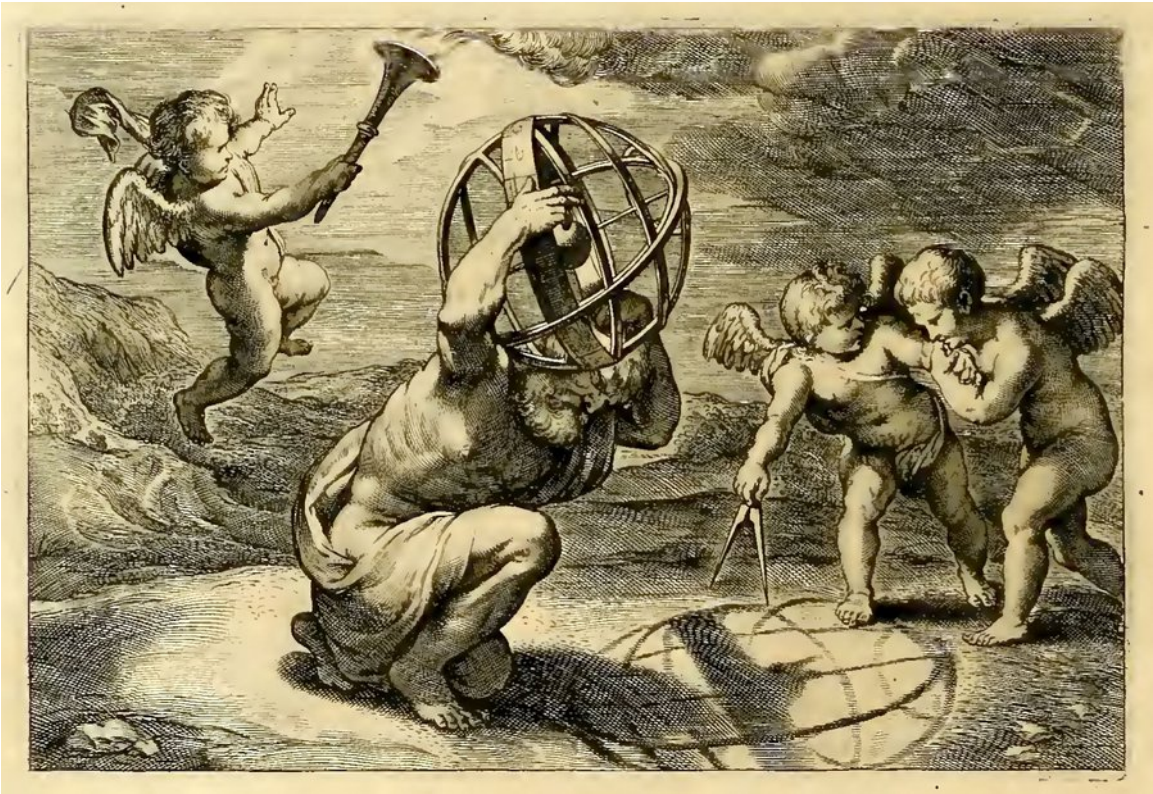

Figure 4.25 Illustration by Peter Paul Rubens showing a globe held by Atlas illuminated by winged putti to illuminate the construction of a stereographic net (de Aguilón, 1613).

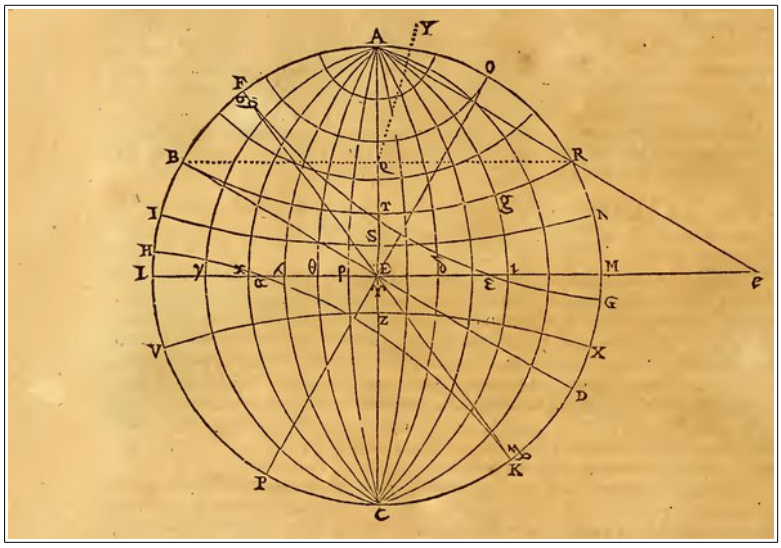

Figure 4.26 *Stereographic net*, or *stereonet*, published by François de Aguilón, 1613.

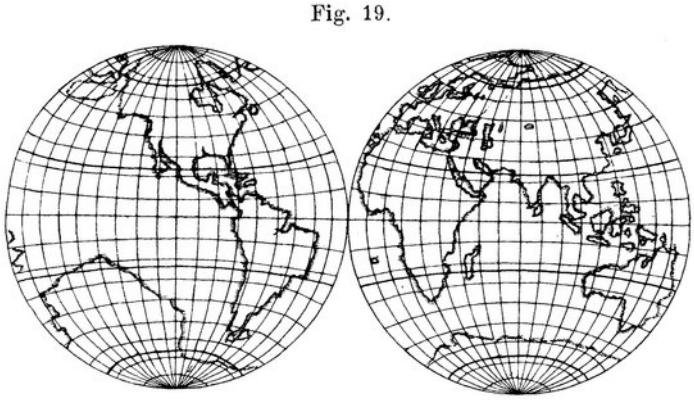

Figure 4.27 Illustration of the Lambert azimuthal equal-area projection by Johann Heinrich Lambert (Lambert, 1722).

In 1925 Walter Schmidt recognized that the stereographic projection was unsuitable for directional data analysis due to its distortion of area (Section 4.6), and introduced the use of the equal-area projection for fabric analysis. Rejecting the stereographic, or Wulff, net used by mineralogists, Schmidt introduced the equal-area net, or Schmidt net, as well as data contouring (Figures 4.28 and 4.29).

In 1944 Walter H. Bucher introduced the *stereonet* for use in structural geology in North America (Bucher, 1944; Billings 1954; Donn and Shimer, 1958; Badgley, 1959). Bucher defined *stereonet* as a shorthand term for *stereographic net* (Bucher, 1944, p. 193), and *stereogram* as a diagram produced using the stereographic net (Bucher, 1944, p. 194). The phrases *equal-area stereonet*, and *equal-area stereogram* are contradictions.

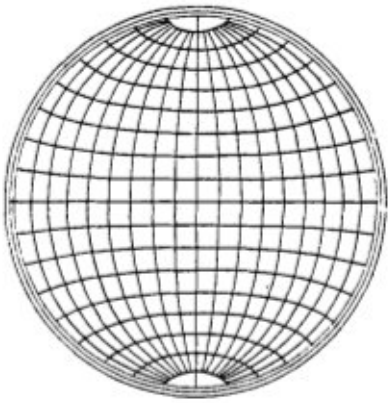

Fig. 1.

Figure 4.28 *Lambert equal-area net*, or *Schmidt net*, as published by Walter Schmidt in 1925.

Fig. 2. Granit, Uhligstal.

Figure 4.29 Lower hemisphere equal-area projection, or *Schmidt plot*, of crystallographic fabric (Schmidt, 1925).

The *equal-area projection* is correctly referred to as the *Lambert azimuthal equal-area projection* (Snyder, 1985), although in the context of directional data analysis, it is usually referred to simply it as the *equal-area projection*. The projected hemisphere should be given, as *lower hemisphere equal-area projection.* Note that other spherical equal-area projections exist, such as the *cylindrical equal-area projection* (Snyder, 1985). Additionally, *hyperboloidal* equal-area and stereographic projections exist, and are used for some geologic data (Yamaji, 2008; Vollmer, 2011). The term *Schmidt projection* has been used for the projection (Mardia and Jupp 2000), and the term *Schmidt plot* is suggested for plots produced using the projection (Vollmer, 2015; Section 4.12).

Early references (Schmidt, 1925; Billings 1942, 1954; Bucher, 1944; Sander, 1948, 1950, 1970; Phillips, 1954; De Sitter, 1956; Donn and Shimer, 1958; Badgley, 1959; Turner and Weiss, 1963; Hills, 1963, Whitten, 1966; Ramsay, 1967, Hobbs et al., 1976) are careful to use correct terminology, as are most current structural geology texts (Marshak and Mitra, 1988; Van der Pluijm and Marshak, 2004; Pollard and Fletcher, 2005; Twiss and Moores, 2007; Ragan, 2009; Fossen, 2016). Note that:

- The equal-area projection is not a *type* of stereographic projection
- A stereonet, or Wulff net, is a stereographic net
- A Schmidt net, or equal-area net, is not a stereonet
- Scatter plots and contour plots are not stereonets
- The phrase *equal-area stereonet* is a contradiction
- The phrase *equal-area stereographic projection* is a contradiction

4.12 Schmidt Plots

The Schmidt net (Schmidt, 1925) was widely used in structural geology (Knopf and Ingerson, 1938; Billings 1942; Turner and Weiss, 1963) prior to the introduction of the stereonet (Bucher, 1944; Billings, 1952; Phillips, 1954), however it is common to see spherical projection scatter plots and contour plots mislabeled as s*tereonets*. As they are not (cf. Figures 4.7 and 4.14), what they represent, and the projection used to make them, is unclear. The equal-area projection and the Schmidt net have a long and important history in structural geology, mislabeling them as stereonets does not give due

credit to their inventor. In 1925 Schmidt recognized that the stereographic projection was not suitable for directional data analysis, and invented the Schmidt net 90 years ago.

Although diagrams produced using Schmidt's equal-area method (Schmidt, 1925) are ubiquitous in structural geology and tectonics, no succinct term exists for them. The term *Schmidt plot* therefore has been suggested for a lower-hemisphere Lambert azimuthal equal-area spherical projection of three-dimensional directional data, such as foliation planes, joints, slickensides, magnetic vectors, crystallographic axes, fold axes, and lineations (Vollmer, 2015). These plots, which are often contoured, have been in common use in structural geology, tectonics, and related disciplines, since their introduction by Walter Schmidt in 1925.

5. Coordinates and Rotations

5.1 Introduction

The rotations used for projection and data display are normally transparent to the user, and the default settings are sufficient in most cases. The default coordinates are local coordinates commonly used in geology (North at the top, and East at the right), however, it is easily configured for other common geographic or spherical coordinate systems, which is the first topic covered in in this section.

The second topic covered here is *coordinate system rotation*, or *projection rotation.* In some cases it is useful or necessary to view data in a more specialized coordinate system, for example centered over a specific location, or chosen parallel to one of the data maxima. The third topic is *data rotation*, which may be required for a number of reasons, such as paleomagnetic fold tests, or rotation of paleocurrent measurements back to horizontal.

Note that for *directed* data, symbols for data not on the current hemisphere will not appear. Rotations involving directed data will therefore often hide those data points. The Directed and Undirected drop-down menus contain options to display hidden directed data, as well as the hidden duals of undirected data. See Section 5.6 for a discussion of these options.

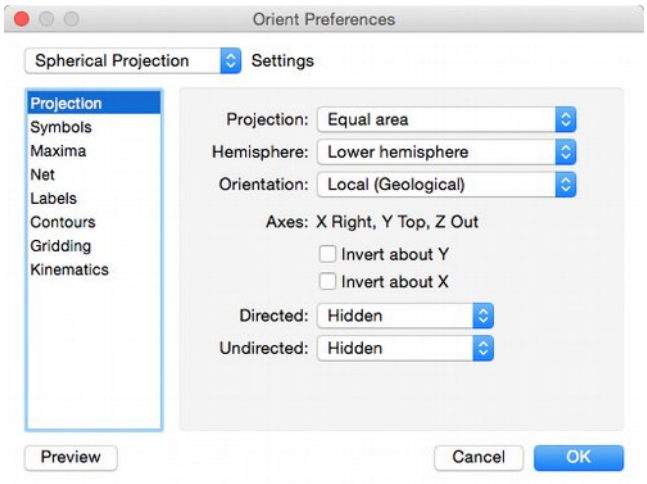

Figure 5.1 The *Preferences* dialog *Spherical Projection Settings* pane displaying options for projections. The *Axes* display, here *X Right, Y Top, Z Out*, gives the current positions of the coordinate axes.

5.2 Geographic Coordinates

The primary coordinate system is selected in the Preferences dialog in the Spherical Projection Projection Settings panel (Figure 5.1). In addition to the Projection and Hemisphere drop-down menus, there is an *Orientation* drop-down menu from which six geographic coordinate systems (Polar, Antipolar, Equatorial 0, Equatorial 90, Equatorial 180, and Equatorial 270) and six spherical systems (XY, ZX, YZ, YX, XZ, and ZY planes) can be selected. These options allow views along any of the three axes in either direction. Additionally, there are checkboxes for inverting the projection about the Y and X axes. These are used, for example, to produce plots like Figure 1.3, a plot of directed magnetic data

displayed on both hemispheres, as they essentially flip the hemisphere over. The Axes display changes when any of these are modified, so the current coordinate system is clear, for example X Right, Y Top, Z Out is displayed for local coordinates.

Figures 5.2 to 5.7 are upper hemisphere equal-area projections of 14,229 earthquake epicenters with magnitudes greater than 4.5 from 1980 to 1990 (data from NOAA) plotted on the six standard geographic coordinate systems.

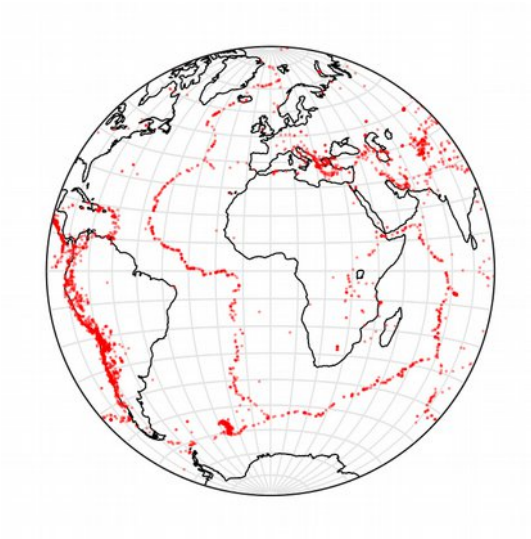

Figure 5.2 Upper hemisphere equal-area projection of 14,229 earthquake epicenters with magnitudes greater than 4.5 from 1980 to 1990, centered at latitude, longitude 0°, 0°, the *Equatorial 0* coordinate system (data from NOAA).

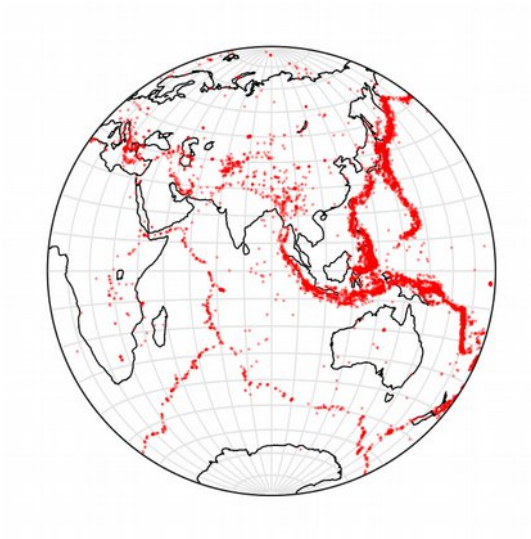

Figure 5.3 Projection as in Figure 5.2, but centered at 0°, 90°, the *Equatorial 90* coordinate system. Compare with Figure 4.26 from Lambert, 1722.

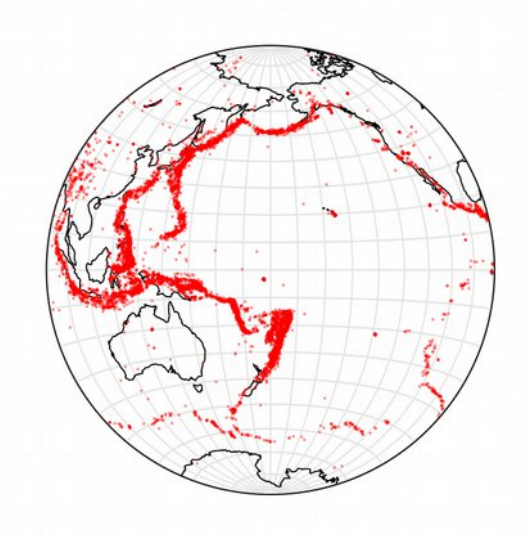

Figure 5.4 Projection as in Figure 5.2, but centered at 0°, 180°, the *Equatorial 180* coordinate system.

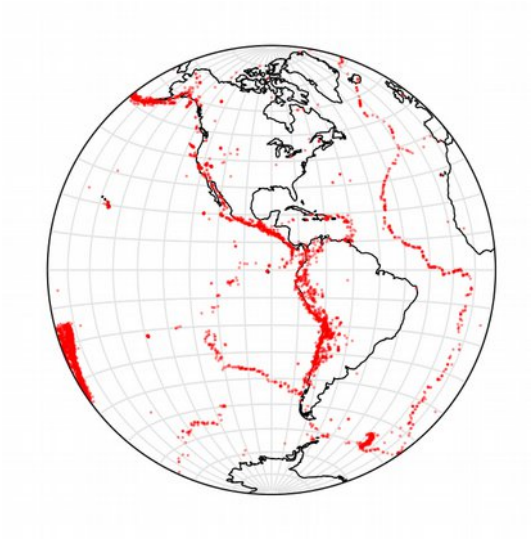

Figure 5.5 Projection as in Figure 5.2, but centered at 0°, -90° , the *Equatorial 270* coordinate system. Compare with Figure 4.26 from Lambert, 1722.

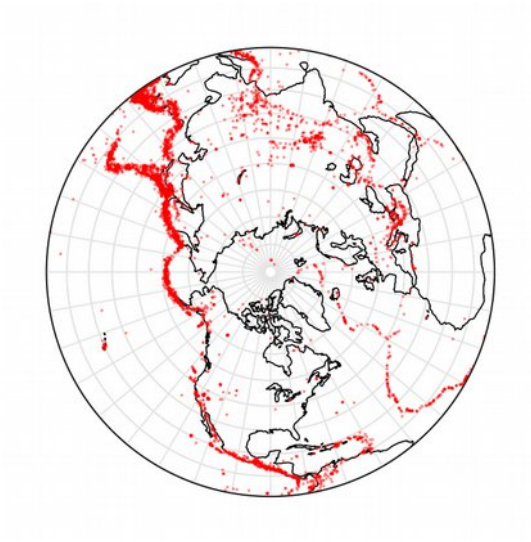

Figure 5.6 Projection as in Figure 5.2, but centered at 90°, 0°, the *Polar* coordinate system.

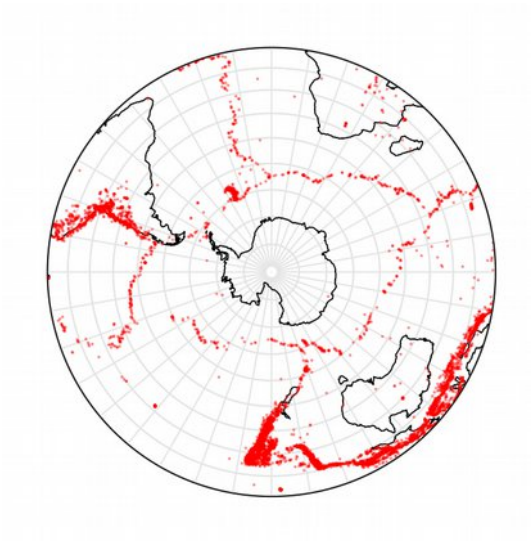

Figure 5.7 Projection as in Figure 5.2, but centered at -90°, 0°, the *Antipolar* coordinate system.

The standard coordinate systems provide views of data along all coordinate axes, however it is also possible to select a view along an arbitrary axis using the Rotate Projection command. The Rotate Projection dialog is shown in Figure 5.8.

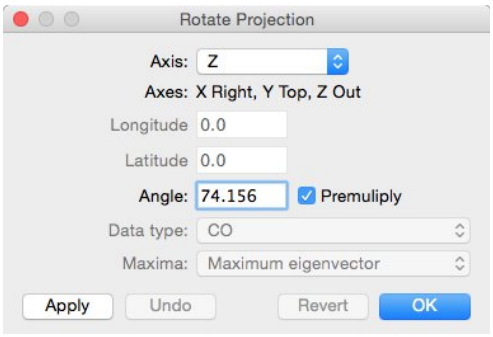

Figure 5.8 The *Rotate Projection* dialog showing the settings for a rotation of 74.156° about the Z axis, which is currently at the top of the projection.

For example, to produce a projection centered at latitude, longitude 41.764, -74.156, first set the coordinate system to Equatorial 0. The projection, as in Figure 5.2, is now centered at 0°, 0°, with X Out, Y Right, Z Top. Set Z as the Axis, enter 74.157 into the Angle edit box, and press Apply. The projection is now centered at 0°, -74.157°. Then set Y as the Axis, enter 41.764 into the Angle edit box, and press Apply. The projection is now centered at 41.764°, -74.157° (Figure 5.9).

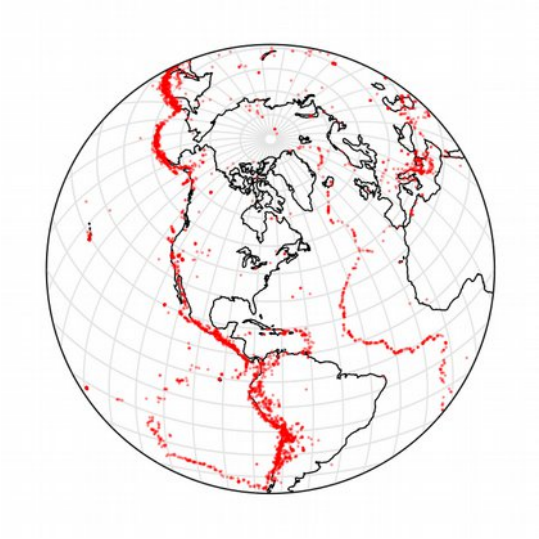

Figure 5.9 Projection as in Figure 5.2, but centered at latitude, longitude 41.764°, -74.157°.

5.3 *Tutorial 6 – Geographic Coordinates*

Open the file Earthquakes With Continents from the Example Data folder, using any of the provided formats, and click on the Spherical Projection icon. The projection will now appear extremely cluttered. To remedy this, open the Preferences dialog and select the Spherical Projections Symbols pane. For the data type CO, uncheck Symbol, check Polyline, and check Directed. For the data type EQ,

set the Symbol Size to 1, the Stroke Color and Fill Color to red, and the Stroke and Fill Opacities to 50%. Check Directed.

Next select the Net pane, uncheck Axes, and check Net. For the Y axis, uncheck both Major and Minor Great Circles and Small Circles. For the Z axis, check Major Great Circles and Major Small Circles, and set both Stroke Colors to a very light gray.

Select the Projection panel, set the Hemisphere to Upper Hemisphere, and the Orientation to Equatorial 0. The projection is now centered at latitude, longitude 0°, 0°, X is out, Y is right, Z is at the top, and the plot should appear as in Figure 5.2.

To center the projection at latitude, longitude 41.764°, -74.156°, open the Rotate Projection dialog (Figure 5.8). Set Z as the Axis, enter 74.157 into the Angle edit box, and press Apply. The projection is now centered at 0°, -74.157°. Then set Y as the Axis, enter 41.764 into the Angle edit box, and press Apply. The projection is now centered at 41.764°, -74.157° (Figure 5.9).

5.4 Projection Rotation

As was shown in the Section 5.2, it is possible to rotate the projection to any orientation. The Rotate Projection dialog (Figure 5.8) allows the sequential application of rotations about any coordinate axis, or about arbitrary axes, by pressing the Apply buttton. The rotations can be undone in the order they were applied, using the Undo button, or can be completely removed using the Revert button.

In examining some data sets, such as crystallographic axes, it may be desirable to produce a plot whose axes are related to the distribution, such as the eigenvectors (Fisher et al., 1987). Figure 5.10 shows the Rotate Projection dialog with settings to rotate a data set to the maximum eigenvector. Any of the three eigenvectors, the mean vector, or the pole to the best fit small circle (Section 7.3), can be selected.

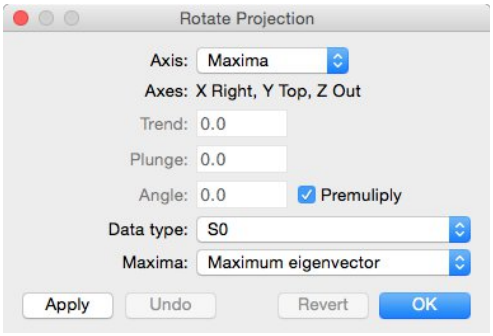

Figure 5.10 The *Rotate Projection* dialog showing the settings for a rotation to center the projection on the maximum eigenvector of the S0 data type.

Figure 5.11 is a Schmidt plot with modified Kamb contours at 20% of the poles to bedding data shown in Figure 4.14, which is then shown rotated to the maximum (Figure 5.12), intermediate (Figure 5.13), and minimum (Figure 5.14) eigenvectors.

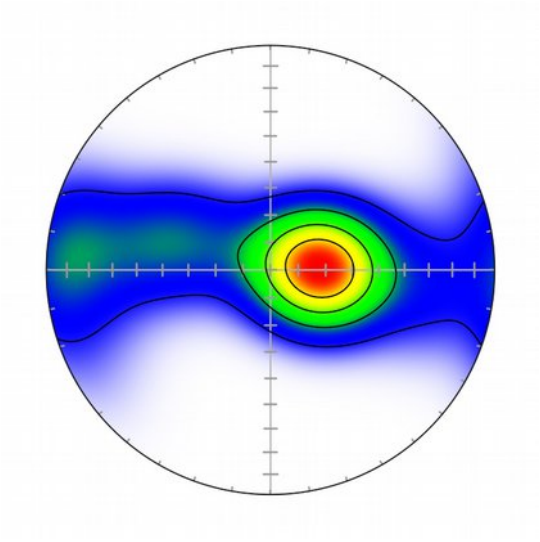

Figure 5.11 Schmidt plot with modified Kamb contours of poles to bedding data from Figure 4.14 with contours at 20% density.

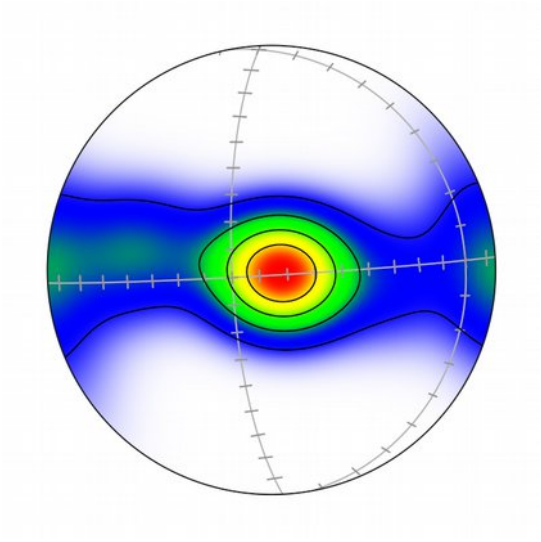

Figure 5.12 Contour plot as in Figure 5.11, rotated to the maximum eigenvector.

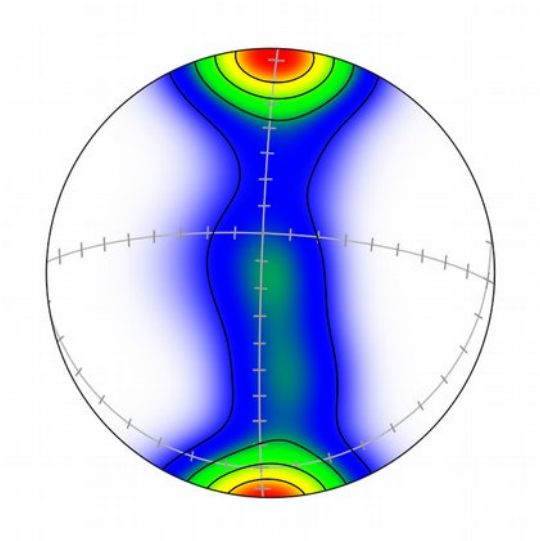

Figure 5.13 Contour plot as in Figure 5.11, rotated to the intermediate eigenvector.

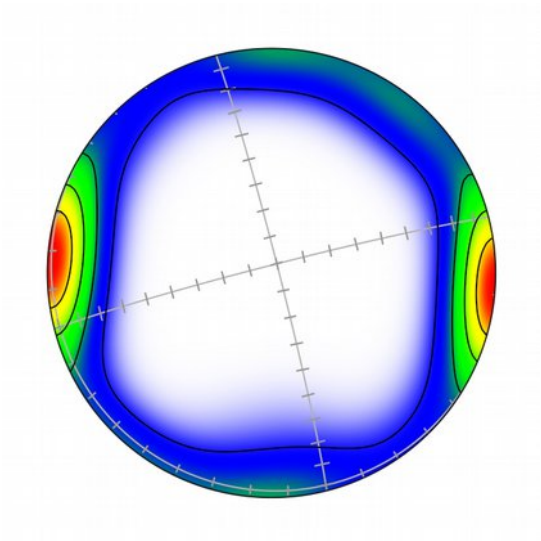

Figure 5.14 Contour plot as in Figure 5.11, rotated to the minimum eigenvector.

5.5 *Tutorial 7 – Rotation to Maxima*

Open the file Vollmer 1981 from the Example Data folder (any of the formats is fine) in Orient, and click on the Spherical Projection icon.

If not already done, remove the Schmidt net from the background. Click on the Preferences icon, and locate the Net pane under the Spherical Projection settings. Uncheck Great circles, Small circles, and Minor Tick marks. Set the Major Tick marks increment (Inc) to 10, and the length (Len) to 4 for the X, Y, and Z axes. Check Above. Next, in the Labels pane, change the Increment to -90, the Offset to 14, and the Size to 12.

In the Spherical Projection settings, restore the projection to Lower Hemisphere and Local coordinates if necessary. In the Symbols pane, uncheck Symbol for the S0 data type, and check both Contour and Gradient. Click on the gradient paint picker and select the WBGYR (White Blue Green Yellow Red) preset. Finally, in the Contours pane set Levels to 5. This gives modified Kamb contours at 20% density levels, and the plot should appear as in Figure 5.11.

Use the Rotate Projection command to open the Rotate Projection dialog (Figure 5.10). Set Axis to Maxima, Data Type to S0, and Eigenvector to Maximum to produce Figure 5.12, Intermediate for Figure 5.13, and Minimum for Figure 5.14.

5.6 *Tutorial 8 – Data Visualization*

It can be difficult to visualize the three dimensional geometry of data plotted on spherical projections. In this tutorial we will use the folded bedding data shown in Figure 4.14 with projection rotation to get a visualization of the geometric significance of poles to folded beds.

Open the example data file Vollmer 1981a, and display a spherical projection using the Graph Spherical Projection command. For this visualization we will use the *orthographic* projection. While it distorts area and density (Section 4.6), it gives an easily visualized image of a sphere as viewed from a distance. You may also want to try using an *upper hemisphere* projection which you may find easier to visualize, but start with the lower hemisphere, which is the standard one for such plots.

From the Spherical Projection pane of the Preferences dialog, select Orthographic. In the Symbols pane, set the symbol Fill Color to yellow, and check the Ray option. Next, in the Maxima pane check Visible. For the Maximum Eigenvector check Symbol and Ray. For the Minimum Eigenvector, check Symbol, Ray, and Great Circle. Set the Stroke Width of the Great Circle to 2. The resulting Schmidt plot is shown in Figure 5.15. Finally, in the Spherical Projection panel, select Undirected 50% Opaque, to give Figure 5.16.

At this point the data elements on the hidden (upper) hemisphere are translucent. Imagine that you can see through them down to the lower hemisphere. Now open the Rotate Projection dialog using the Graph Rotate Projection command, set Axis to X and Angle to 10. Apply increments of rotation using the Apply button, example results are shown in figures 5.17 and 5.18.

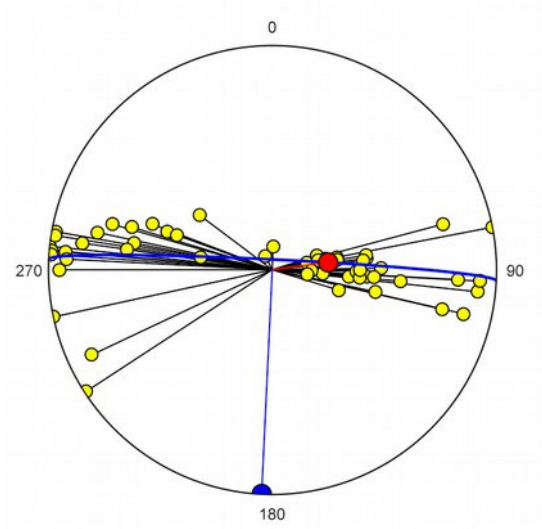

Figure 5.15 Schmidt plot of data from Figure 4.14 with symbol rays, and maximum (red) and minimum eigenvectors (blue) displayed with rays and a great circle girdle.

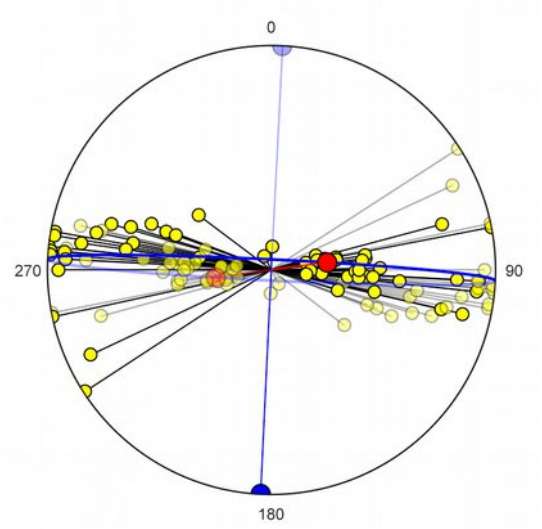

Figure 5.16 Plot as in Figure 5.15 with *Undirected 50% opaque* selected in the *Spherical Projection* pane, so data on the hidden (upper) hemisphere is transparent.

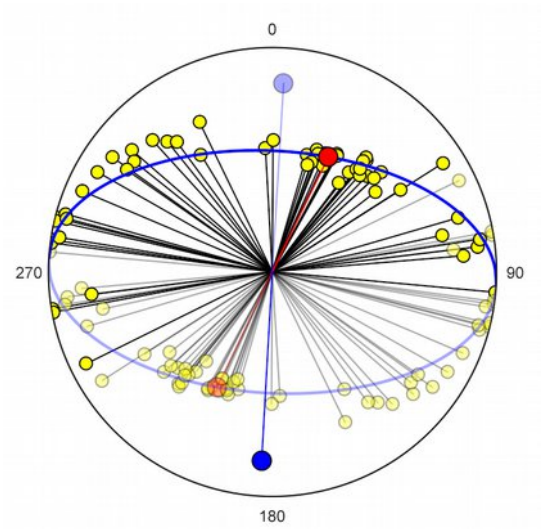

Figure 5.17 Plot at in Figure 5.15 after a rotation of 30° about the X axis.

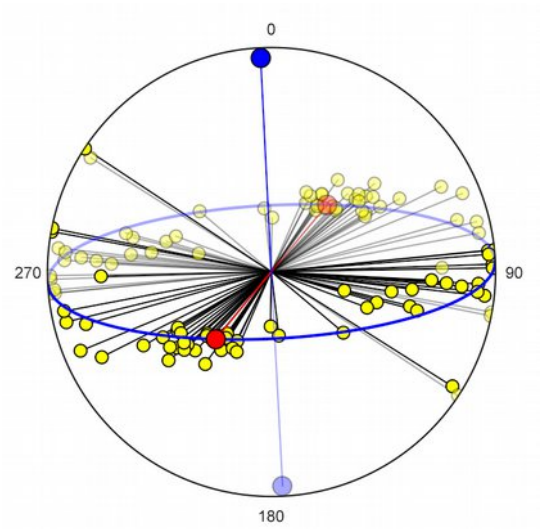

Figure 5.18 Plot as in Figure 5.16 after a rotation of 160° about the X axis.

5.7 Data Rotation

The final topic in this section is *data rotation*. The principal is the same as *projection rotation* however the rotations are applied to the data, not the projection. The data can be sequentially rotated about any of the coordinate axes (Figure 5.19). Before using this command be sure you have a backup file of your data, as this will change the values in the data window spreadsheet.

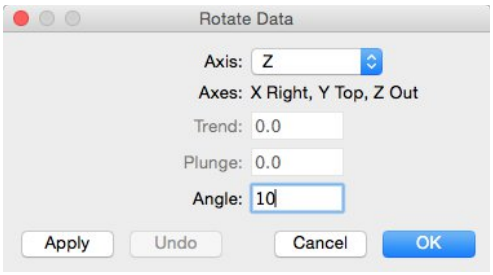

Figure 5.19 The *Rotate Data* dialog allows rotation of the data about any of the coordinate axes, or about an arbitrary axis of any orientation.

To try this command, open the file Vollmer 1981 as in Section 5.5, select all or part of the data, and apply several rotations using the Rotate Data command. Pressing the Apply button sequentially applies rotation by premultiplication of a rotation matrix, and updates any open projections. Press OK to accept the rotated data, or Cancel to revert.

6. Confidence Cones and Bootstrapping

6.1 Introduction

Section 4.7 introduced the concept of calculating maxima for samples of directional data. In particular, the maximum, intermediate, and minimum *eigenvectors* for undirected, or axial, data, and the *vector mean* for directed, or vector data. The *maximum eigenvector* and vector mean are measures of the mean value, or direction about which the samples cluster. The *minimum eigenvector* is used to locate the center of a great circle girdle, such as a cylindrical fold axis. The relative magnitudes of the eigenvectors give additional information about the type of distribution, this is discussed further in Chapter 9. The *best fit small circle* is discussed in Section 7.3.

The concept of a mean value is of great significance, but it does not say anything about the certainty of the estimate. This chapter discusses ways to provide uncertainty estimates, in particular deriving confidence cones about the mean. Only a basic overview is provided here, the statistical analysis of directional data is discussed in detail by Fisher et al. (1987), and Mardia and Jupp (2000). These texts should be consulted for additional details and statistical tests.

6.1 Spherical Distributions

There are a number of models for distributions of spherical directional data (Mardia, 1972; Fisher et al., 1987; Mardia and Jupp, 2000). By analogy, the Gaussian, or normal, distribution is a familiar model for scalar data. Four important distributions on the sphere are the Fisher, Kent, Watson, and Bingham distributions.

The *Fisher* (or *von Mises-Fisher*) distribution is the basic model for *unimodal rotationally symmetric directed* data, so, for example, is applicable to paleomagnetic vectors. This is a general and useful statistic for directed data. A confidence region is calculated for a symmetrical unimodal distribution, which gives a circular confidence cone.

The *Kent* distribution (Kent, 1982) is also a model for unimodal directed data, but does not assume the distribution is rotationally symmetric, so the confidence cone is elliptical, rather than circular. The Kent statistic is calculated using moment estimation, similar to the Watson and Bingham statistics, but is centered on the vector mean.

The *Watson* distribution serves as the basic model for rotationally symmetric *undirected* lines (axes). The distribution has rotational symmetry as a *bipolar* or *girdle* distribution. The confidence region is bipolar, giving two confidence cones centered 180° apart in opposing hemispheres. Confidence cones can be calculated for the three axes of asymmetrical polar, girdle, or multimodal distributions, giving elliptical confidence cones. This distribution can be used for features such as normals to joint planes, or quartz c-axes. It is common to determine the axes of folded bedding surfaces using the pole to a girdle, however note that assigning a younging direction to bedding allows it to be treated as vector data.

The *Bingham* distribution is also for undirected lines (axes), but does not assume rotational symmetry. It can be regarded as an extension of the Watson distribution, which is the Bingham distribution with rotational symmetry (Mardia and Jupp, 2000). Confidence cones are similarly bipolar. Fisher et al. (1987) recommend the simpler Watson model in most cases. Confidence cones can be calculated for each of the three axes, giving elliptical cones.

Using these models, confidence cones can be drawn around either the mean direction (Fisher or Kent), or the eigenvectors (Watson or Bingham), at confidence levels of 90%, 95%, or 99%. Note that a *minimum sample size of 25* is required for these, bootstrapping (Section 6.2) should be applied for sample sizes less than 25.

Figure 6.1 shows the directed paleomagnetic data from Figure 1.3 with a 95% confidence cone based on the Fisher distribution. Figure 6.2 shows the same data with a 95% confidence cone based on the Kent distribution.

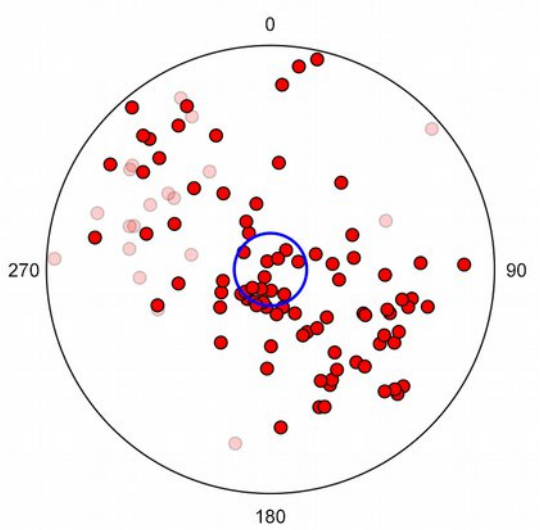

Figure 6.1 Schmidt plot of paleomagnetic data as in Figure 1.3 with 95% confidence cone based on a Fisher distribution. Upper hemisphere data shown as 30% opaque.

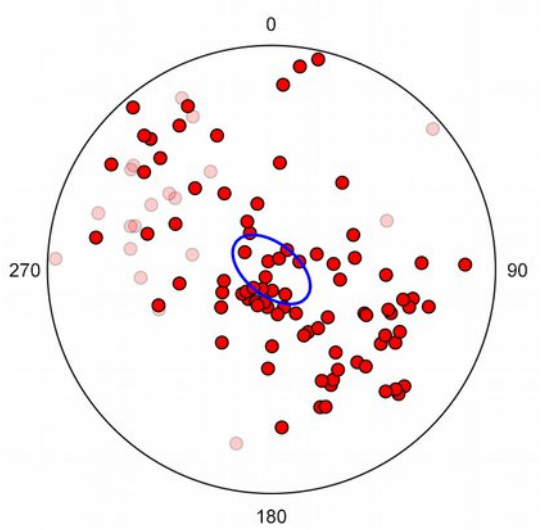

Figure 6.2 Paleomagnetic data as in Figure 6.1 with 95% confidence cone based on a Kent distribution.

Figure 6.3 shows 95% confidence cones using the Watson distribution for folded bedding data. Note that, because of the strong girdle pattern in this data, the semiapical angles of the confidence cone about the minimum eigenvector are small, while the maximum is strongly elliptical within the girdle. This shows that the minimum is well constrained, while the position of the maximum within the girdle is less well defined. Figure 6.4 shows similar confidence cones for ice crystallographic data. Figures 6.5 and 6.6 show confidence cones based on the Bingham distribution for the same data sets.

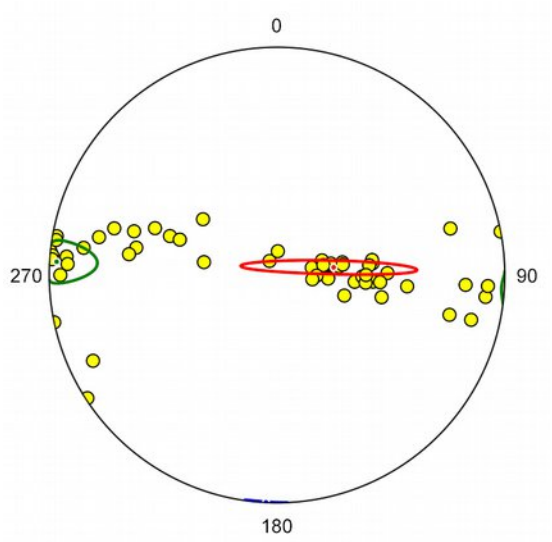

Figure 6.3 Schmidt plot of poles to folded greywacke beds, as in Figure 4.14 with 95% confidence cones based on a Watson distribution about the maximum (red), intermediate (green), and minimum (blue) eigenvectors.

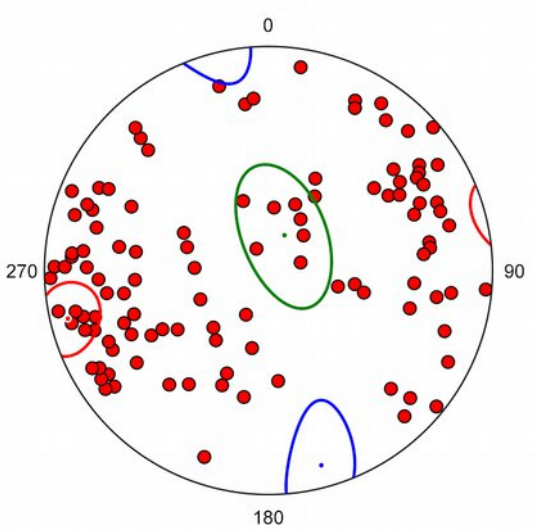

Figure 6.4 Ice crystallographic axes as in Figure 4.17 with 95% confidence cones based on the Watson distribution. Colors are as in Figure 6.3.

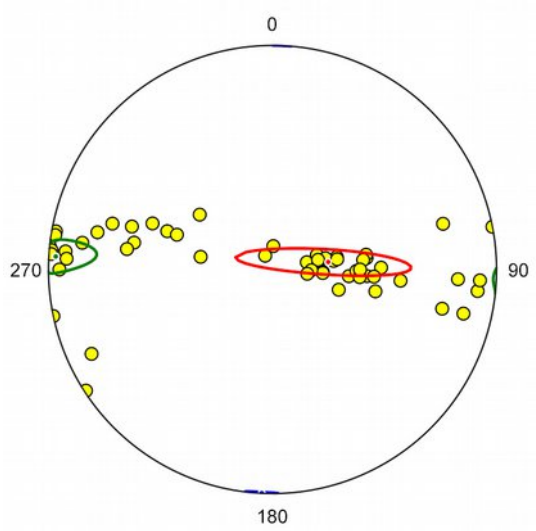

Figure 6.5 Plot as in Figure 6.3 with 95% confidence cones based on the Bingham distribution.

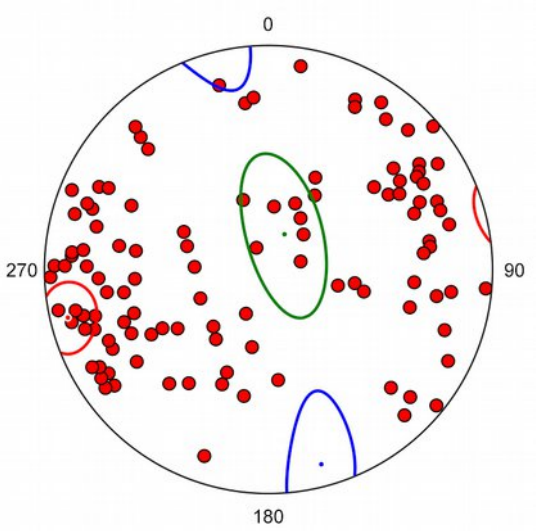

Figure 6.6 Plot as in Figure 6.4 with 95% confidence cones based on the Bingham distribution.

Data point weighting is implemented for Fisher, Kent, Watson, and Bingham confidence cones, but is not for bootstrap confidence cones (Section 6.3). Bootstrapping creates replicates by random selection, and assumes each data point is equally weighted.

6.3 Bootstrapping

The models discussed in section 6.2 assume an underlying distribution model and require a minimum sample size of 25. An alternate method is to use *bootstrapping* to infer confidence regions about the mean. The data set is resampled numerous times and the mean calculated each time to give a large number of *replicate means*, which can be used to determine elliptical confidence regions (Fisher et al., 1987; Mardia and Jupp, 2000; Davis et al., 2015; Figures 6.3 and 6.4). This approach is particularly useful for small samples (and is required for sample sizes less than 25), or where the underlying distribution model is not known.

Bootstrapping requires creating a large number of replicates, the default is 1000, with an allowed range from 100 to 100,000. The means of the replicates can be displayed (Figures 6.8, 6.10) if desired. The process involves pseudorandom (mersenne twister) number generation, and the resulting confidence regions will vary slightly each time. Confidence results are presented in the Log window by giving the axis of the elliptical cone (a direction, which may differ from the mean), the semiapical angle of the rotationally symmetric (circular) cone, and the semiapical angles and directions of the major and minor semiaxes of the elliptical cone.

Note that, while data point weighting is implemented for Fisher, Kent, Watson, and Bingham confidence cones (Section 6.2), it is *not* implemented for bootstrap confidence cones because bootstrapping creates replicates by random selection, and assumes each data point is equally weighted.

Figure 6.7 illustrates bootstrap confidence cones for folded graywacke bedding planes treated as undirected axes, Figure 6.8 shows an example of the bootstrap replicates used to calculate the cones. Figure 6.9 shows similar bootstrap cones for ice crystallographic data, with an example of replicates shown in Figure 6.6. While no underlying model is assumed, the confidence cones generated are comparable to those generated using the Watson distribution, as shown in Figures 6.3 and 6.4.

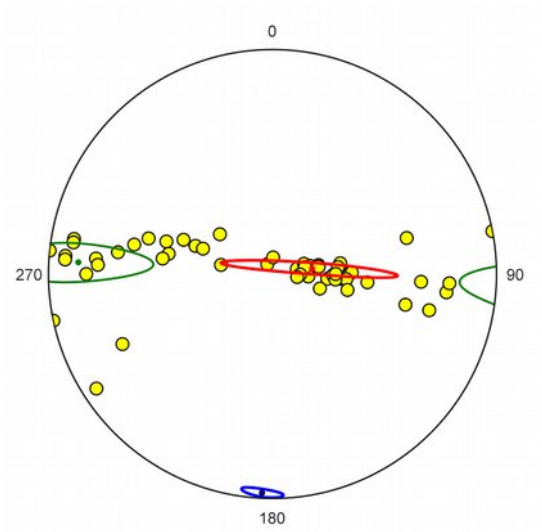

Figure 6.7 Bedding data as in Figure 6.3 with 95% confidence cones from 5000 bootstrapped replicate means. This gives confidence cones similar to the Watson model in Figure 6.3.

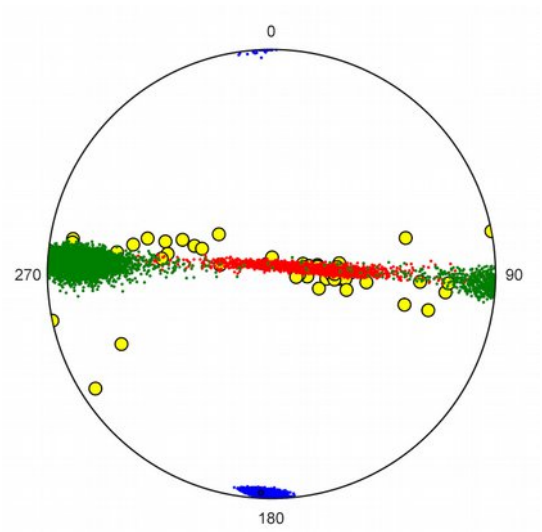

Figure 6.8 Bedding data as in Figure 6.3 showing the means of 5000 bootstrap replicates used to calculate the ellipses as in Figure 6.7.

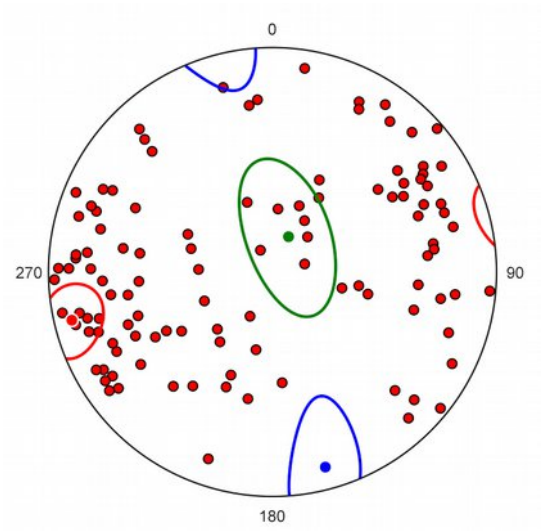

Figure 6.5 Schmidt plot of ice c-axis data, as in Figure 1.1, with bootstrapped elliptical confidence regions. This gives confidence cones similar to the Watson model in Figure 6.2.

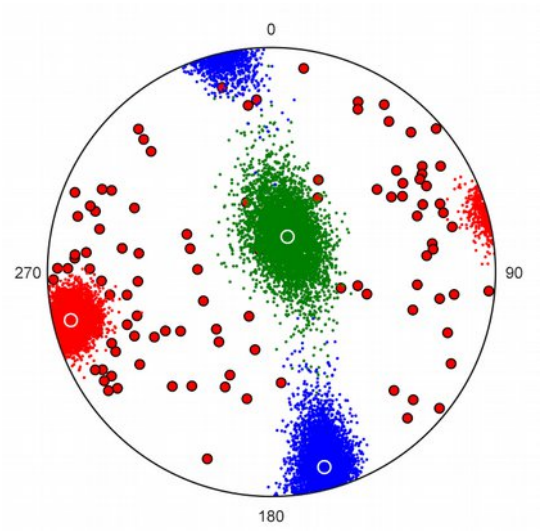

Figure 6.6 Plot of data as in Figure 6.5, with the means of 5000 bootstrap replicants on each of the eigenvectors.

The Log file generates a large number of results, however in most cases it is probably sufficient to report one or two mean values, either the *vector mean* for directed data, the *maximum eigenvector* for undirected data, or the *minimum eigenvector* for a girdle pole, along with a measure of uncertainty, such as the 95% symmetric cone semiapical angle. This confidence cone is plotted if the *Circular* option is selected for bootstrapping, the confidence cone is then calculated using the angular deviation from the mean, giving a circular confidence cone which encloses 95% of the replicate means. Examples are shown in Figure 6.7 of bedding data, in Figure 6.8 of ice crystallographic axes.

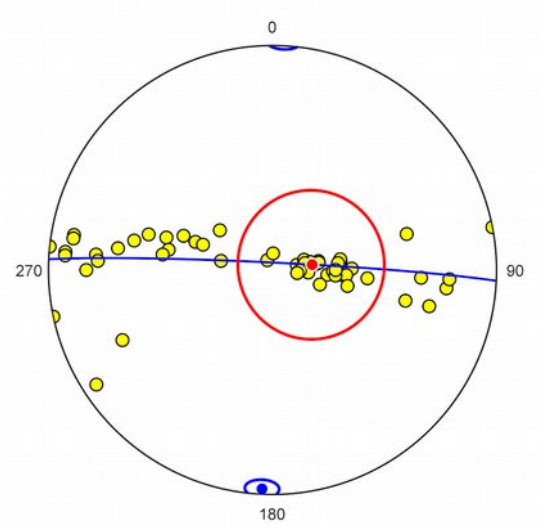

Figure 6.7 Plot as Figure 6.7 showing symmetric 95% confidence cones about the maximum and minimum eigenvectors. The mean bedding as strike, dip is 172.29°, 14.52° with 95% confidence of 26.72°. The mean fold axis as trend, plunge is 182.76°, 2.69° with 95% confidence 4.61°.

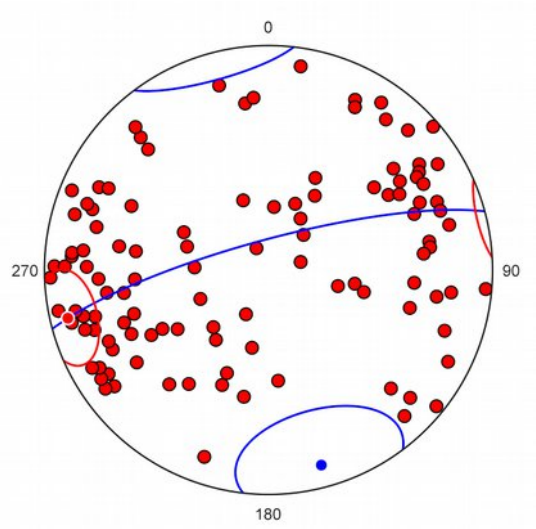

Figure 6.8 Plot as in Figure 6.2 showing symmetric 95% confidence cones about the maximum and minimum eigenvectors. The mean axis as trend, plunge is 256.52°, 8.74° with 95% confidence of 13.74°. The mean girdle pole is 164.84°, 10.90° with 95% confidence 25.66°.

Figure 6.9 illustrates bootstrap analysis applied to directed data, magnetic remnant vectors. In this diagram the upper hemisphere is inverted on the left using the Invert about Y option. Figure 6.10 is a projection of the same data using a 30% transparent upper hemisphere, and Figure 6.11 shows the projection rotated to the vector mean to more clearly show the distribution.

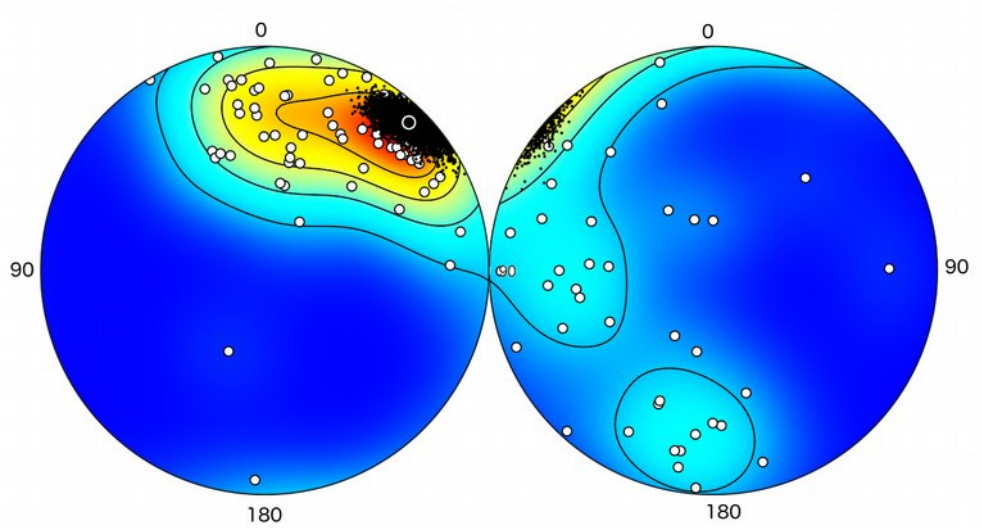

Figure 6.9 Schmidt plots (data inverted on left) of magnetic remanence data, an example of directed or vector data, from Figure 1.3 with the means of 5000 bootstrap replicants on the mean vector.

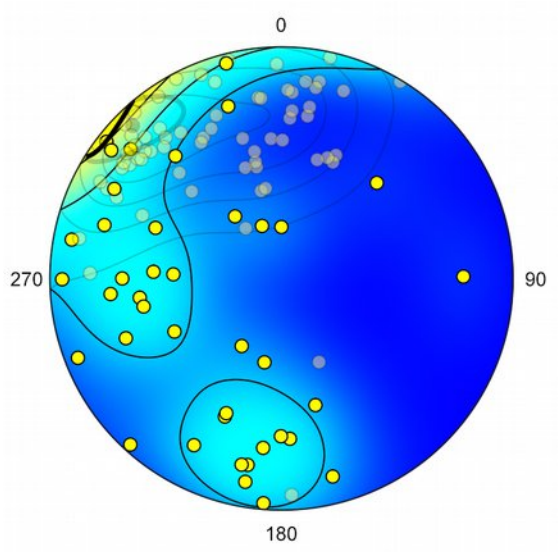

Figure 6.10 Magnetic data as in Figure 6.9 with 95% bootstrap confidence cone about the mean, and 30% transparency of upper hemisphere.

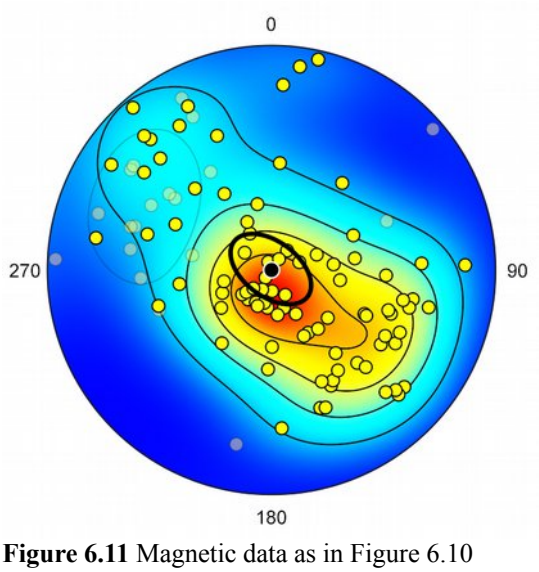

Figure 6.11 Magnetic data as in Figure 6.10 rotated to the vector mean. Compare this to the confidence cone generated using the Kent distribution in Figure 6.2.

Figure 6.12 shows the replicate means used to calculate the confidence cones. Figure 6.13 shows the symmetric confidence cone generated with the Circular option. For comparison, the corresponding circular Fisher confidence cone is shown in Figure 6.14.

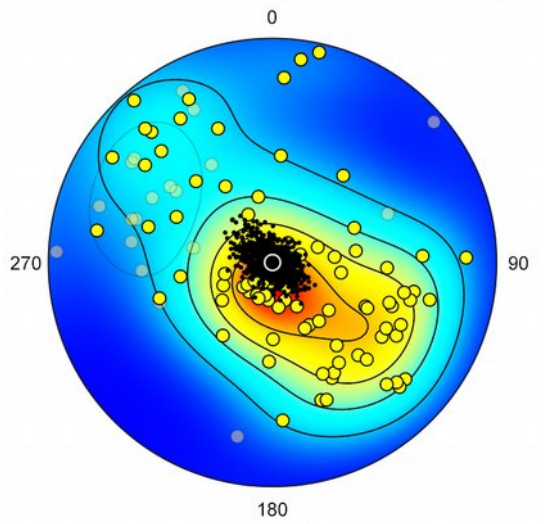

Figure 6.12 Magnetic data as in Figure 6.11 with 5000 bootstrap replicate means displayed. A set of such means is used to calculate the confidence cone.

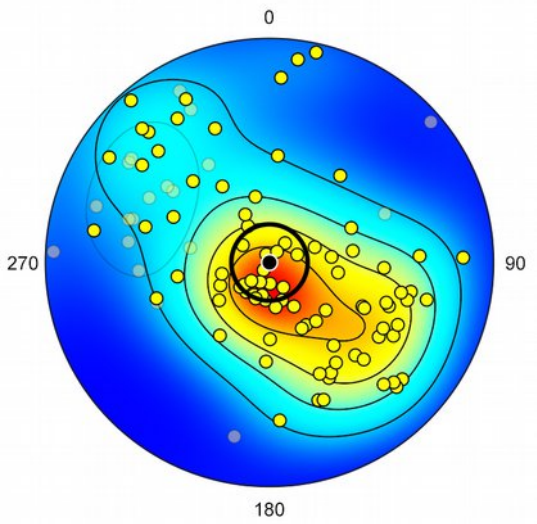

Figure 6.13 Magnetic data as in Figure 6.11 with circular bootstrap confidence cone. The vector mean as trend, plunge is 315.78°, -8.65° with 95% confidence 13.84°. This gives similar confidence cones as the Fisher model shown in Figure 6.3.

One final option is to display the confidence region using the Hull option, this displays the convex hull of all points that fall within the confidence region calculated using the angular deviations. Figure 6.14 shows an example using undirected crystallographic data and centered on the maximum eigenvector. Figure 6.15 is an example using directed magnetic data centered on the vector mean.

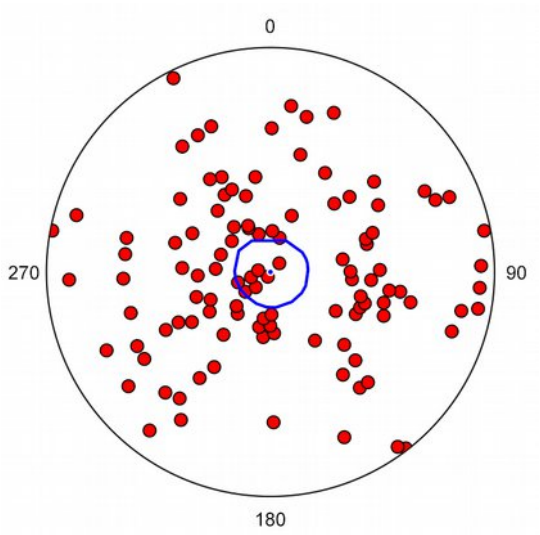

Figure 6.14 Ice crystallographic data as in Figure 6.5 centered on the maximum eigenvector with bootstrap 95% confidence region. The polygonal hull encloses 95% of the replicate means sorted by distance from the maximum.

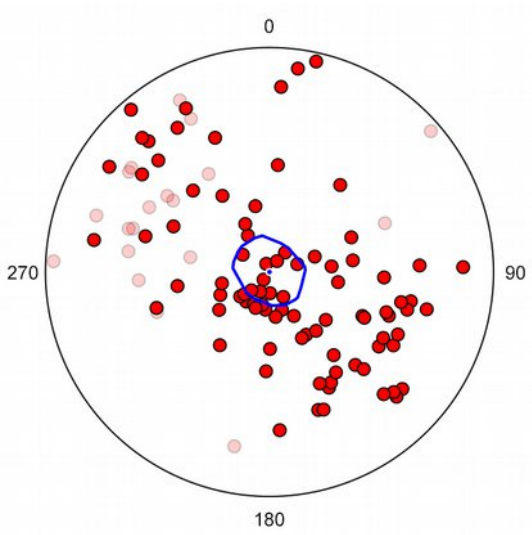

Figure 6.15 Magnetic data rotated to the vector mean as in Figure 6.11 with 95% bootstrap confidence region. The polygonal hull encloses 95% of the replicate means sorted by distance from the mean.

7. Conical Data and Small Circles

7.1 Introduction

This chapter concerns two distinctly different topics, data that is entered as a direction and an angle, and data that can be fitted to a cone.. An example of the first are drill core data from cores that penetrate layers at a measured angle. Each data point is characterized by three angles (θ, φ, α), where θ, φ give the direction (e.g., trend and plunge) of the core, and α is the half apex, or semiapical, angle defining the circular cone.

The second topic, fitting to a cone, is most commonly applied to fitting bedding or foliation data to a conical fold. Folds are treated as approximately cylindrical when possible (Badgley, 1959; Turner and Weiss, 1963; Whitten, 1966; Ramsay, 1967; Hobbs et al., 1976), however non-cylindrical folds are common in nature, and conical folds are an alternate model that may be applicable in some locations (Wilson, 1967; Kelker and Langenberg, 1982).

A tutorial on *data point weighting* is included in this chapter as well, using the example of fitting a small circle. The weighting of individual points applies to other plots and calculations, such as circular plots and kinematic analysis, but the fitting of small circles provides a useful example for visualization.

7.2 Conical Data

Data that are characterized by both a direction and an angle define a cone, which projects as a small circle on a spherical projection. In exploration geology it is common to drill a core to determine rock composition and structure. If the core intersects a plane of interest, such as a bedding plane, the angle between the core with orientation (θ, φ), and the plane gives a core-plane angle, α, defining the cone (θ, φ, α). When the core is extracted the orientation of the plane is lost, however it must lie tangent to the cone (θ, φ, α).

This is one of a class of geometric problems that are commonly solved using a stereographic net, or stereonet (Bucher, 1944; Phillips, 1954; Donn and Shimer, 1958; Badgley, 1959; Lisle and Leyshorn, 2004; Ragan, 2009). An advantage of the stereographic projection is that, because of its equal-angle property, small circles project as circular arcs (Section 4.4), and can be constructed using a compass. Unless this equal-angle property is required, such problems can also be solved using a Schmidt net.

Orient allows such conical data to be entered and will plot small circles, avoiding manual construction, and aiding in the visualization and solution of drill hole problems. The direction of the drill core (θ, φ) is typically given by its trend and plunge, enter these, and then the half apex (semiapical) angle α in the spreadsheet column Alpha. Use the View Data Columns command to display the column if not visible.

As an example, Table 7.1 gives the orientations of three drill cores with core-plane angles of bedding planes (from Ragan, 2009), the problem is to determine the bedding plane orientation.

ID	Trend	Plunge	Alpha
1	0	60	51
2	270	50	67
3	45	55	38

Table 7.1 Example drill core data (from Ragan, 2009). Given the trend and plunge of three drill cores, and the core-plane angle α (*Alpha*) of bedding planes, determine the orientation (strike and dip) of the bedding.

To solve the problem, open a new data sheet in Orient, and display a projection using the Graph Spherical Projection command. In the Symbols pane of the Preferences dialog, check Small Circle.

Use the View Data Columns command to display the Alpha column if not visible, and enter the data from Table 7.1. The resulting Schmidt plot is shown in Figure 7.1, and lower-hemisphere stereographic projection (stereogram) in Figure 7.2. The three cones intersect at a single point, which represents the bedding plane orientation. Use the mouse to determine the solution on either projection. The bedding normal trend, plunge is TP = 120°, 60°, and the plane strike dip is SD = 210°, 30°. While an analytical solution can be calculated (Ragan, 2009), a visualization of the solution is desirable, and precision to less than a degree unlikely to be required.

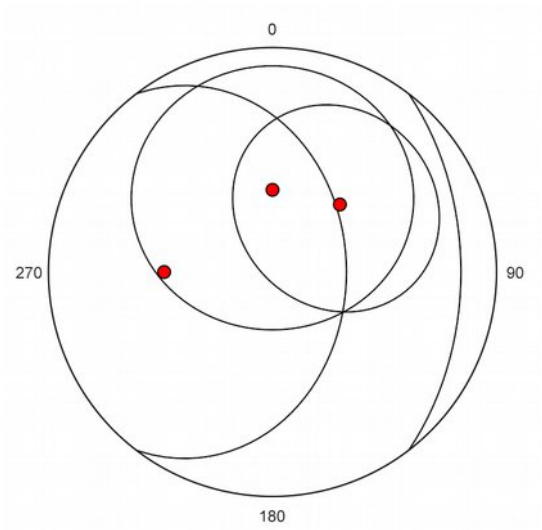

Figure 7.1 Schmidt plot of drill core data from Table 7.1 showing cones defined by the core-plane angles. The solution is the intersection of the three cones.

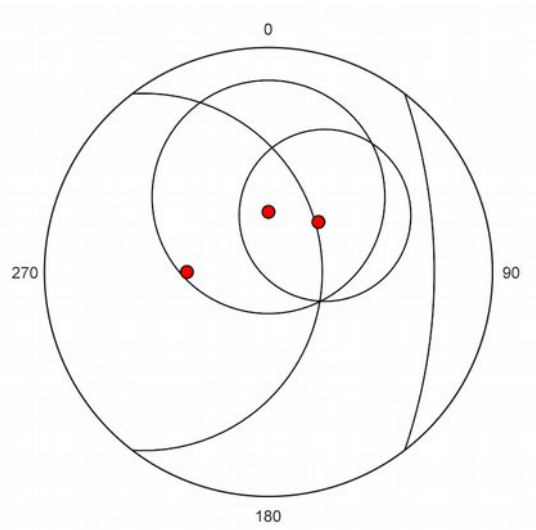

Figure 7.2 Lower hemisphere stereographic projection, or stereogram, of data as in Figure 7.1. Either projection can be used to find the solution.

7.3 Fitting Small Circles

In some cases it may be required to fit directional data to a cone. The most common case in geology is to determine the best fit axis, **λ** (a vector, specified, for example, by trend and plunge)**,** and half apex (semiapical) angle, ψ, of conical folds. The most common model for folds is *cylindrical*, however the alternate model of *conical* folds may be useful in some cases (Wilson, 1967; Gray et al., 1980; Kelker and Langenberg, 1982, 1988; Mulchrone et al., 2013).

This may also be viewed as a general model for fitting *vector* data to *great or small circles*, since great circles are given by $\psi = 90°$. Note that the data (θ_i, φ_i) are treated as *directed* (vector) data, if these are bedding measurements, any overturned beds should be entered using negative dips $(\theta + 180°, -\varphi)$.

The problem, given a data sample (θ_i, φ_i), find the cone (λ, ψ), which can be formulated by minimizing the sum of either the distance or angular residuals, requires an iterative solution (Mardia and Gadsden, 1977; Gray et al., 1980; Mancktelow, 1981; Fisher et al., 1987; Mulchrone et al., 2013). The fitting method used here follows Fisher et al. (1987) after Mardia and Gadsden (1977) with modifications (Vollmer, in preparation).

Figure 7.3 is a Schmidt plot of data from an area of cylindrical folding in Australia (Cohen, 1983, from Fisher, 1987; example data file Cohen 1983). The fitted cone is $(\lambda, \psi) = (3.23°, 18.38°, 76.19°)$ given as azimuth, declination, semiapical angle. Figure 7.4 shows the folded graywacke bedding data with the best fit small circle $(\lambda, \psi) = (183.63°, 8.09°, 85.57°)$, very close to the great circle $(\psi = 90°)$ shown in Figure 4.15.

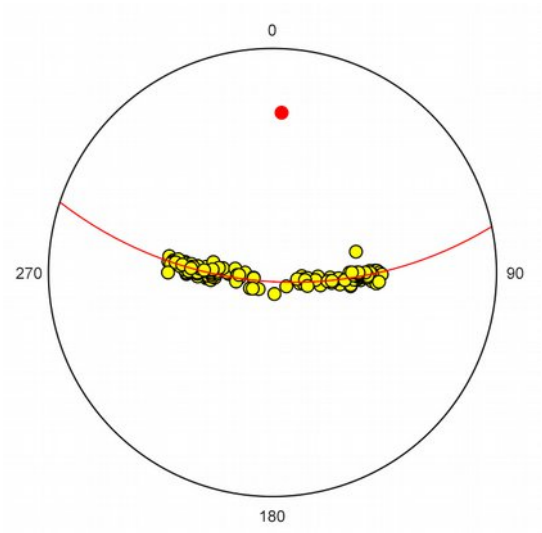

Figure 7.3 Schmidt plot of 155 facing directions of conically folded planes to a small circle. Data from Cohen (1983), in Fisher et al. (1987).

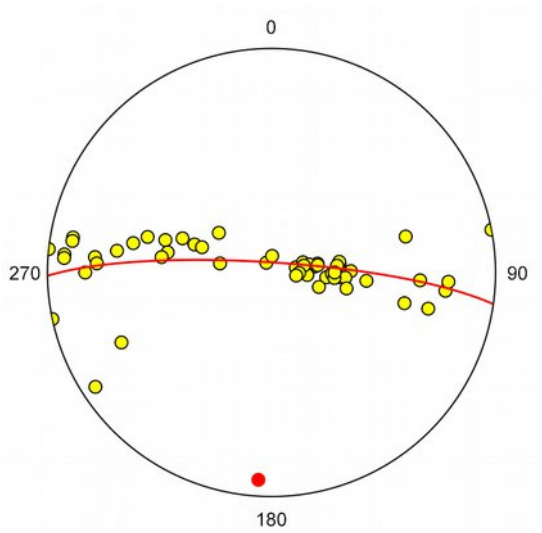

Figure 7.4 Schmidt plot of folded graywacke bedding data from Figure 4.14 with best fit small circle. Compare with Figure 4.15, which shows the best fit great circle.

7.4 Small Circle Confidence

The method for fitting a small circle can be extended to estimate confidence regions by using bootstrapping methods similar to that discussed in Section 6.3 (Fisher et al., 1987). A large number of estimates of the mean are calculated from resampled replicates, and used to estimate confidence regions. Figure 7.5 shows the 95% confidence for the cone axis of the fold data in Figure 7.3 calculated using 1000 replicates, and Figure 7.6 shows the data rotated to the cone axis, and the means of 1000 replicates.

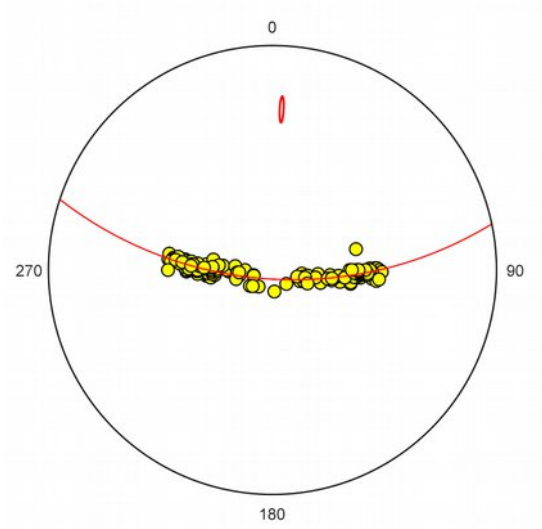

Figure 7.5 Plot of conical fold data as in Figure 7.3 with 95% bootstrap confidence cone.

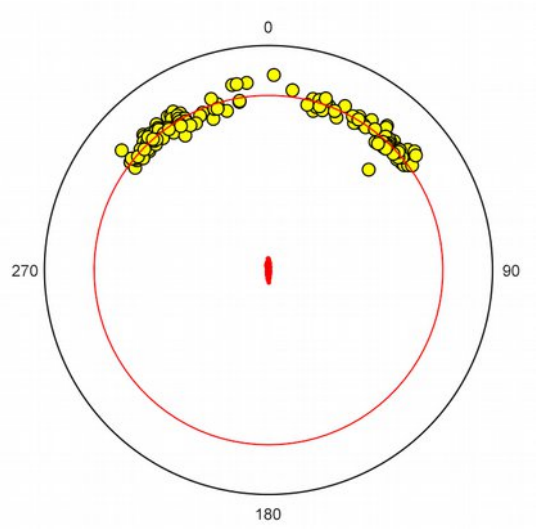

Figure 7.6 Plot of conical fold data as in Figure 7.4, rotated to the best fit cone axis, with means of 1000 bootstrap replicates used to calculate the confidence ellipse as in Figure 7.5.

If the Circular option is selected, the confidence cone is calculated using only the angular distance, producing a circular cone. In this case it is possible to draw confidence rings about the best fit small circle by checking the Ring option. Figure 7.7 shows the conical fold data with a circular confidence cone and small circle confidence rings, Figure 7.8 is a plot rotated to the small circle axis.

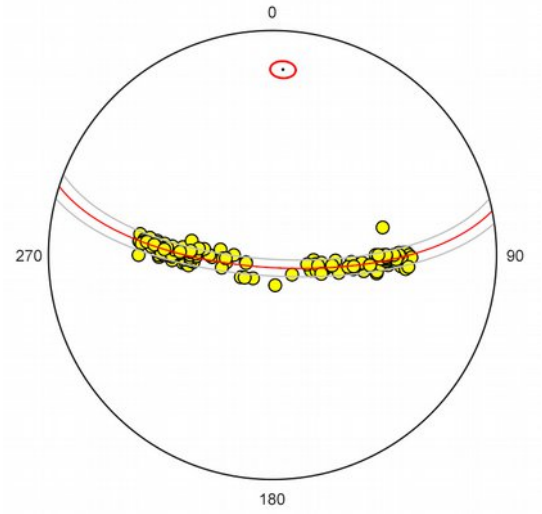

Figure 7.7 Conical fold data as in Figure 7.3 displayed with 95% circular confidence cone and small circle confidence rings. The best fit small circle is (λ, ψ) = (3.23°, 18.38°, 76.19°) with 95% confidence about (λ, ψ) as (3.10°, 2.39°).

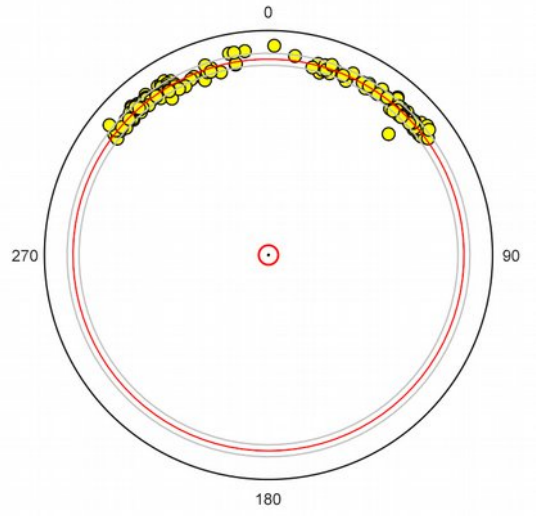

Figure 7.8 Plot of conical fold data as in Figure 7.7 rotated to the small circle axis.

Figure 7.9 is a Schmidt plot of the folded graywacke beds from Figure 4.14 with 95% circular confidence cones and small circle confidence rings. The best fit small circle is ($\boldsymbol{\lambda}$, ψ) = (183.63°, 8.09°, 85.95°) with 95% confidence about ($\boldsymbol{\lambda}$, ψ) estimated as (7.04°, 11.91°). Figure 7.9 shows the same data rotated to the small circle axis. Note that the axis is calculated with the bedding data as *vectors*, even if they are displayed as axes with the Symbols panel Directed option unchecked. From Figure 7.10 it is clear that one of the 95% confidence includes the plane normal to the axis, that is, ψ (85.95°) plus the confidence estimate on ψ (11.91°) is greater than 90°. Figure 7.11 shows the same data with the symmetrical confidence cone for the minimum eigenvector, the standard method for determining the axis of a cylindrical fold.

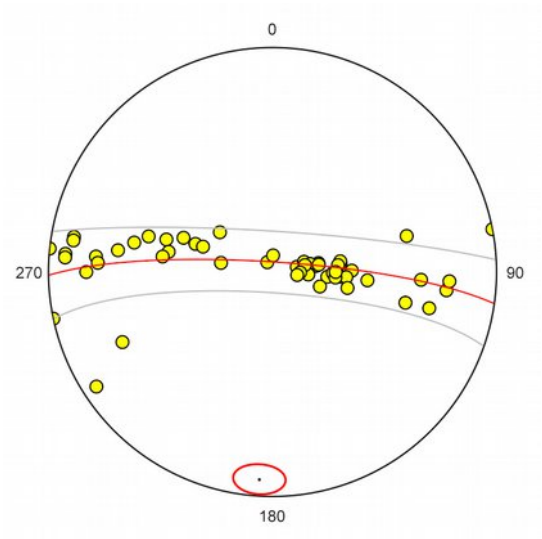

Figure 7.9 Schmidt plot of folded graywacke beds from Figure 4.14 with 95% circular confidence cones and small circle confidence rings. The best fit small circle is ($\boldsymbol{\lambda}$, ψ) = (183.63°, 8.09°, 85.95°) with 95% confidence on ($\boldsymbol{\lambda}$, ψ) estimated as (7.04°, 11.91°).

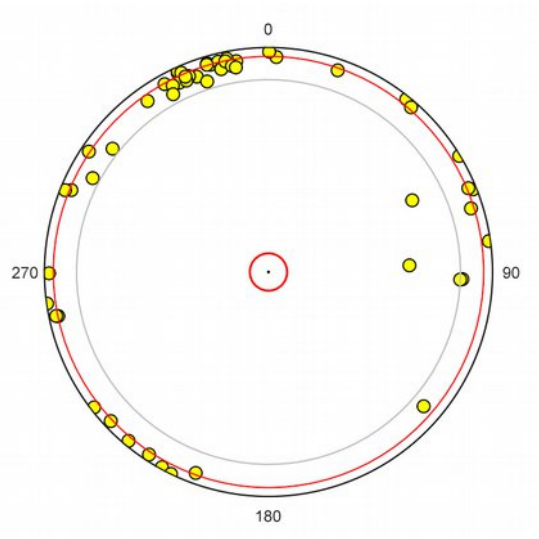

Figure 7.10 Plot as in Figure 7.8 rotated to the fitted small circle axis. Note that confidence rings on ψ include the plane normal to the axis.

Due to the long processing time required for the small circle fitting algorithm, bootstrap statistics are not calculated in the Log window unless either the bootstrap Cone, Hull, or Replicates options are on (e.g, Figures 7.4 to 7.11). Increasing the number of replicates can cause the calculation to take a very long time, depending on your processor speed, 1000 resamples should only take a few seconds however.

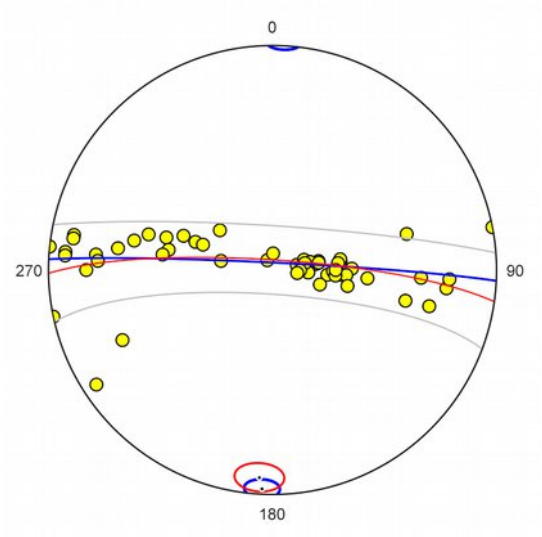

Figure 7.11 Plot as in Figure 7.9 with the minimum eigenvector, its pole, and 95% circular confidence region displayed (blue), the standard method for determining a cylindrical fold axis.

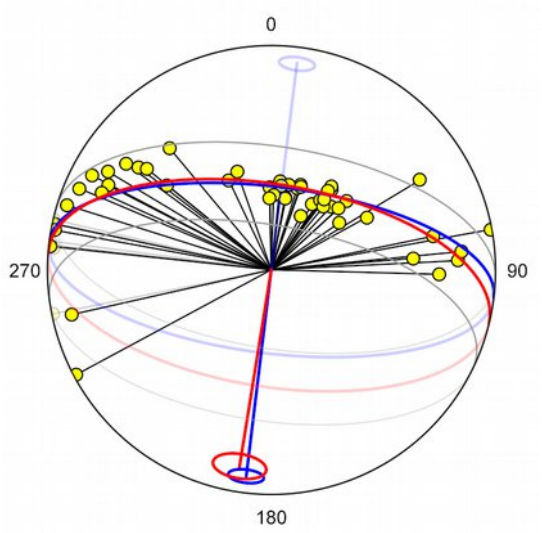

Figure 7.12 Plot as in Figure 11, but using lower hemisphere orthographic projection and visualization techniques discussed in Section 5.6.

7.5 *Tutorial 9 - Data Point Weighting*

As noted in Section 2.4, individual data points can be weighted. While this applies to all calculations (except bootstrap confidence cones), including circular plots and kinematic analysis, the fitting of a small circle gives a good visualization of the effect of weighting a data point.

Make the Weight column visible by using the View Data Columns command if necessary. Select Small Circle in the Preferences dialog Maxima pane, and enter the following data. The Schmidt plot should appear as Figure 7.13.

ID	Trend	Plunge	Weight
1	30	60	
2	60	20	
3	120	60	
4	180	60	
5	270	60	

Table 7.2 Example data to illustrate data point weighting.

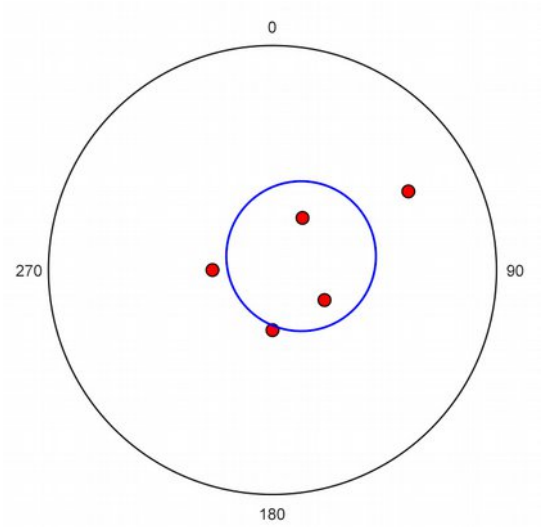

Figure 7.13 Schmidt plot of data from Table 7.2 with fitted small circle to illustrate data point weighting.

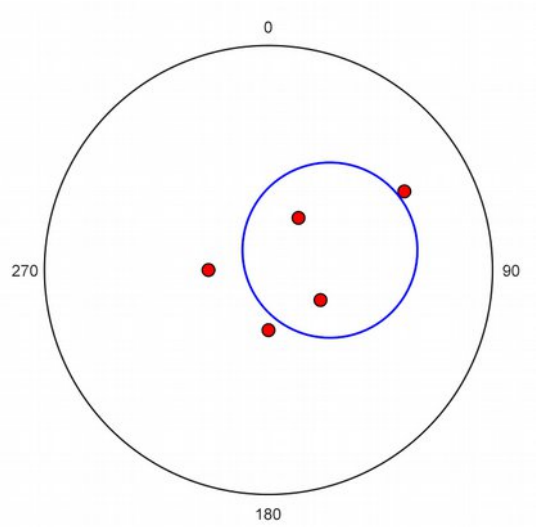

Figure 7.14 Data as in Figure 7.6 with a weight of 5 entered for data point 2. Data point 2 now counts the same as 5 points, shifting the small circle towards it.

Enter 5 in the Weight column for data point 2, this data point now counts the same as 5 points, shifting the small circle towards it (Figure 7.14). Finally, enter 0 for the weight of data point 2, it is now not included in the calculation and has no effect as shown in Figure 7.15.

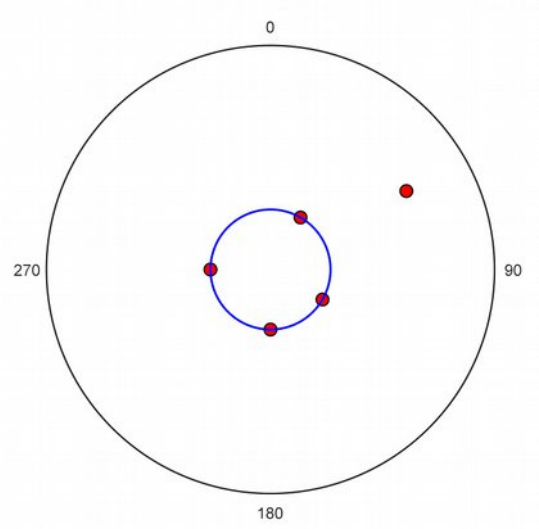

Figure 7.15 Example data as in Figure 7.6 with a weight of 0 entered for data point 2. Data point 2 is now discounted, with no effect on the small circle calculation.

8. Kinematic Analysis

8.1 Introduction

Some data comprise planes that contain lines. These data may indicate movement along faults or shear directions, such as striae on slickenside surfaces. Other data, such as hinge lines in fold axial planes, or current directions in bedding planes, also have that characteristic, however this section deals only with the kinematic analysis of faults and shear zones. Numerous methods exist for the determination of stresses, strains, or displacements from populations of faults, Orient implements a kinematic analysis based on *M-plane*, or *movement plane*, geometry (Angelier, 1979; Marshak and Mitra, 1988; Twiss and Unruh, 1998; Marrett and Allmendinger, 1990; Twiss and Moores, 2007).

8.2 Entering Line-Plane Pairs

Kinematic analysis requires entering plane-line pairs, as each data point includes both a plane, such as a fault plane, and a directed line contained in that plane, such as a fault striation. Data is commonly entered as *strike, dip, trend, plunge*, however it is also possible to enter *strike, dip* and just one of the three values *trend, plunge,* or *rake*. and have Orient calculate the other values. Given the strike and dip of a plane, only a single additional angle is required to completely specify the orientation of the contained line.

Three additional columns are provided for kinematic analysis, Sense, Rake, and Error, and an additional command, Calculate Lines, is provided to calculate missing values, or to recalculate existing values exactly. Use the View Data Columns command to set these columns visible. The Sense column is used to indicate if the fault has a normal or reverse component (it is also possible to enter negative values for the plunge of reverse faults, and add 180° to the trend). The Rake column is for the positive (clockwise) angle between the strike of the plane and the striation direction, this will be from 0° to 180°, and is positive for faults with a normal component, and negative for faults with a reverse component.

The Error column is read only, and contains the calculated angular error between the plane and its contained line. A common problem with field data is that it is over constrained, only three angles are required for plane-line pairs, while four are often measured. The Calculate Line command is used to calculate, or recalculate line-plane pairs.

Given the orientation of a plane and one of the angles *trend* (or other horizontal angle), *plunge* (or other vertical angle), or *rake* (or pitch), the other two can be calculated using the Calculate Line command. The resulting line-plane pair will have a 0° angular mismatch error.

8.3 Orthonomalization

If both the plane and line have been measured directly, then the line-plane pair is over-constrained with a mismatch error (Davis et al., 2015). In this case the *Error* column will contain a non-zero angular value. The Calculate Line command has two options to recalculate the line-plane pair and remove the angular error. The Projection option recalculates the line as its projection on the plane. The Orthonormalize option recalculates *both* the line and the plane to create a normalized orthogonal frame.

Given over-constrained data, the selection of the Calculate Line option requires judgement of the source of measurement error. The angular errors should be checked first, any data point with a large

error should be discarded or corrected. It is common that the plane is easier to measure accurately than the contained line, if so, the Projection option is the best. The Orthonormalize option will modify both, and is better if no assumption is made about the source of error. Alternatively, the line-plane data can be corrected using the trend, plunge, or rake, possibly taking into account the dip. Note that potential measurement errors depend on the orientation of the line or plane, for example, the likely error in the strike of a plane increases with decreasing dip (Ragan, 2009).

8.4 M-Planes

Each data point for kinematic analysis must include the orientation of a kinematic plane, such as the strike and dip of a fault plane, and the orientation of a movement direction in that plane, such as the trend and plunge of a fault striation, signifying the motion of the hanging wall (upper) block. Upward directed vectors, with a reverse component, can be entered using negative plunges, or by entering Reverse (r) in the Sense column. Note that this is equivalent to adding 180° to the trend, and multiplying the plunge by -1. Normal (n) may also be entered into the Sense column, but has no effect.

Although the term *fault* is used here, the kinematic analysis can be applied to shear zones if the displacement directions can be determined. As the slip lineation lies within the fault plane, the displacement direction must lie in the plane containing the lineation and the pole to the fault, this plane is the M-plane. Figure 8.1 shows the geometric relationships with the M-plane shown in gray.

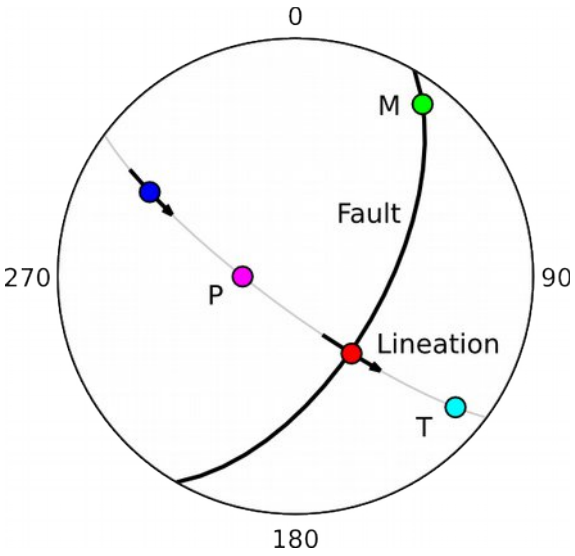

Figure 8.1 Schmidt plot of a normal fault, with a slip lineation (red), pole to the fault (blue) and the M-axis, or movement axis, (green), the M-plane is shown in gray. Directions P and T bisect the angle between the pole and slip line. Arrows are *tangent lines* that show the displacement sense of the *hanging wall* with respect to the footwall.

Two additional kinematic axes can be defined within the M-plane, at ±45° from the lineation (Figure 8.1). These are commonly referred to to as the P-axis and T-axis, terms derived from first motion studies in seismology, however they should not be confused with *stress* axes. Rather P is an incremental *shortening* axis, and T is an *extension* axis.

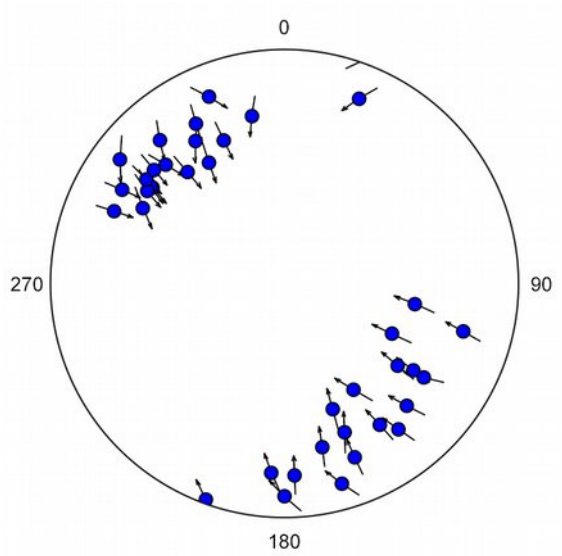

Figure 8.2 A lower hemisphere equal-area *slip-linear,* or *pole tangent line,* diagram of a population of 38 Neogene normal faults from central Crete, Greece. The arrows through the fault pole projections show the displacement sense of the *hanging wall* with respect to the footwall (data from Angelier, 1979).

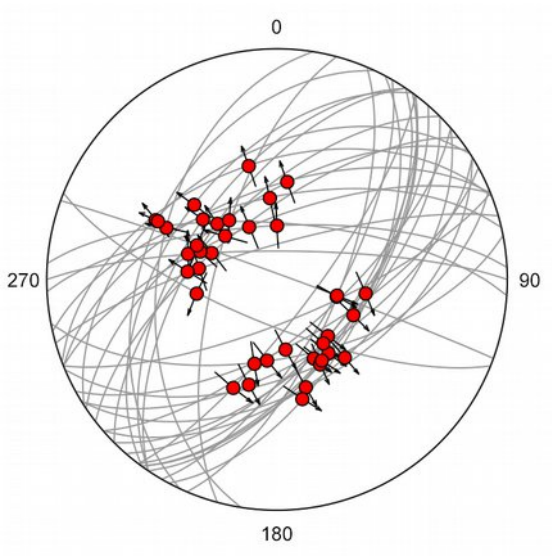

Figure 8.3 A lower hemisphere equal-area *slip tangent line* diagram of the data shown in Figure 8.2. The arrows through the slip lineation projections show the displacement sense of the *hanging wall* with respect to the footwall (data from Angelier, 1979).

The arrows drawn though the lineation and the fault normal are *tangent lines*, directed lines tangent to a projected point on a sphere. In Figure 8.1 tangent lines are drawn through the lineation and the fault pole projections to show the placement sense of the *hanging wall* with respect to the *footwall*. They can be viewed as instantaneous rotation vectors about the M-axis. The term *slip-linear* has been used for a tangent line drawn through the fault pole using this reference frame (Marshak and Mitra, 1988). Figure 8.2 shows a slip-linear diagram of a population of 38 Neogene normal faults from central Crete, Greece (data from Angelier, 1979).

The term *tangent-lineation* has been used for the tangent line drawn through the fault pole showing the placement sense of the *footwall* with respect to the *hanging wall* (Twiss and Unruh, 1998; Twiss and Moores, 2007). However, the reference frame used in Figures 8.1 and 8.2 for slip-linears is compatible with the definition of fault slip as a displacement vector of the hanging wall with respect to the footwall, and has priority, so is the default setting. Since Orient offers both conventions, the term *pole tangent line* (tangent line through the projected fault pole) is used to include both *slip-linear* and *tangent-lineation* reference frames.

A second type of tangent line can be drawn through the slip lineation within in the M-plane. This is referred to here as a *slip tangent line* (tangent line through the projected slip line), drawn though the projected lineation towards, or away from, the pole to the fault (Figure 8.1). This contains the same information as a pole tangent line. Note that many spherical projections of fault data in the literature show ticks or arrows parallel to the *trend* of the slip lineation, which is not the same.

8.5 Moment Tensors

The P and T axes (Figure 8.1) indicate shortening and extension axes respectively, and fault kinematic analysis can therefore done by examining populations of P and T axes independently using moment tensors (Marrett and Allmendinger, 1990). These tensors are orientation matrixes discussed in Sections 4.7. When fault data is entered, normally a strike and dip for a fault plane, and a trend and plunge for a slip lineation, Orient automatically generates M-planes, P-axes, and T-axes. An extension is added to the data type indicate each of the five data elements (Table 8.1).

Data Type Extension	Data Element
.S	Plane, fault, slickenside, or shear plane
.L	Line, slip direction, slickenline, or shear direction
.M	M movement plane
.P	P shortening axis
.T	T extension axis

Table 8.1 Data type extensions automatically generated for kinematic data.

Each of these extended data types can be plotted and analyzed independently. For kinematic analysis the P and T axes are contoured (Figures 8.5 and 8.6; Section 4.9), and their maximum values and scatter determined by eigenvector analysis (Section 4.7), and for the construction of *beachball plots* (Figure 8.7).

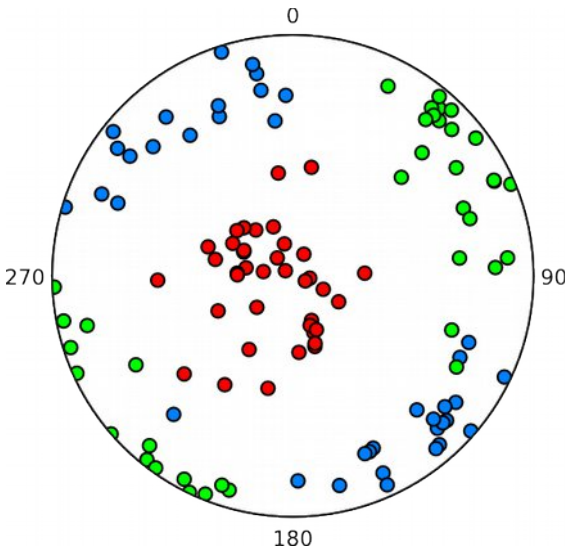

Figure 8.4 Lower hemisphere equal-area projection of poles to M-planes (green), P shortening axes (red), and T extension axes (blue) for data in Figure 5.2.

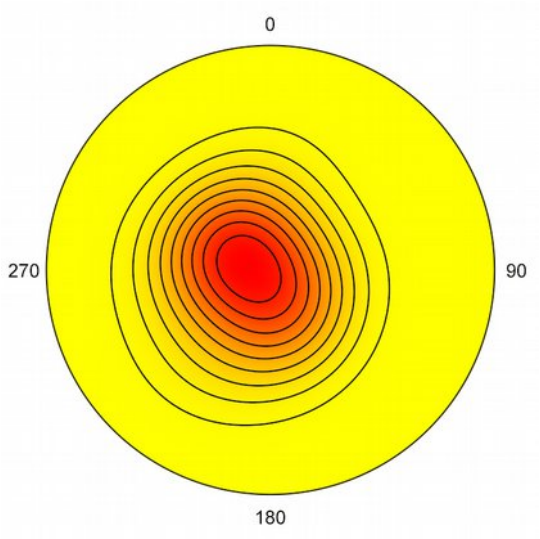

Figure 8.5 Schmidt plot with modified Kamb contours of the fault data from Figure 5.3 with 10% density contours on the P shortening axes.

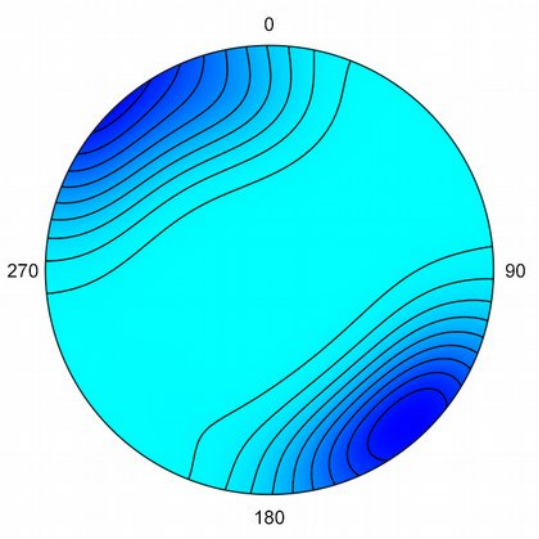

Figure 8.6 Projection as in Figure 8.4 with contours on the T extension axes.

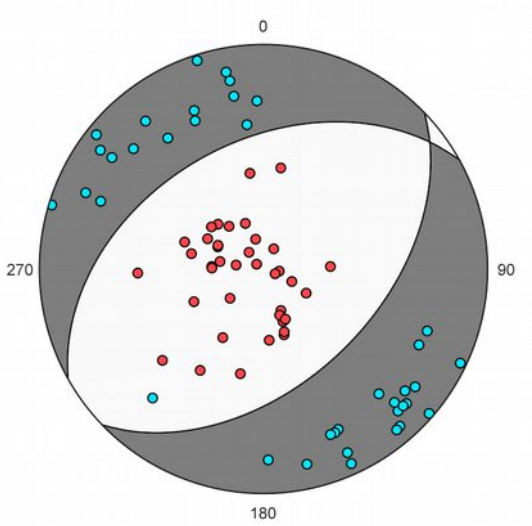

Figure 8.7 Lower hemisphere equal-area beachball plot showing the P shortening and T extension quadrants using the data shown in Figure 8.3.

8.6 *Tutorial 10 – Kinematic Analysis*

Open the file Angelier 1979 from the Example Data folder (any of the csv, tsv. ods, or xlsx versions) in Orient, and click on the *Spherical Projection* icon. If no settings have been previously modified the projection will look as in Figure 8.8. The Help Restore Defaults command can be used to reset the preferences if desired.

To remove the Schmidt net from the background, click on the Preferences icon, and locate the Net pane under the Spherical Projection Settings. Uncheck both *Axes* and *Net*. Next, in the Labels pane, change the Increment to -90, the Offset to 14, and the Size to 12.

Next, go to the *Symbols* pane. Note that there are 5 data types displayed in the Data Type pulldown list. Select SL.P, check Visible, then select SL.T and check Visible. At this point all data type elements should be displayed with a symbol as in Figure 8.9.

The first step is to prepare a *pole tangent line*, or slip-linear, plot. In the Symbols pane uncheck Visible for all the elements *except* SL.S so only the poles to the fault planes are displayed. Now go to the Kinematics pane and check Tangent Lines. The resulting plot is shown in Figure 8.2.

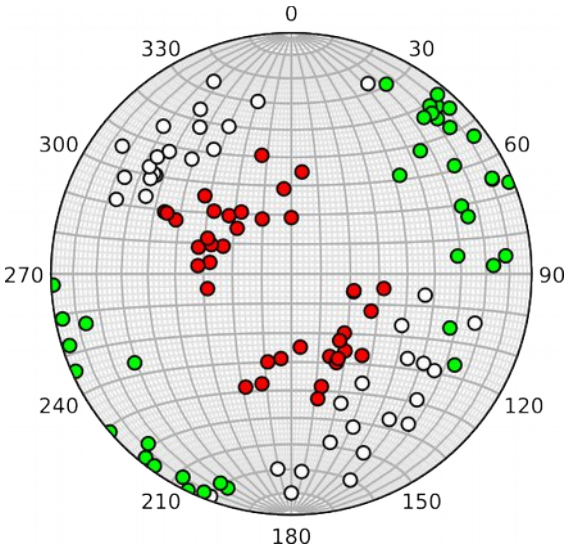

Figure 8.8 Lower hemisphere equal-area scatter plot of fault data in Figure 5.2 showing fault normals (white), slip lines (red), and M-planes (green), with Schmidt net.

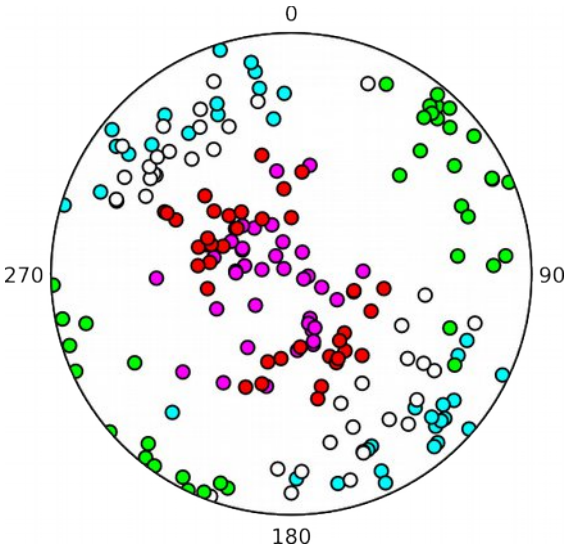

Figure 8.9 Projection as in Figure 5.7 after turning off display of the Schmidt net, and showing the P shortening (magenta) and T extension (cyan) axes.

Next prepare modified Kamb contour plots of the P shortening and T extension axes. Uncheck Tangent Lines in the Kinematics pane, and open the Symbols pane. Uncheck Visible for SL.S. For SL.P, check the following: Visible, Symbol, Contour, and Gradient. Modify the defaults as follows. Set the Symbol Fill Color to white, and the Symbol Size to 6. Click on the gradient color picker, and select YR (yellow red) from Preset. Next go to the Contours pane and set Levels to 5 to give modified Kamb contours at 20% density. The resulting plot is shown in Figures 8.10.

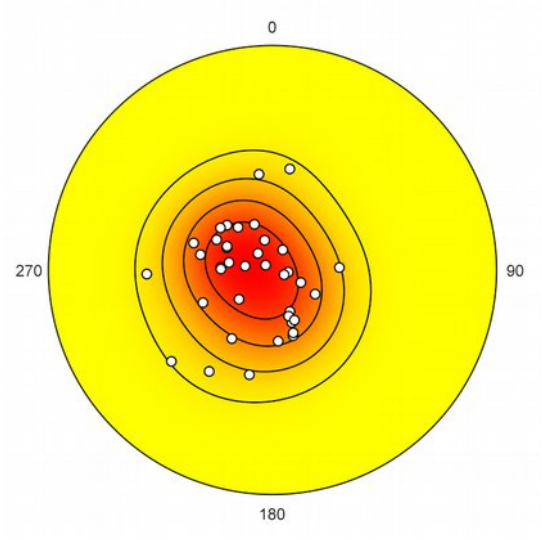

Figure 8.10 Lower hemisphere equal-area modified Kamb contour plot of the fault data from Figure 5.2 with 20% density contours of the P shortening axes.

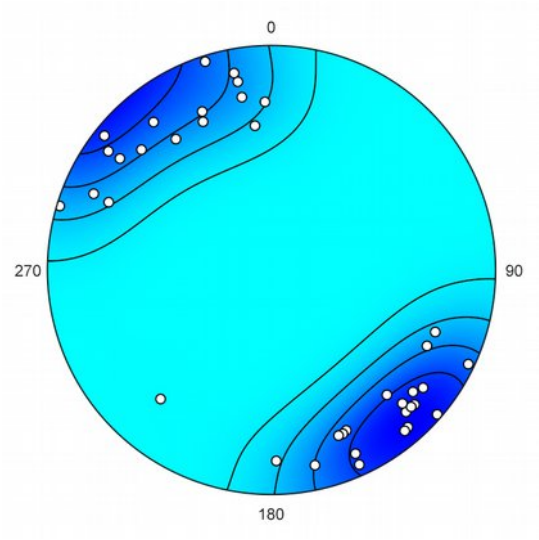

Figure 8.11 Projection as in Figure 5.10 with contours of the T extension axes.

To prepare a contour plot for the T extension data, uncheck Visible for SL.P. For SL.T, check: Visible, Symbol, Contour, and Gradient. Set the Symbol Fill Color to white, and the Symbol Size to 6. Click on the gradient color picker, and select CB (cyan blue) from Preset. The resulting plot is shown in Figure 8.11.

Finally, to prepare a beachball plot, uncheck the SL.T options for Contour and Gradient, and set the Symbol Fill Color to cyan. For SL.P, check *Visible*, uncheck Contour and Gradient, and set the Symbol Fill Color to red. In the Kinematics pane check Beachball. The resulting plot is shown in Figure 8.7.

8.7 Confidence Levels, Synoptic Plots, and Weighting

This section explains the use of additional options, including determining confidence cones, using the same example fault plane data set as in previous sections. Following Section 8.3, note that the line-plane data should be adjusted to insure that each line-plane pair form an orthogonal frame. This is easily done by selecting all the data with Edit Select All, and then Data Calculate Line with the Orthonormalize option. Other options are discussed fully in Section 8.3.

It may be desirable to produce a contoured summary, or *synoptic*, plot of both the P and T axes. Figure 8.12 is a such a diagram with combined contours as displayed in Figures 8.10 and 8.11. Both the P and T axes have contours and gradients (Symbols Contour and Symbols Gradient selected), with the Contours Fill Contours option selected, and Gradient set to Gray. Contours Levels is set to 5 to give contours at 20%.

Note that the P gradient obscures the T gradient because both are opaque, and the P gradient bitmap is on top of the T gradient bitmap. To fix this, click on the P Gradient Picker, and set the opacity to 50%. The result is an overlay as shown in Figure 8.13. The use of overlays can be similarly applied to any plot with multiple data types, such as bedding and cleavage.

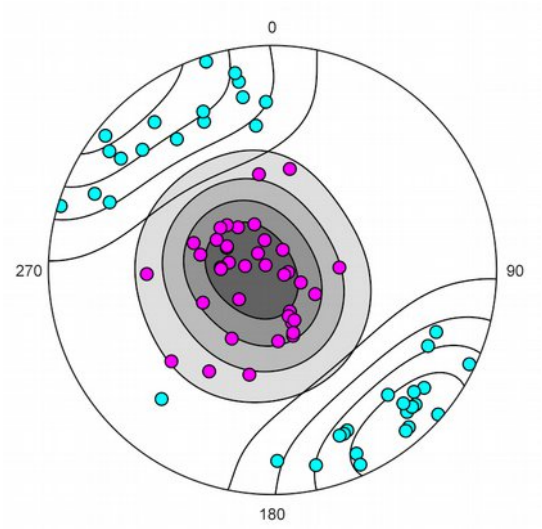

Figure 8.12 Schmidt plot of P and T axes as in Figure 8.9 with modified Kamb contours for each at 20%. The *Gradient* option is selected for each, but only one is displayed.

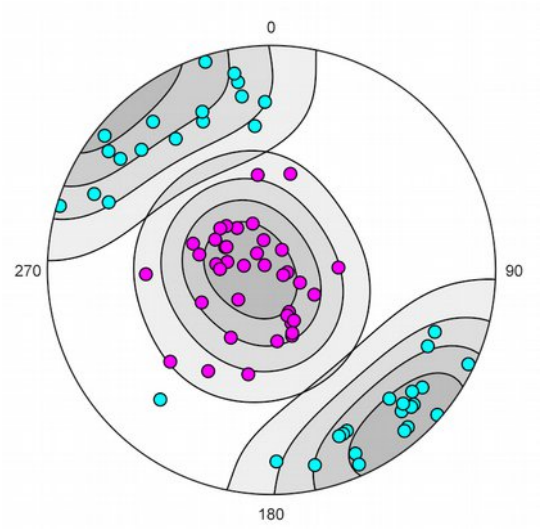

Figure 8.13 Schmidt plot as in Figure 8.12 with the P contour gradient transparency set to 50%, to create a transparent overlay.

The bootstrapping technique discussed in Section 6.3 can be applied to kinematic analysis to derive confidence intervals about the P and T axis. Figure 8.14 shows the confidence intervals as elliptical cones about both P and T axes, and Figure 8.15 shows 5000 means of the bootstrap replicants used to calculate the cones. The confidence values are displayed in the Log window after running the Data Statistics command. Locate the maximum eigenvectors for the P and T data elements in the log, these give the 95% confidence radii for the P axis as 7.59°, 6.32°, and for the T axis as 9.87°, 7.99° (Figure 8.14; these will vary randomly a small amount). Points defining endpoints of the long and short ellipse axes are also given.

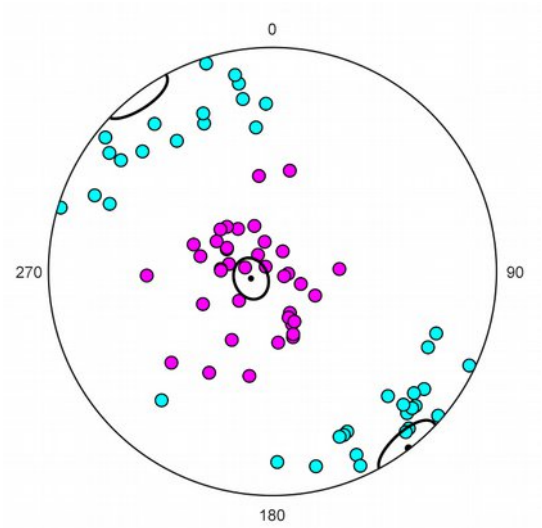

Figure 8.14 Schmidt plot as in Figure 8.12 with 95% confidence cones about the P and T axes.

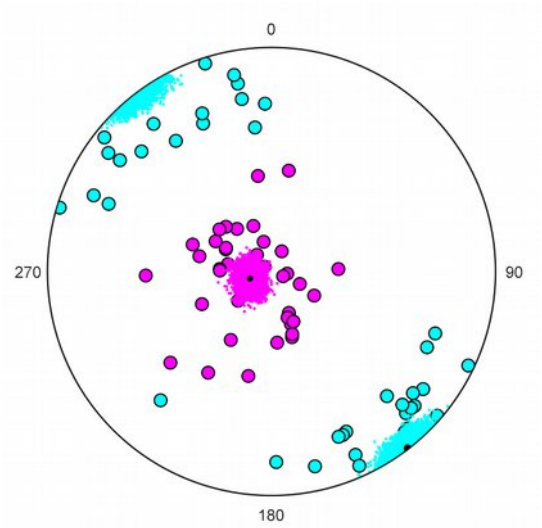

Figure 8.15 Schmidt plot as in Figure 8.14 displaying the means of 5000 bootstrap replicates used to calculate the confidence cones.

Finally, as discussed in Sections 2.4 and 7.4, individual data points can be *weighted* by entering a positive value in the Weight column. The default weight is 1, a weight of 0 will discount the data point. In kinematic analysis it may be desirable to weight data points, for example by using a weight related to the estimated area of a fault.

To see the effect of data weighting on kinematic analysis, make the Weight column visible using the *View Data Columns* command if necessary, then use the Angelier 1979 data set to create a plot such as shown in Figure 8.13. Enter weight values, such as 0, 2, or 10 for some of the line-plane pairs to see the effect on the analysis.

9. Orientation Plots

9.1 Introduction

The *orientation matrix*, orientation tensor, or scatter matrix (Fisher, Lewis, and Embleton, 1987; Mardia and Jupp, 2000), can be interpreted as a *moment tensor* associated with the spherical distribution of *axial* direction data, by regarding the intersection points of each axis with the sphere as unit masses. Such a weighted sphere would have three perpendicular moment axes. Section 4.3 showed how the eigenvectors of this tensor can be used to determine the maximum, intermediate, and minimum directions. The eigenvectors, however, have relative magnitudes, the *eigenvalues*, which are treated in this chapter. Note, for example, that if are three eigenvalues are all equal, there is no preferred direction and the measurements are randomly, or uniformly, distributed.

9.2 Triangular Orientation Plot

A triangular eigenvalue plot (Point Girdle Random) is particularly useful when a summary diagram is required of numerous data sets. On the triangular plot a single point summarizes the type of directional data distribution among point (or cluster), girdle, and random (or uniform) distributions. The plot is also used in map domain analysis, where domains are defined in the *Orientation Map* portion of the program, by maximizing the total cylindricity index.

Given the orientation matrix eigenvectors $\boldsymbol{\varepsilon}_1$, $\boldsymbol{\varepsilon}_2$, and $\boldsymbol{\varepsilon}_3$ for n data points, where the magnitudes $\varepsilon_1 \geq \varepsilon_2 \geq \varepsilon_3$, the following are defined (Vollmer 1989):

Point	$P = (\varepsilon_1 - \varepsilon_2)/n$
Girdle	$G = 2(\varepsilon_2 - \varepsilon_3)/n$
Random	$R = 3\varepsilon_3/n$
Cylindricity	$C = P + G$

these have the property that:

$$P + G + R = 1$$

and form the basis of the triangular plot. Cylindrical data sets plot near the top of the graph, along the P-G join, point distributions plot near the upper left (P), girdle distributions plot near the upper right (G), and random or uniformly distributed data will plot near the bottom of the graph (R). Figure 9.1 is a plot of bedding plane poles from a cylindrical fold in Ordovician graywackes (Vollmer, 1981), and Figure 9.2 is the corresponding triangular plot graph. These indicate a well defined girdle with a distinct maximum.

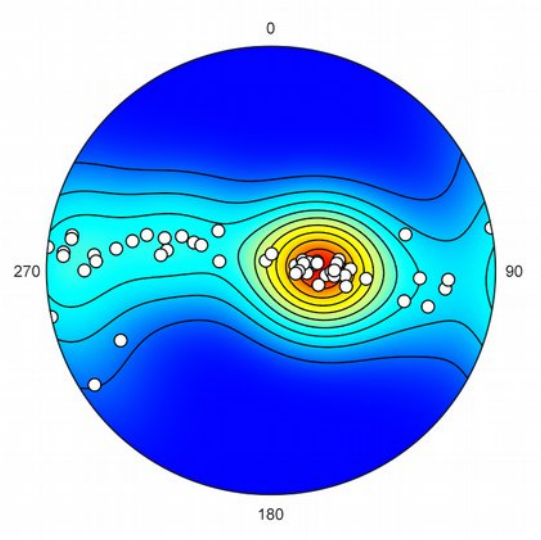

Figure 9.1 Schmidt plot with modified Kamb contours of poles to bedding from a fold in graywackes (data from Vollmer, 1981).

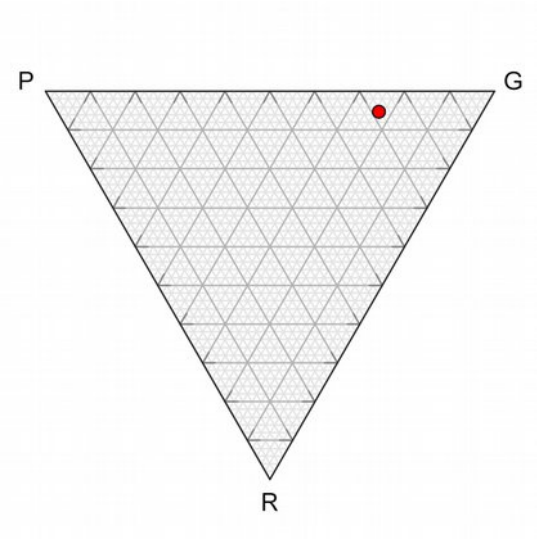

Figure 9.2 Triangular orientation plot of data shown in Figure 9.1.

A contour plot of ice fabric c-axes (Kamb, 1959) is shown in Figure 9.3, which shows a much more scattered distribution, and plots nearer to the bottom of the plot (Figure 9.4). Finally a plot of fold axes associated with the bedding data in Figure 4.14 is shown in Figure 9.5, and the associated triangular plot in Figure 9.6 showing a strong point cluster.

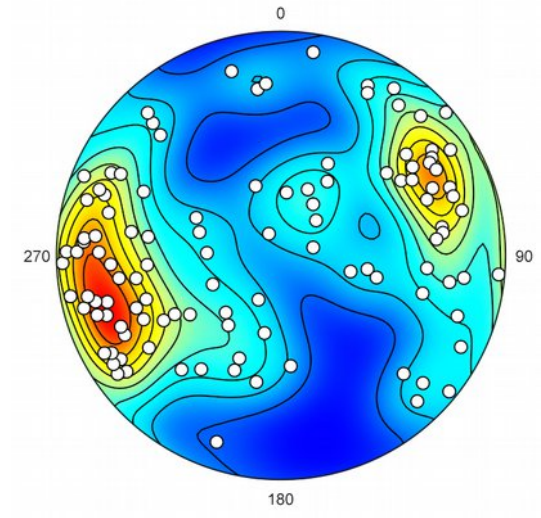

Figure 9.3 Schmidt plot with modified Kamb contours of ice c-axes (data from Kamb, 1959).

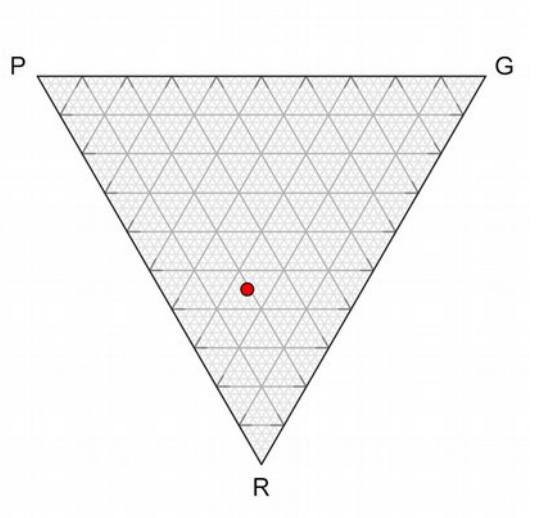

Figure 9.4 Triangular orientation plot of data shown in Figure 9.3.

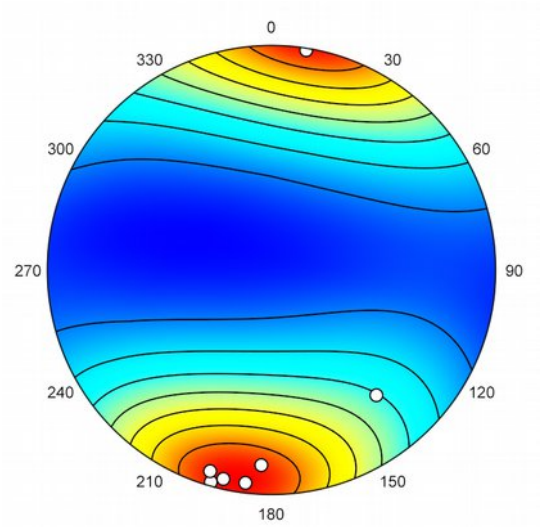

Figure 9.5 Schmidt plot with modified Kamb contours of minor fold axes associated with the folded bedding data in Figure 4.12.

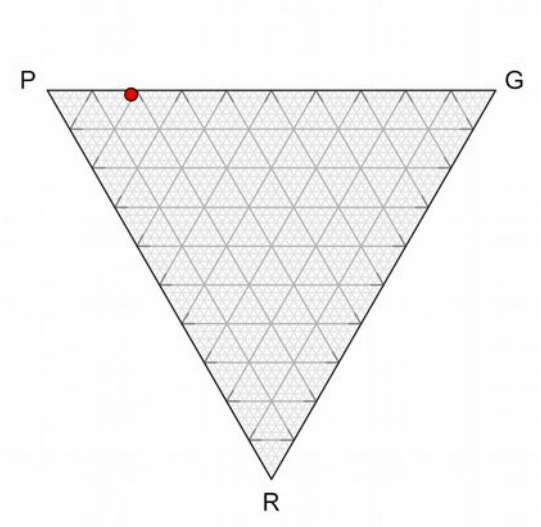

Figure 9.6 Triangular orientation plot of fold axis data in Figure 9.5 showing strong point cluster.

10. Cluster Analysis

10.1 Introduction

Many directional data samples are multimodal, and, while contouring (Section 4.9) may be sufficient to locate likely modes (e.g., Schmidt, 1925; Section 4.9), it may be desirable to use numerical techniques to partition the sample into discrete clusters (e.g., Press et al., 2007). One application is from geological fracture analysis, in which the orientations of fracture or joint planes are measured, with no basis other than orientation to use for subdividing the sample. This chapter discusses methods to attempt to partition such multimodal samples into clusters or *cluster domains*.

Visual cluster analysis of directional data began with the work of Schmidt (1925), who used contouring to identify modes, or deviations from uniformity. Shanley and Mahtab (1976) used a Schmidt projection based counting method to identify clusters. Klose et al. (2005) give a summary of other work, and present a numerical minimization method. The approach used here differs significantly from that of Klose et al. (2005), however similarly attempts to locate a solution that minimizes residuals of a measure of distance from the cluster centers (centroids). The present method allows weighting of data points, and is implemented for vector, axis, and girdle distributions (Vollmer, in preparation; see Yamaji and Sati, 2011, for a related method).

The method requires selecting the number of clusters, the *cluster count*, from $k = 2$ to 9. This will be based on user expertise, either through theoretical expectation, or by examination of a contour plot. Minimization may not converge to a unique solution for distributions that do not have distinct modes, or where the number of modes is less than the input cluster count. The method selected, *Axis*, *Vector*, or *Girdle* controls the minimization procedure. Data display for symbols and maxima should be selected to correspond to the method, and set as either directed or undirected.

10.2 Axis Cluster Partitioning

Figure 10.1 is a Schmidt plot of ice crystallographic data as in Figure 4.17, after cluster partitioning with two clusters. The two modes initially identified by contouring are clearly selected by the partitioning method, although due to asymmetry, the axes are not precisely aligned with the contoured maxima.

The clusters can be visualized more clearly by rotating the projections to the maximum eigenvectors of the two cluster domains. Figure 10.2 shows the data rotated to the maximum of cluster domain 1 (yellow symbols), and Figure 10.3 shows the data rotated to the maximum of cluster domain 2 (green symbols). Two distinct maxima are indicated by contouring the cluster domains, and by bootstrap confidence cones. Figure 10.4 is a triangular orientation plot summarizing the change in fabric type following partitioning, with the two domains plotting closer to the point, or cluster, vertex than the total data set (red symbol).

The total data set maximum eigenvector (red symbols in Figures 10.4 and 6.5) as trend, plunge, 95% confidence is (256.52°, 8.74°, 13.63°), cluster domain 1 (yellow in Figure 10.1) is (58.95°, 36.91°, 10.19°), and cluster domain 2 (green in Figure 10.1) is (261.17°, 28.23°, 8.98°).

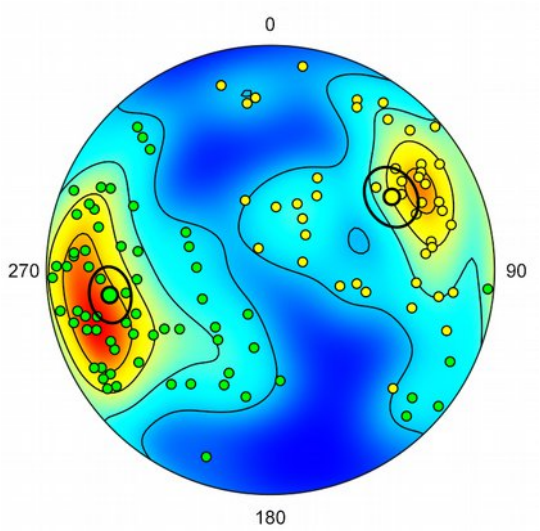

Figure 10.1 Schmidt plot of ice crystallographic data as in Figure 4.17, after cluster partitioning with two clusters. 20% modified Kamb contours on full data set, and 95% symmetric confidence intervals on the two cluster axes.

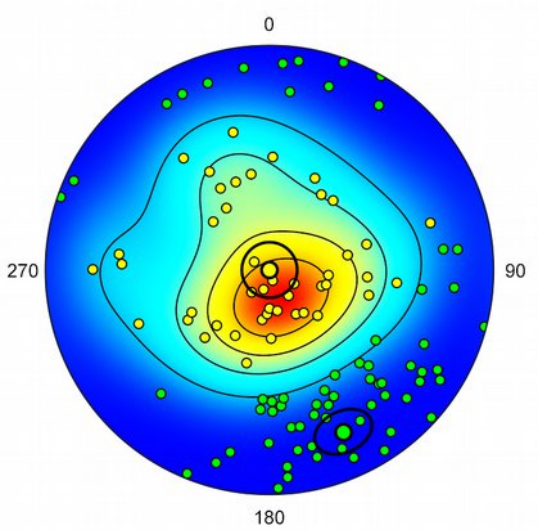

Figure 10.2 Plot as in Figure 10.1, rotated to the maximum of cluster domain 1, with contours on cluster domain 1.

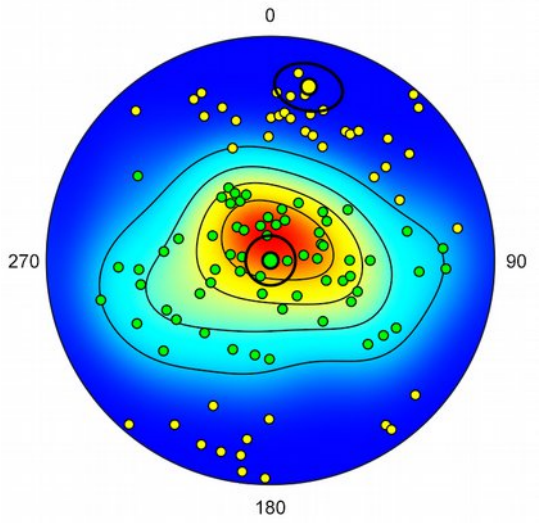

Figure 10.3 Plot as in Figure 10.1 rotated to the maximum of cluster domain 2, with contours on cluster domain 2.

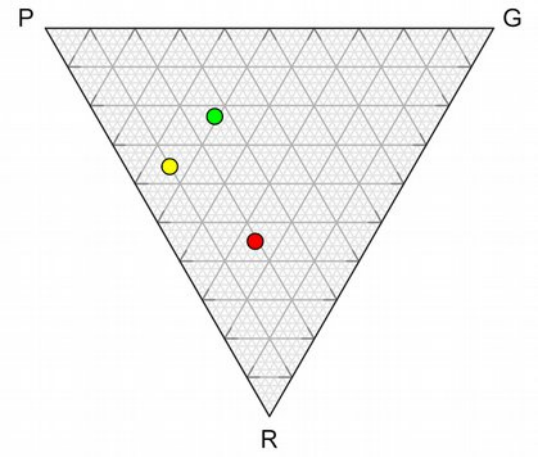

Figure 10.4 Triangular orientation plot, showing the full data set (red symbol), cluster domain 1 (yellow), and domain 2 (green). Note that the axis domain clusters plot closer to the point, or cluster, vertex.

Figure 10.5 illustrates a similar analysis on the folded graywacke bedding data displayed in Figure 4.14. In this case there is a reasonable expectation to find two modes, corresponding to the two the fold limbs. Figure 10.6 shows the data rotated to the maximum of cluster domain 1, and Figure 10.7 shows the data rotated to the maximum of cluster domain 2. As expected, two distinct maxima are indicated

by contouring the cluster domains, and by the confidence cones. Figure 10.8 is a triangular orientation plot summarizing the change in fabric type following partitioning. Note again, that the cluster domains plot closer to the point, or cluster, vertex than the full data set.

The axis cluster partitioning gives the two clusters (estimated fold limbs) as strike, dip, 95% confidence equal to (4.10°, 58.79°, 11.84°) for cluster domain 1 (yellow symbols in Figure 10.5), and (180.05°, 23.54°, 6.06°) for cluster domain 2 (green symbols in Figure 10.5).

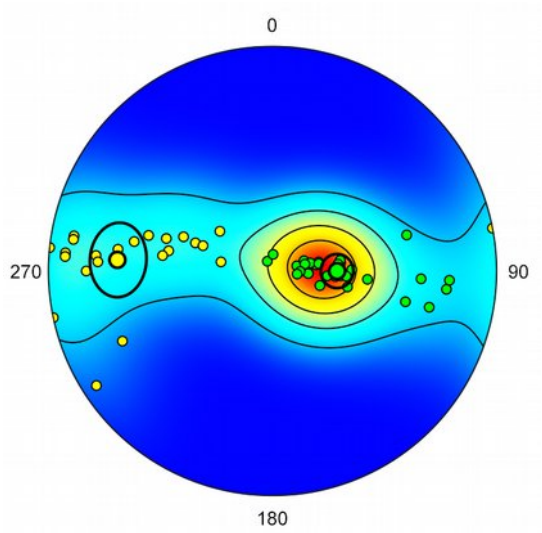

Figure 10. 5 Schmidt plot of folded graywacke bedding data as in Figure 4.14, with 20% modified Kamb contours on the full data set, and 95% symmetrical confidence intervals on the two cluster axes.

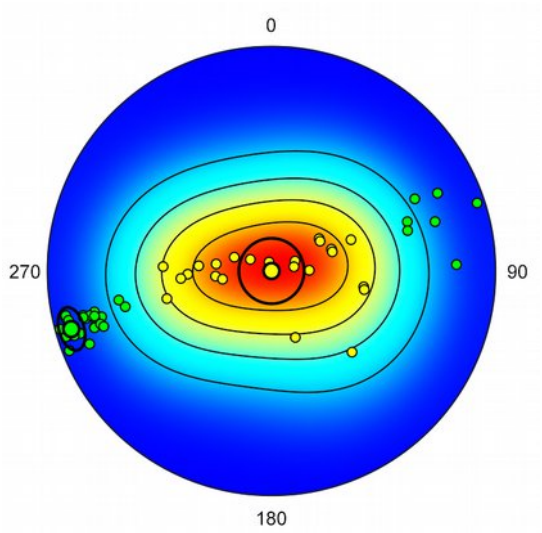

Figure 10.6 Plot as in Figure 10.5 rotated to cluster domain 1 maximum, with contours on cluster domain 1.

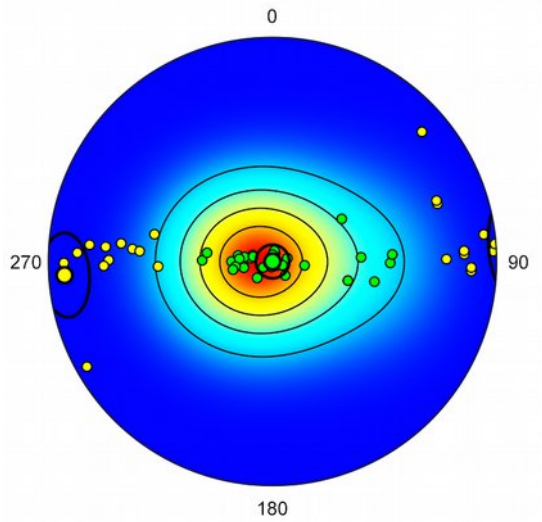

Figure 10.7 Plot as in Figure 10.5 rotated to domain 2 cluster axis, with contours on cluster domain 2.

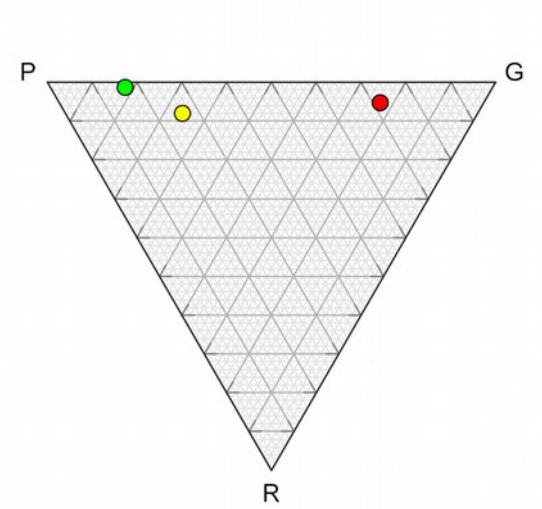

Figure 10. 8 Triangular orientation plot, with full data set (red symbol), cluster domain 1 (yellow), and domain 2 (green). Note that the domains (estimated fold axes) plot closer to the point, or cluster, vertex than the full data set.

10.3 Vector Cluster Partitioning

An analysis similar to axis cluster partitioning can be done on vector data. Figure 10.9 is a Schmidt plot of the magnetic remanence data from Figure 1.3, after vector cluster partitioning. Data ploted on the upper hemisphere are semi-transparent. Figure 10.10 shows the data rotated to the vector mean of cluster domain 1, and Figure 10.11 shows the data rotated to the vector mean of cluster domain 2.

The two clusters given as [trend, plunge, 95% confidence] are (224.39°, 42.41°, 15.63°) for cluster domain 1 (yellow symbols in Figure 10.9), and (333.87, -23.13, 7.37) for cluster domain 2 (green symbols in Figure 10.9).

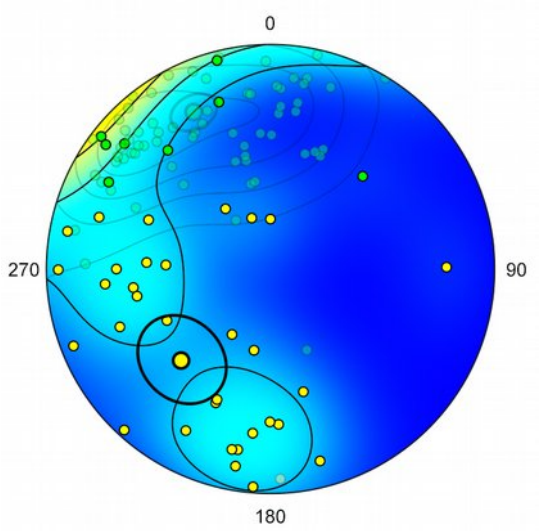

Figure 10.9 Schmidt plot of magnetic remanence vectors as in Figure 1.3, after vector cluster partitioning. 20% modified Kamb contours on the full data set, and 95% symmetric confidence intervals on the cluster domain vector means. Symbols on upper hemisphere are 30% transparent.

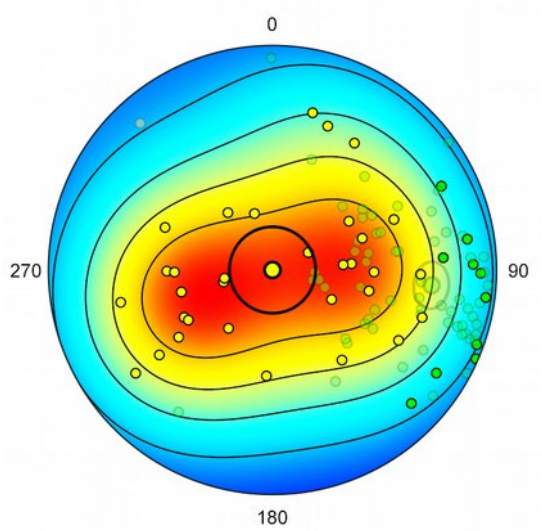

Figure 10.10 Plot as in Figure 10.9 rotated to the vector mean of cluster domain 1 (yellow symbols), with contours on cluster domain 1.

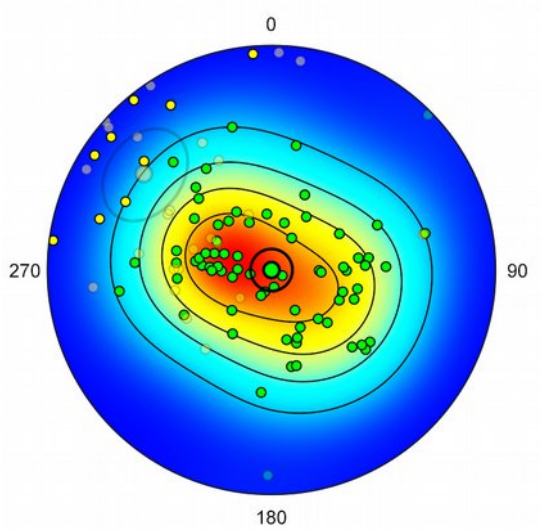

Figure 10.11 Plot as in Figure 10.9 rotated to the vector mean of cluster domain 2 (green symbols), with contours on cluster domain 1

10.4 Girdle Cluster Partitioning

This section concerns girdle cluster partitioning, where an attempt is made to partition more than one girdle distribution from a sample. A synthetic test example is shown in Figure 10.12, produced by combining the data from Figure 10.5 with the same data rotated 30° about the Z (vertical) axis . The best-fit great circles with confidence cones illustrate the effect of the partitioning. To more clearly visualize the partitioning, Figure 10.10 shows the data rotated to the maximum eigenvector of cluster domain 1, with contours on domain 1, and Figure 10.11 shows the data rotated to the maximum eigenvector of cluster domain 2, with contours on domain 2.

The minimum eigenvector (estimated cylindrical fold axis) of the original data as trend, plunge, 95% confidence was (182.76°, 2.69°, 4.70°) (Figure 6.7). The combined synthetic data after girdle cluster partitioning gives the domain 1 axis as (187.38°, 3.38°, 1.88°), and domain 2 axis as (153.83°, 2.45°, 4.29°). Rotating domain 2 by -30° about Z gives the (restored) axis (183.8° 2.5°, 4.29°). Note that the girdle cluster analysis has largely partitioned the combined data into the two original components, a complete restoration can not be expected. Finally, Figure 10.15 is a visualization of the cluster analysis results using methods discussed in Section 5.6.

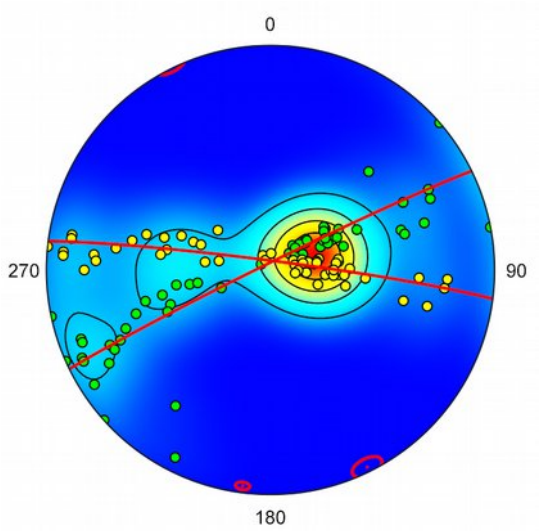

Figure 10.12 Girdle partitioning of synthetic data produced by combining the data from Figure 10.5 with the same data rotated 30° about Z. 20% modified Kamb contours on the full data set.

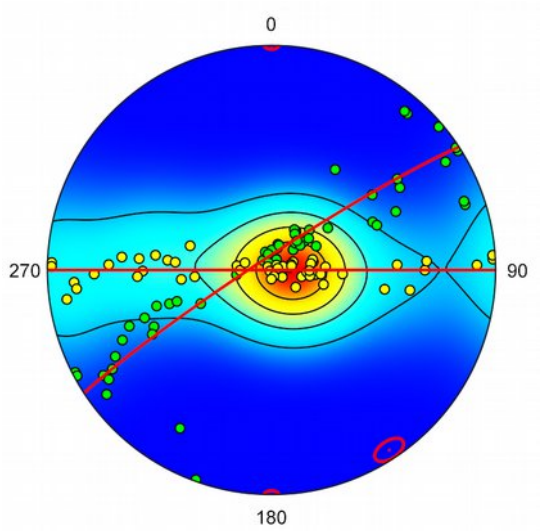

Figure 10.13 Plot as in Figure 10.12 rotated to the maximum eigenvector of girdle domain 1, with contours on domain 1.

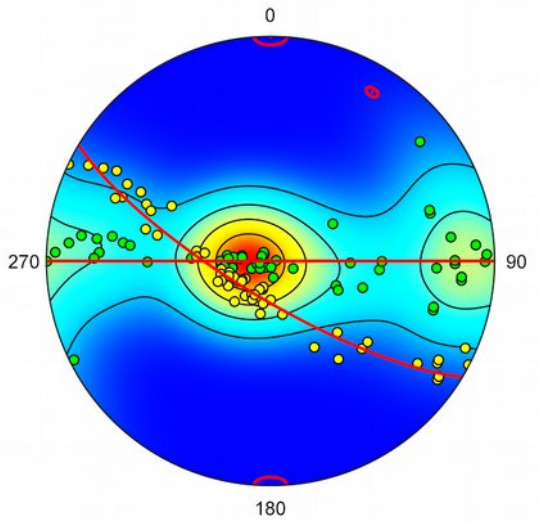

Figure 10.14 Plot as in Figure 10.12 rotated to the maximum eigenvector of girdle domain 2, with contours on domain 2.

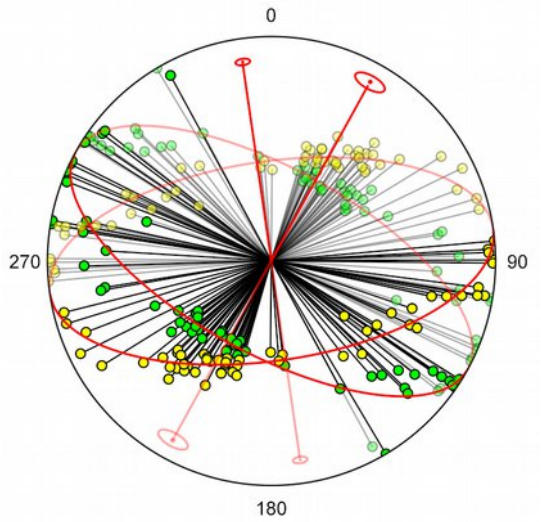

Figure 10.15 Plot as in Figure 10.12 using orthographic projection, rotation, and transparency as discussed in Section 5.6.

11. Orientation Maps

11.1 Introduction

Spherical projections aid in the analysis of the directional data, such as rock foliations, but they do not display their spacial distribution. Understanding the spacial relationships of directional data is often one of the primary goals of a geologist, particularly a structural geologist. A number of tools are provided in Orient to assist with spacial analysis. These include coordinate conversions, integration with mapping websites, and integration with Google Earth. Orient is designed to plot the spacial distributions of directional data, and has the capability of calculating orientation data fields that can be used to study regional tends and to do structural domain analysis. For example, a common problem in mapping areas of complex geological structure is to identify domains of cylindrical folding. Orient provides unique capabilities to automatically search for such domains (Vollmer, 1990).

11.2 UTM, Latitude, Longitude, Conversion

Orient includes UTM to latitude, longitude and latitude, longitude to UTM conversions (Snyder, 1987; Dutch, 2015). Conversion among 14 datums, including WGS 1984 an, NAD 1983, is available. The Data UTM Conversion dialog (Figure 10.1) can be accessed when there are either easting, northing coordinates, or latitude, longitude coordinates. Select the conversion, and the desired datum. The hemisphere can be specified using the UTM grid zone, or by hemisphere.

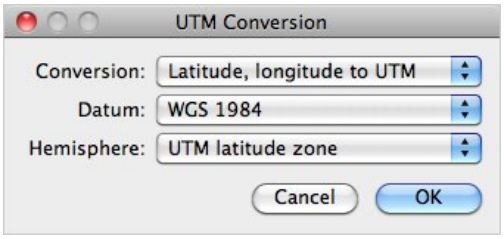

Figure 11.1 UTM, latitude, longitude conversion dialog.

11.3 *Tutorial 11 – UTM Conversion*

Open the file World Earthquakes 1980-1990 Map from the included Example Data folder (any of the provided file formats, csv, tsv, ods, or xlsx, is fine). Note that the file World Earthquakes 1980-1990 Sphere is formatted to plot the data on a spherical projection, and is not the one for this tutorial. This data is a set of 14,229 earthquake epicenters between 1980 and 1990 with magnitudes greater than 4.5 (data from NOAA).

Next, open the UTM Conversion dialog (Figure 11.1), select Latitude, Longitude to UTM, WGS 1984, and UTM latitude zone. Press OK, and the conversion is done. Finally, select View Data Columns and check Zone, Easting, and Northing if not already checked. UTM grid zones and coordinates should all be displayed.

Tutorial 12 covers web map integration, but you may wish to select one of the earthquake data rows, and select Data Show Location Google Maps Satellite. As this is a global data set, you may need to

zoom out before determining where you are. Data point ID 49 is an interesting example of a non-plate boundary seismic event.

11.4 Google and Web Maps

A number of internet web sites offer access to maps, including street maps, topographic maps, and terrain maps, by entering search terms or geographic coordinates. Google Maps is probably the most well known of these. Orient has commands to open many of these sites, including Google Maps, ACME Mapper (which has many topographic maps), Bing Maps, HERE Maps, OpenStreetMaps, and others in your default browser. If a data file contains latitude and longitude coordinates, these can be opened directly from Orient. If the data contains UTM coordinates, they must first be converted to latitude, longitude as covered in Section 11.1. To see the location displayed in your default browser, select a data row containing latitude, longitude coordinates, and choose a website from the Data Show Location menu.

11.5 Google Earth

The program Google Earth is an invaluable tool in numerous areas, and has become a widely used tool in geologic mapping. Google provides an interface using KLM (Keyhole Markup Language) files that can contain geographic coordinates, viewing instructions, and many other details. Orient uses this interface to display outcrop locations, and symbols for directional data measurements. Symbols are selected from the Preference dialog Orientation Map Settings Symbols pane where various symbols can be selected, as well as color, size, and line width. The symbol size is set in meters in the KML Length edit box, and the width in the KML Width edit box. To save the file, use the File Export to Google Earth KML command. Double click the resulting file to open in Google Earth.

11.6 *Tutorial 12 – Web and Google Earth*

This tutorial covers internet web maps, such as Google Maps, as well as Google Earth integration. Open the file Sky Top from the included Example Data folder (any of the provided file formats is fine, csv, tsv, ods, or xlsx). This is a demonstration file with simulated geologic data for use in this tutorial. You may wish to use the View Data Columns command to close some of the unused columns.

The file contains the latitude, longitude coordinates of one marker location, and eight simulated data points of four different types of geologic data, bedding, cleavage, joints, and slickenside lineations. For web map access, select one of the locations and choose a websites from the Data Show Location menu. The selected web map will display the location of the data point, you can then zoom in, or change display options as needed.

In order to display directional data symbols, as well as location, Orient writes KML files for Google Earth, so directional symbols and complete data sets can be viewed. Open the Preferences dialog by clicking on its icon, select the Orientation Map Settings option, and the Symbols pane. Select the data types from the pulldown menu, and check just one symbol for each data type. For J, check Strike, select a strike line with two ticks, and set Stroke Color to light green. For L, check Line, select an arrow symbol, and set Stroke Color to magenta. For S0 check Strike, select a strike line symbol, and set Stroke Color to red. For S1, check Strike, select a strike line with a tooth, and set Stroke Color to red. Press OK when done.

Save the file as Sky Top.klm using the File Export to Google Earth KML command. Double click on it to open in Google Earth. The location (that I can see from the window in my university office) should come into view with the data symbols (Figure 11.2). For a quicker demonstration, there is a copy of the resulting file in the Example Data folder.

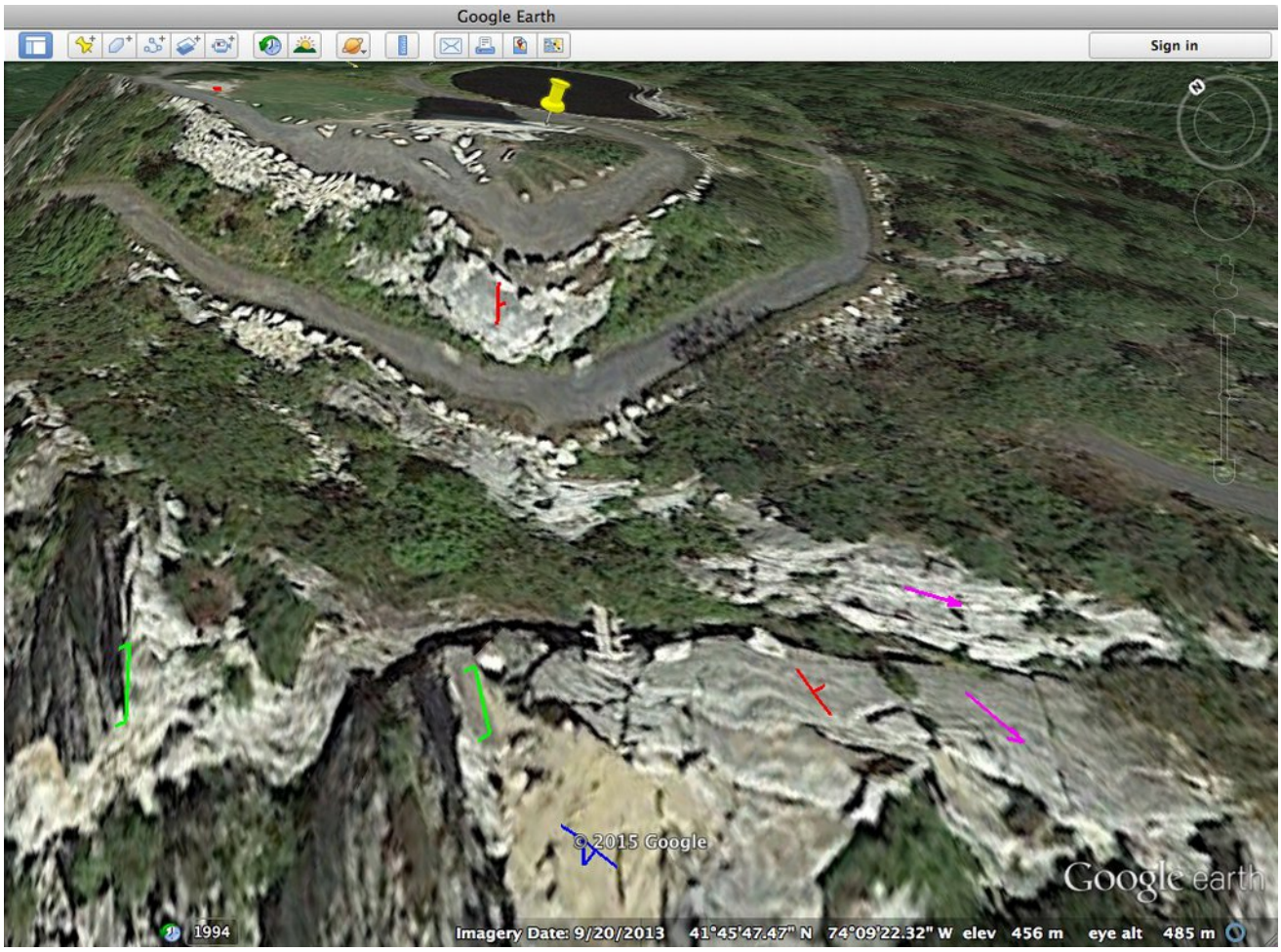

Figure 11.2 Example data from the file *Sky Top* viewed in Google Earth. Example data types are S0 (bedding, red), S1 (cleavage, blue), J (joints, green), and a lineation (L, magenta).

11.7 Orientation Fields and Domain Analysis

Spherical projections aid in the analysis of directional data, but they do not show their spacial distribution. Therefore Orient provides tools for analyzing the spacial variation of directional data, including *orientation fields* and *structural domain analysis*. Orientation fields are a way to look for regional patterns in data by defining *eigenfoliations* and *eigenlineations* on a grid over the area (Vollmer, 1990). One method is to define discrete subdomains that include all data within them, for example a one kilometer square area. A second method is to apply a weighting function to produce area-smoothed orientation values. The fields are defined by calculating an orientation matrix at grid locations, and using its eigenvectors and eigenvalues to characterize the fabric.

For example, a common problem in mapping areas of complex geologic structure is to identify cylindrical domains within the map area (Ramsay, 1967). Figure 11.3 is an equal-area lower

hemisphere projection of poles to foliations from the Doverfjell mountains, Norway, and Figure 7.4 is a modified Kamb contour plot of the data. Their spacial distribution is shown in Figure 7.5, plotted using the Orientation Map command.

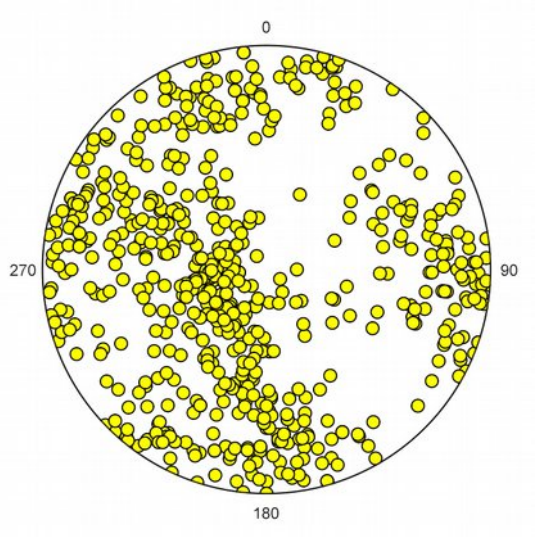

Figure 11.3 Lower hemisphere equal-area projection of poles to 625 foliation planes from the Doverfjell Mountains, Norway (data from Vollmer, 1985).

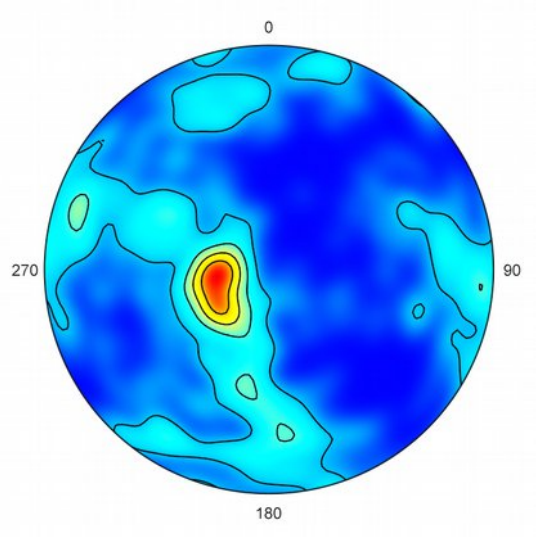

Figure 11.4 Modified Kamb contour plot of the data shown in Figure 7.3 with contours at 20% density.

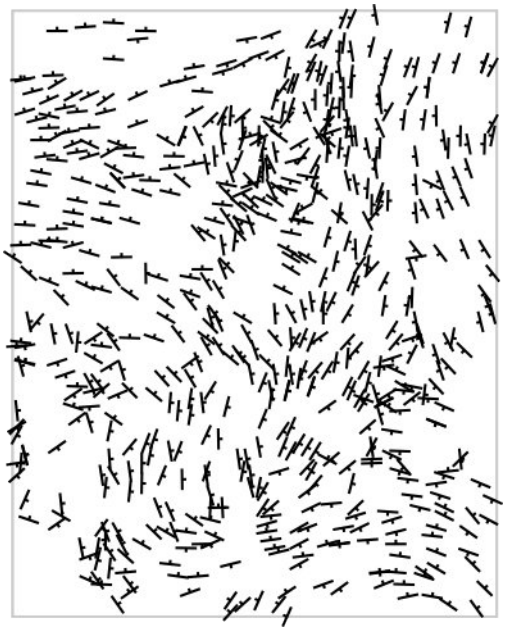

Figure 11.5 Orientation map of foliation strikes of the data shown in Figure 7.3.

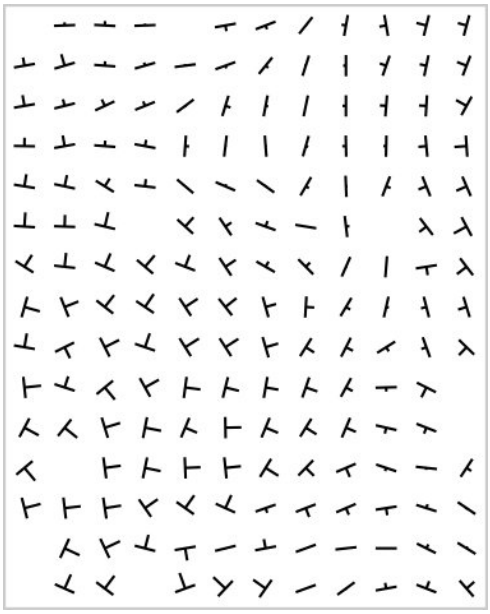

Figure 11.6 Subdomain orientation field of eigenfoliation strikes generated from the data shown in Figure 7.3. The strike tick marks represent the horizontal projection of the dip line.

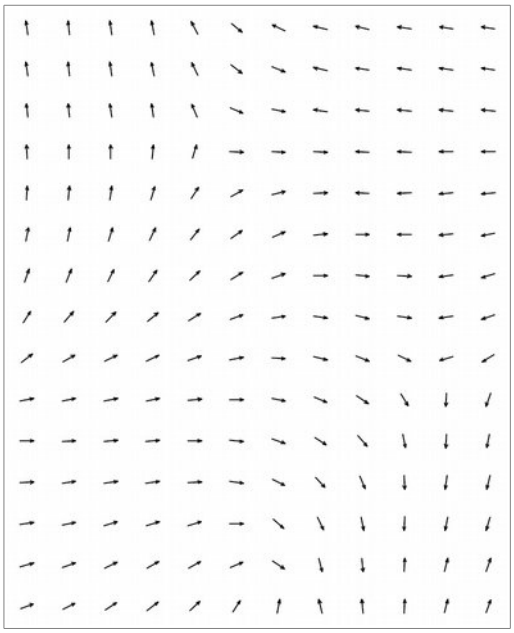

Figure 11.7 Weighted orientation field of eigenfoliation dip lines generated from the data shown in Figure 7.3. The arrows represent the horizontal projections of the dip line.

The geometry of the structure defined by the foliations is not obvious. Figure 11.6 is a *subdomain orientation field* defined on a one kilometer grid. Note that the number of data points within each subdomain varies, and that each has a discrete boundary. Figure 11.7 is a *weighted orientation field* where each grid node is generated as a weighted sum of all other data points. This map shows the *horizontal projection* of the dip lines, with steeper dips displayed as shorter lines.

Structural domain analysis (Vollmer, 1990) is done by attempting to maximize a quantity, or index, related to the given problem. Orient provides several indexes that may be maximized, including *point*, *girdle*, and *cylindricity* indexes. To locate areas of cylindrical folding the cylindricity index is maximized:

$$C = (\varepsilon_1 + \varepsilon_2 - 2\varepsilon_3) / n$$

Where $\boldsymbol{\varepsilon}$ is the orientation matrix eigenvalue for n data points, and $\varepsilon_1 \geq \varepsilon_2 \geq 2\varepsilon_3$.

For a set of *domains* the sum of the products of the domain indexes (C_1, C_2, C_3, ...) and the number of data points within each domain (n_1, n_2, n_3, ...):

$$Z = C_1n_1 + C_2n_2 + C_3n_3 + ...$$

is maximized. Because:

$$n = n_1 + n_2 + n_3 + ...$$

the maximum possible value for Z is equal to n. The normalized sum is:

$$C' = Z/n$$

The settings for the Orientation Map command are in the Preferences dialog Orientation Map panels. For each data point, or field value, it is possible to plot a symbol in four directions, Line, Dip Line, Strike, and Strike 180 (Figure 11.8).

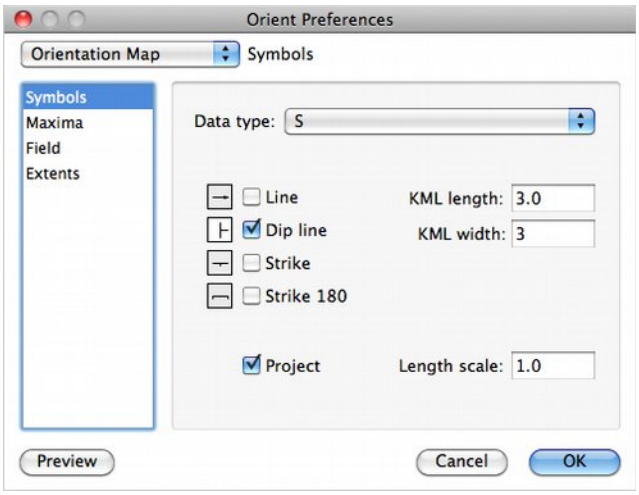

Figure 11.8 Orient *Preference* dialog showing the *Orientation Map Symbols* pane. The options shown are to project strike lines as in Figure 10.6.

Figure 11.9 The *Domain Search* dialog box.

Line is the direction of a line, or of the plane normal (θ). Dip Line is the opposing direction (θ + 180°), and used to display a plane's dip direction. Strike is the plane strike (θ + 90°), and Strike 180 is the opposing direction (θ – 90°). Only Line and Dip line can be projected. To display a projected strike symbol, select Dip Line and the strike symbol shaped like a sideways T (Figures 11.6 and 11.8). The Length Scale scales the length of the symbol. The KLM settings are for the display of data in Google Earth (Section 11.3).

To conduct a domain search, define the extents of the map area in the Extents panel, select the Subdomain Method in the Field panel, along with the number of subdomains. Then use the Domain Search command, which displays the dialog shown in Figure 11.9. This is used to maximize the orientation index using an automated search process. The Value is the current value of the index, and N is the number of points used to calculate it. Domains are numbered from 1 to 9, zero represents an unassigned domain. Clear resets all subdomains to zero. Initialize sets all domains to the search domain. Search will attempt to grow the search domain. The search process iteratively checks to see if subtracting a subdomain from one domain and adding it to the search domain will increase the index. It can only do so if both domains remain connected.

The user can manually edit domains, moving the mouse over the map will display subdomain information in the status bar, and clicking on a subdomain will add it to the search domain if possible. The constraint that the domains remain connected can cause edge effects, and vacant subdomains may also effect connectivity. The general procedure is to do a search on a desired number of domains, then manually edit them, and search again to see if a better solution is found.

Once the search is completed, pressing OK will assign domains to each of the data points. The domains are added as attributes of the data, use the View Data Columns to view the Domain column. Extended data types are formed by appending domain extensions, D1 to D9, to the data type so each domain can be plotted independently, for example on a spherical projection. To update the results during a search,

click on the Apply button. This will apply the domains to the data and will update other graphs that are open. If a spherical projection of the data is open it is possible to color code the data by domain to get a visualization of the distribution.

10.8 *Tutorial 13 – Domain Analysis*

Open the file Vollmer 1985 included Example Data folder (any of the provided file formats). This is the data displayed in Figures 11.3 to 11.7, 625 foliation planes from the Doverfjell mountains, Norway. While folds are clearly present, the spherical projections (Figure 11.3 and 11.4) do not display a girdle pattern that would indicate cylindrical folding (there are spectacular sheath folds in the Doverfjell and adjacent Trollheimen ranges). The map of foliations (Figure 11.5) shows some areas of consistent orientation, but the location of cylindrical domains is not obvious.

Click on the Orientation Map icon to display a map of the foliation data, then in the Orientation Map window, click on the Preferences icon. In the Orientation Map Extents pane, uncheck Auto Scale, and enter the 890 for the minimum X (Easting) coordinate, 150, for the minimum Y (Northing) coordinate, 1010 for the maximum X coordinate, and 300 for the maximum Y coordinate. To view the data, uncheck all symbols in the Maxima pane, and check only Strike in the Symbols pane. The result should appear as in Figure 11.5.

To set up the domain search, uncheck Strike in the Symbols pane, and check Strike in the Maxima pane. In the Field pane the Method should be Subdomain, and Directed should be unchecked. Enter 12 and 15 for the number of X and Y subdomains respectively. The coordinates are UTM based in meters, so this gives one square kilometer subdomains. The resulting map should be as in similar to Figure 11.6, except that the strikes are not projected. Press OK when done.

To begin the domain search, select the Graph Domain Search command from the menu (Figure 11.9). Press Initialize to set all subdomains to 1, then press Search to grow domain 2. Change the search domain to 3, and press Search again. The result is should in Figure 11.10, which has a cylindricity index, c = 0.738. There are some edge effects, particularly where domain 1 wraps around the other two. Move the mouse over the map to see information about each subdomain. Clicking on one will change it to the current search domain, if all domains remain connected.

Edit the domains by selecting a search domain and clicking on the map. When done, go back to the dialog and search on each domain again. If the domains are stable, they will not change. Figure 11.11 shows a stable solution with C = 0.851, an improvement over the previous value. Press OK when done.

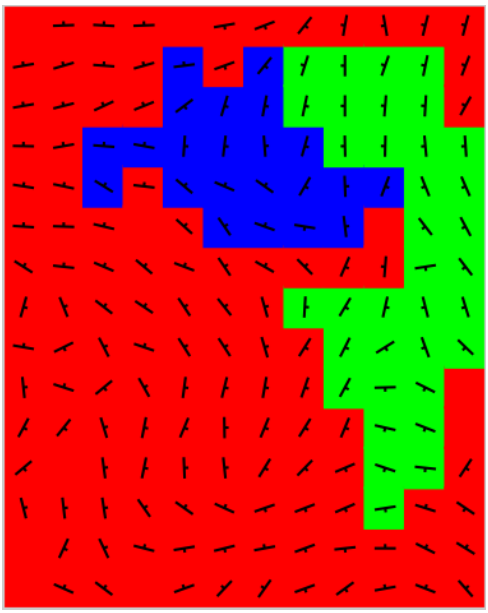

Figure 11.10 Initial automatic domain search formed by grouping the subdomains of Figure 7.6 into three domains maximizing cylindricity. This configuration has a cylindricity index, C' = 0.738.

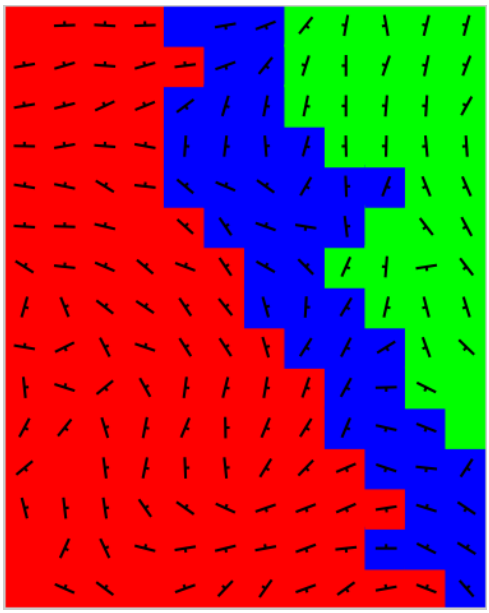

Figure 11.11 Final domain configuration after iterative manual editing and automatic searching to find a stable configuration. This configuration has a cylindricity index, C' = 0.851.

The map will now be cluttered with symbols, as the three new domains are plotted in addition to the field. Before cleaning up the map, open a spherical projection by clicking on the Spherical Projection icon in the data spreadsheet window, and then the Preferences dialog. In the Spherical Projection Net pane, uncheck Axes and Net, and in the Labels pane set Increment to -90, Offset to 14 and Size to 12, as in previous tutorials.

In the Symbols pane, uncheck Symbol the for data type S. Then for data types S.D1, S.D2, and S.D3, the new data types, set the Symbol Fill Color to red, green, and blue respectively. In the Maxima pane, select *only* the Minimum Eigenvector for S.D1, S.D2, and S.D3, and set the fill and stroke colors the same. The result should be as in Figure 11.12. Note that the three domains show well defined girdles. Turning off the data symbols give Figure 11.13, which suggests refolding of earlier folds about a northwest plunging axis.

Next, open a triangular orientation (Point Girdle Random) plot using the PGR Plot icon in the data spreadsheet window. In the Preferences dialog PGR Plot Symbols pane set the Symbol Fill Color for S to white, and then for S.D1, S.D2, and S.D3, to red, green, and blue respectively, and increase the symbol sizes to 16. The resulting triangular plot (Figure 7.14) shows the relative changes in cylindricity from the whole area to the three domains. Note that domain 2 (green) has the strongest point distribution, and domain 3 (blue) has the strongest girdle distribution.

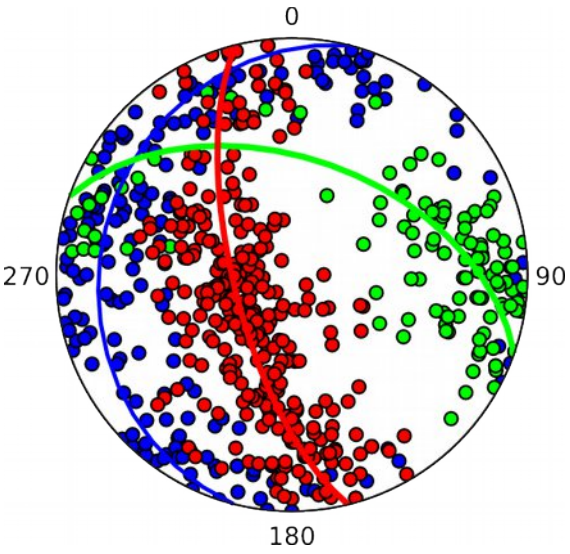

Figure 11.12 Lower hemisphere equal-area projection of data from Figure 7.3, with foliation poles color-coded by domain, and the great circle normal to the minimum eigenvector drawn for each domain.

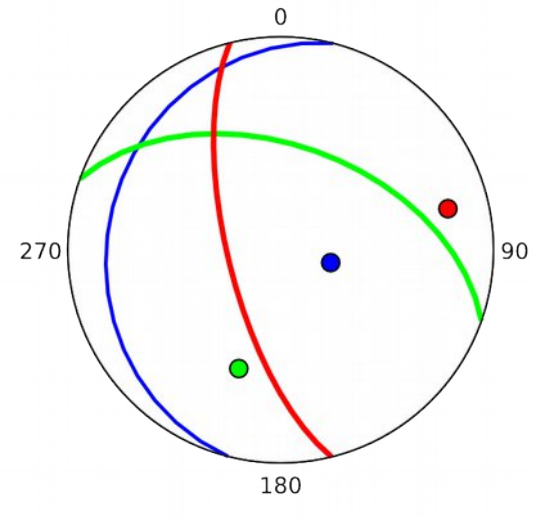

Figure 11.13 Synoptic plot of best fit girdles and axes of data shown in Figure 7.12.

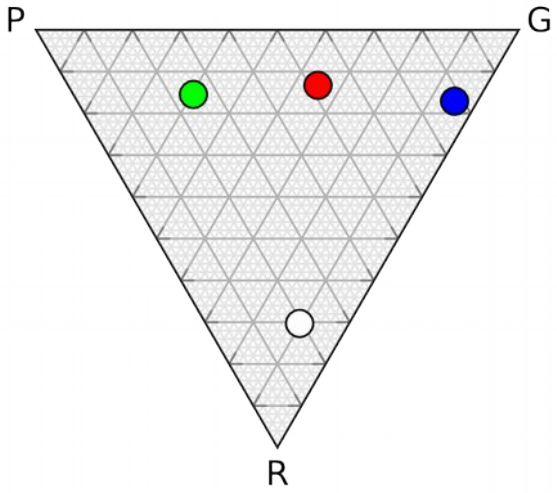

Figure 11.14 Triangular orientation plot of the three domains compared to the total data set (white).

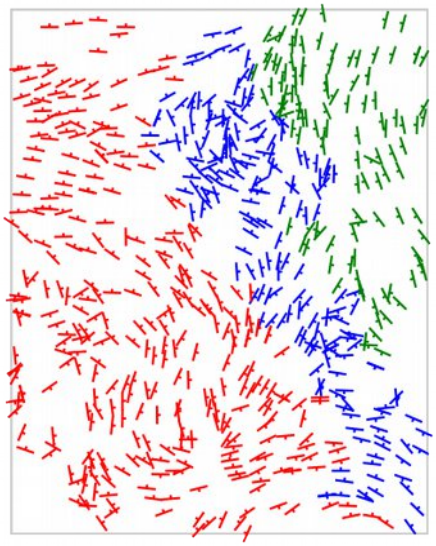

Figure 11.15 Data from Figure 7.5 color-coded by domain.

To clean up the map, turn off the display of the maxima in the Orientation Map Maxima pane, turn off display of data type S symbols, and set Strike on with Stroke Color for S.D1, S.D2, and S.D3, to red, green, and blue respectively, giving the map in Figure 11.15.

As a final step, prepare lower hemisphere equal-area modified Kamb contour plots (Section 4.9) of the three domains (Figures 11.16, 11.17, and 11.18).

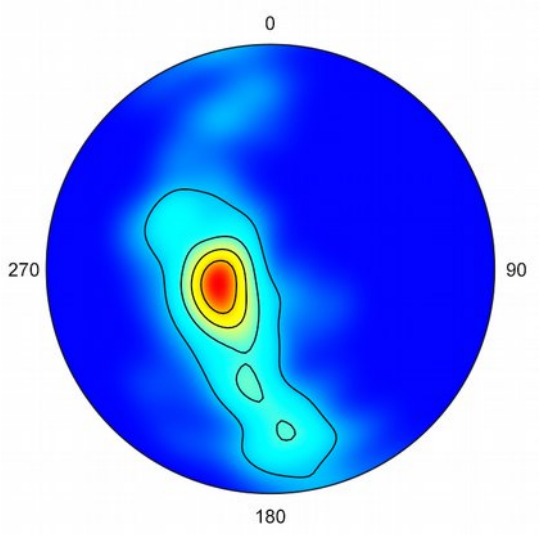

Figure 11.16 Lower hemisphere equal-area midified Kamb contour plot of poles to foliation for domain 1 (red domain in Figures 11.10 to 11.15) contoured at 20% .

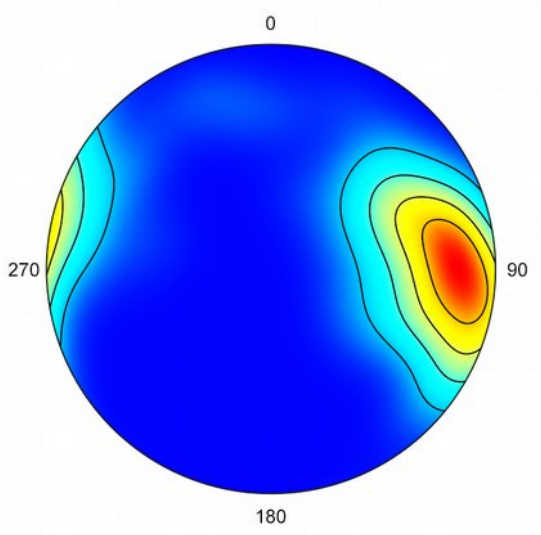

Figure 11.17 Projection as in Figure 11.16 for domain 2 (green domain in Figures 11.10 to 11.15)

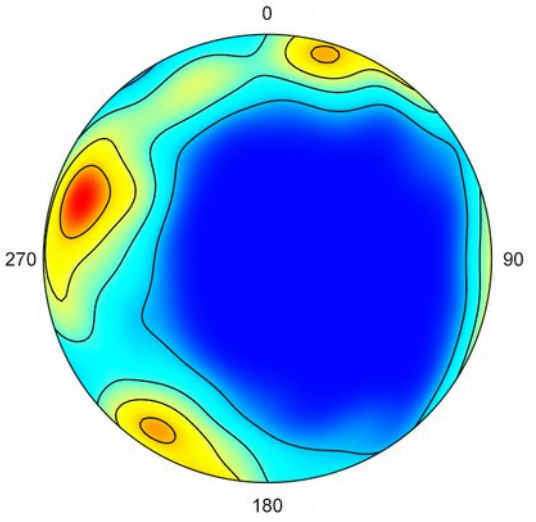

Figure 11.18 Projection as in Figure 11.16 for domain 3 (blue domain in Figures 11.10 to 11.15) .

Acknowledgements

An early draft of this document was prepared for Teaching Structural Geology, Geophysics, and Tectonics in the 21st Century, On the Cutting Edge, held July 15-19, 2012 at the University of Tennessee, Knoxville, which rekindled my enthusiasm for completing this new version of Orient. I thank the conveners Barbara Tewksbury, Gregory Baker, William Dunne, Kip Hodges, Paul Karabinos, and Michael Wysession. I thank Eric Erslev, Steven Wojtal, Haakon Fossen, Christian D. Klose, Josh Davis, Sarah Titus, Yvette Kueiper, Peter Hudleston, Robert Bauer, Mark Brandon, and Dazhi Jiang for discussions at various times.

Thanks to Emily Lubicich (City College of New York), Chistopher Gahn (Vassar College), Ben Michael Frieman (Colorado School of Mines), Haakon Fossen (University of Bergen), Josh Davis (Carlton College), Tammy Xinran He (Colorado School of Mines), Steven Coombes (Rio Tinto Exploration, Canada), and Andrea Bistacchi (University of Milano-Bicocca) for suggestions and bug reports.

References

Angelier, J., 1979. Determination of the mean principal directions of stresses for a given fault population. Tectonophysics, v. 56, p. T17-T26.

Badgley, P.C., 1959. Structural methods for the exploration geologist. Harper and Brothers, New York, 280 pp.

Barnes, J.W., 1995. Basic geologic mapping, 3rd Edition. Open University Press, Milton Keynes, UK.

Billings, M.P., 1942. Structural geology. Prentice-Hall, New York, 473 pp.

Billings, M.P., 1954. Structural geology, 2nd edition. Prentice-Hall, New York, 514 pp.

Bingham, C., 1974. An antipodally symmetric distribution on the sphere. Ann. Stats., v. 2, p. 1201-1225.

Borradaile, G.J., 2003. Statistics of earth science data: their distribution in time, space, and orientation. Springer, Berlin.

Bucher, W.H., 1944. The stereographic projection, a handy tool for the practical geologist. Journal of Geology, v. 52, n.3, p. 191-212.

Cheeney, R.F., 1983. Statistical methods in geology. George Allen & Unwin, London. 169 p.

Davis, J.C., 1986, Statistics and data analysis in geology. Wiley, 646 pp.

Davis, J.R., Titus, S.J., and Tikoff, B., 2105. Statistical treatment of structural geology data. Geological Society of America Short Course Notes.

De Aguilon, François, 1613. Opticorum libri sex philosophis juxta ac mathematicis utiles (Six books of optics, useful for philosophers and mathematicians alike). Anvers.

De Sitter, L.U, 1956. Structural Geology. McGraw-Hill Book Company, Inc., London, New York, Toronto. 552 p.

Downs, T.D., 1972. Orientation statistics. Biometrika, v. 59, n. 3, p. 665-676.

Dutch, S., 2015. Converting UTM to latitude and longitude (or vice versa). www.uwgb.edu/dutchs/usefuldata/utmformulas.htm (accessed 27 April 2015).

Diggle, P.J., and Fisher, N.I., 1985, Sphere: a contouring program for spherical data. Computers & Geoscience, v. 11, p. 725-766.

Donn, W.L., and Shimer, J.A., 1958. Graphic methods in structural geology. Appleton-Century-Crofts, Inc., New York, 180 p.

Fisher, N.I., Lewis, T., and Embleton, B.J., 1987. Statistical analysis of spherical data (errata, 2000). Cambridge University Press, Cambridge, 329 pp.
Fosson, H., 2016. Structural geology, 2nd Edition. Cambridge University Press, Cambridge, 463 pp.
Gray, N., Geiser, P., Geiser, J., 1980. On the least-squares fit of small and great circles to spherically projected orientation data. Mathematical Geology 12, 173–184.
Haughton, S., 1856. On slaty cleavage, and the distortion of fossils. Philosophical Magazine, 12, p. 409-421.
Hills, E.S., 1963. Elements of structural geology. Chapman & Hall, London, 483 p.
Hobbs, B.E., Means, W.D., and Williams, P.F., 1976. An outline of structural geology. Wiley, New York, 571 pp.
Howarth, R.J., 1999. Measurement, portrayal and analysis of orientation data and the origins of early modern structural geology (1670-1967). Proceedings of the Geologists' Association, v. 110, p. 273-309.
Kamb, W.B., 1959. Ice petrofabric observations from Blue Glacier, Washington, in relation to theory and experiment. Journal Geophysical Research, v. 64, p. 1891-1909.
Kelker, D., and Langenberg, C. W., 1982. A mathematical model for orientation data from macroscopic conical folds. Mathematical Geology, v. 14, n. 4, p. 289-307.
Kelker, D., Langenberg, C.W., 1988. Statistical classification of macroscopic folds as cylindrical, circular conical, or elliptical conical. Mathematical Geology 20, 717–730.
Kent, J.T., 1982. The Fisher-Bingham distribution on the sphere. Journal of the Royal Statistical Society B, v. 44, n. 1, p. 71-80.
Klose, C.D., Seo, S., and Obermayer, K, 2005. A new clustering approach for partitioning directional data. International Journal of Rock Mechanics & Mining Sciences v. 42, p. 315-321.
Knopf, E.B., and Ingerson, E., 1938. Structural petrology. Geological Socity of America Memoir 6, 270 p.
Lambert, F.H., 1772. Anmerkungen und zusätze zur entwerfung der land und himmelscharten. Verlag von Wilhelm Engelmann, 1894, Leipzig.
Lisle, R.J. and Leyshorn, P.R., 2004. Stereographic projection techniques for geologists and civil engineers, 2nd edition. Cambridge University Press, Cambridge, 112 pp.
Mancktelow, N.S., 1981. A least-squares method for determining the best-fit point maxima, great circle, and small circle to nondirectional orientation data. Mathematical Geology, v. 13, p. 507-521.
Mardia, K.V., 1972. Statistics of directional data. Academic Press.
Mardia, K.V., Gadsden, R.J., 1977. A circle of best fit for spherical data and areas of volcanism. Applied Statistics 26, 238–245.
Mardia, K.V., and Jupp, P.E., 2000. Directional statistics. John Wiley & Sons, Ltd., Chichester, UK. 430 p.
Mardia, K.V., and Zemroch, P.J., 1977. Table of maximum likelihood estimates for the Bingham distribution. Journal of Statistical Computation and Simulation, v. 6, p. 29-34.
Marrett, R., and Allmendinger, R.W., 1990. Kinematic analysis of fault-slip data. Journal of Structural Geology, v. 12, p. 973-986.
Marshak, S., and Mitra, G., 1988. Basic methods of structural geology. Prentice Hall, 446 p.
Mulchrone, K.F., Pastor-Galán, D., Gutiérrez-Alonso, 2013. Mathematica code for least-squares cone fitting and equal-area stereonet representation. Computers & Geoscience, v. 54, p. 203-210.
Parker, J.M., 1942. Regional systematic jointing in slightly deformed sedimentary rocks. Geological Society of America Bulletin, v. 53, p. 381-408.
Phillips, F.C., 1954. The use of stereographic projection in structural geology. Edward Arnold, London, 86 pp.

Pollard, D.D. and Fletcher, R.C., 2005. Fundamentals of structural geology. Cambridge University Press, Cambridge, 463 500 pp.
Press, W.H, Teukolsky, S.A., Vetterling, W.T., and Flannery, B.P., 2007. Numerical Recipes: The Art of Scientific Computing, 3rd edition. Cambridge University Press, Cambridge, 1235 p.
Ragan, 2009. Structural geology: an introduction to geometrical techniques, 4th edition. Cambridge University Press, Cambridge. 602 pp.
Ramsay, J.G., and Huber, M.I., 1987. The techniques of modern structural geology, volume 2: folds and fractures. Academic Press, 700 pp.
Sander, B., 1970. An introduction to the study of fabrics of geological bodies, 1st English edition. Pergamon Press, Oxford. 641 p. [Translated from Sander, 1948, 1950. German edition. Springer-Verlag.
Schmidt W., 1925. Gefügestatistik. Tschermaks Mineralogische und Petrographische Mitteilungen 38, p. 392–423.
Shanley R.J., and Mahtab, M.A., 1976. Delineation and analysis of clusters in orientation data. Mathematical Geology, v. 8, n. 1, p. 9–23.
Snyder, J. P., 1987. Map projections: a working manual. United States Geological Survey Professional Paper 1395, 383 p.
Swan, A.R.N., and Sandilands, M., 1995. Introduction to geological data analysis. Blackwell Science, Oxford, 446 p.
Swinbank, Richard, and Purser, R. James, 2006. Fibonacci grids: a novel approach to global modeling. Quarterly Journal of the Royal Meteorological Society, v. 132, n. 619, p. 1769-1793.
Turner, F.J. and Weiss, L.E., 1963. Structural analysis of metamorphic tectonites. McGraw-Hill Book Company, New York, 545 pp.
Twiss, R.J., 1990. Curved slickenfibers; a new brittle shear sense indicator with application to a sheared serpentinite. Journal of Structural Geology, v. 11, p. 471-481.
Twiss, R.J., and Unruh, J.R., 1998. Analysis of fault slip inversions: do they constrain stress or strain rate? Journal of Geophysical Research,. v. 103, p. 12205-12222.
Twiss, R.J. and Moores, 2007. Structural geology, 2nd edition. W.H. Freeman, New York, 736 pp.
Van der Pluijm, B.A. and Marshak, S., 2004. Earth structure, 2nd edition. W.W. Norton, New York, 656 p.
Vollmer, F.W., 1981. Structural studies of the Ordovician flysch and melange in Albany County, New York: M.S. Thesis, State University of New York at Albany, Advisor W.D. Means, 151 p.
Vollmer, F.W., 1985. A structural study of the Grovudal fold-nappe, western Norway. Ph.D. Thesis, University of Minnesota, Minneapolis, Advisor P.J. Hudleston, 233 p.
Vollmer, F.W., 1988. A computer model of sheath-nappes formed during crustal shear in the Western Gneiss Region, central Norwegian Caledonides. Journal of Structural Geology, v. 10, p. 735-743.
Vollmer, F.W., 1989. A triangular fabric plot with applications for structural analysis (abstract). Eos, v. 70, p. 463.
Vollmer, F.W., 1990. An application of eigenvalue methods to structural domain analysis. Geological Society of America Bulletin, v. 102, p. 786-791.
Vollmer, F.W., 1993. A modified Kamb method for contouring spherical orientation data. Geological Society of America Abstracts with Programs, v. 25, p. 170.
Vollmer, F.W., 1995. C program for automatic contouring of spherical orientation data using a modified Kamb method: Computers & Geosciences, v. 21, p. 31-49.
Vollmer, F.W., 2011. Automatic contouring of two-dimensional finite strain data on the unit hyperboloid and the use of hyperboloidal stereographic, equal-area and other projections for strain analysis. Geological Society of America Abstracts with Programs, v. 43, n. 5, p. 605.

Vollmer, F.W., 2015. Orient 3: a new integrated software program for orientation data analysis, kinematic analysis, spherical projections, and Schmidt plots. Geological Society of America Abstracts with Programs, v. 47, n. 7, p. 0.
Vollmer, F.W., 2015. Orient 3 User Manual www.frederickvollmer.com. [this document]
Vollmer, F.W., 2015. Orient 3: Spherical projection and orientation data analysis program. www.frederickvollmer.com.
Watson, G.S., 1966. The statistics of orientation data. The Journal of Geology, v. 74, n. 5, p. 786-797.
Whitten, E.H.T., 1966. Structural geology of folded rocks. Rand McNally, Chicago, 663 pp.
Wilson, G., 1967. The geometry of cylindrical and conical folds. Proceedings of the Geologists' Association, 1967, v. 78, part 1, p. 179-209.
Yamaji, A., 2008. Theories of strain analysis from shape fabrics: A perspective using hyperbolic geometry. Journal of Structural Geology, v. 30, p. 1451-1465.
Yamaji, A., and Sato, 2011. Clustering of fracture orientations using a mixed Bingham distribution and its application to paleostress analysis from dike or vein orientations. Journal of Structural Geology, v. 33, p, 1148-1157.

History

3.4.2.3 (2016-06-11)
- Now allows a minimum spherical projection contour level of 0.
- Added automatic range setting for spherical projection contour grid, now the gradient automatically scales to full grid range by default.
- Added rescaling of spherical projection contour grid to expected uniform density to contour in multiples of uniform density.
- Added gradient scale bar option to spherical projection.
- Added WBGYR gradient preset.
- Added an option to place spherical net above the gradient or beachball bitmaps.
- Fixed rotation of spherical projection tick marks.

3.4.1.3 (2016-03-25)
- Fixed orientation map subdomain maxima symbol drawing bug.
- Fixed orientation map subdomain maxima symbol count bug.
- Centered orientation map on page.
- Changed orientation map status display from one to two decimal places.
- Moved orientation map maxima symbols above data symbols.
- Fixed reading and display of explicit NaN values and, therefore, display of polylines (such as the Modern Continental Outlines example data).
- Fixed domain search bug failure to assign domains when multiple files were open.
- Added Apply button to Domain Search dialog.
- The visibility of symbols on the orientation map is no longer linked to their visibility on the spherical projection.
- Domain search subdomains are now saved and optionally displayed after Domain Search dialog is closed.
- Added an option in the Preferences dialog Orientation Map pane to show or hide the subdomains when Domain Search dialog is closed.

3.4.0.16 (2016-03-20)
- Bound Windows and Linux resources into executable.
- Optimized with FPC 3.0.0 and LCL 1.6.0.
- Improved memory management by freeing unused forms.
- Added View Image Window command, moved location of File Open Image command.
- Replaced Timers with IdleTimers for better performance.
- Settings for Rotate Data, Rotate Projection, and UTM Conversion are now stored between sessions.
- Consolidated raster and vector image saving under *Export Image As* command.
- Improvements to digitize commands.
- Added Kent distribution confidence cones.
- Added Kent statistics to Log output.
- Added Bingham statistics to Log output.
- Data input behavior now more spreadsheet compatible. Pressing *Enter* to accept input moves down, additional rows are always available for input, fixed bug causing a scroll up when on last data line.

3.3.3.11 (2016-02-03)
- Fixed Watson confidence cone weighting error, was dividing by count instead of weighted count.
- Added process cancelation code for lengthy operations in bootstrap routines.
- Added progress display status for lengthy operations in bootstrap routines.
- The preferences dialog now displays only the data types available in the current file, instead of all files.
- The spherical projection settings are now saved by file name, instead of globally.

- Only graphs of the current data are now redrawn, instead of all graphs.
- When selecting a plot window the associated file in the spreadsheet is now displayed.

3.3.2.9 (2016-01-24)
- Fixed Page Size dialog display failure.
- Fixed Replicates symbol picker display.
- Fixed several User Manual images in Chapter 6.
- Added Watson confidence cone data to Log.
- Watson confidence cones now rotate on projection rotation.
- Bingham confidence cones now rotate on projection rotation.
- Fixed preferences initialization bug.
- Preferences dialog now reopens on last panel.
- Preferences dialog now reopens with last data type selected.
- Weighting now works with Fisher confidence cones.
- Weighting now works with Watson confidence cones.
- Added translucent display of data polygons on hidden hemisphere.
- Fixed divide by zero bug.
- Fixed additional Windows and Linux control display issues.
- No longer asks twice on quitting with modified file.
- Added translucent display of tangent lines on hidden hemisphere.
- Status bar now indicates if a file is modified.
- Can now display kinematic beachball and tangent lines at same time.

3.3.1.13 (2016-01-17)
- Fixed some dialog control display issues in Linux.
- Added translucent display of contour lines on hidden hemisphere.
- Added translucent display of confidence ellipses on hidden hemisphere.
- Fixed XML creator to correctly translate [&”<>] characters in file paths. Project files are validated XML.
- Project files now save open file paths.
- Added commands to save and open project files.
- Fixed bug causing crash when closing a tabbed window.
- Fixed bug that was naming “untitled” “untitled 1”.
- Fixed some tab orders and control spacing.
- Modified status bar display to include calculated angle for two selected data points. Clicking on the status bar toggles between line and plane units.

3.3.0.8 (2016-01-11)
- Corrected the name of the *Calculate Line Orthorectify* option to *Orthonormalize.*
- Changed *Orthonormalize* algorithm from QR decomposition to polar decomposition, to give the closest orthogonal frame. The difference should be minimal.
- Fixed sorting in *Weight, Error, Rake, Sense,* and *Alpha* columns.
- Tweaked the tangent-normal wrapping algorithm used in bootstrap covariance calculation. The difference should be minimal.
- Plot windows now save their placement on the screen based on name.
- Added *Cluster Partitioning,* see User Manual Chapter 10.
- Added hidden small circle display.

3.2.1.4 (2016-01-02)
- Fixed numerous control display issues in Linux.
- Cleaned up control alignments in *Preferences* dialog.
- Fixed Beachball to rotate with projection.

- Modified small circle bootstrapping work with psi close to 90.
- Added small circle bootstrap estimation of confidence in psi.
- Added drawing of small circle bootstrap confidence rings about psi.
- Added *Fibonacci Sphere* command.
- Added opacity options to plot symbols, rays, and great circles on hidden hemisphere.
- Numerous updates to the user manual.

3.2.0.7 (2015-12-29)
- Added best-fit small circles.
- Modified labels in Columns Dialog to show current data angles, e.g., *Strike*.
- Fixed control spacing in Linux *Calculate Lines* dialog.
- *Rotate Projection* dialog now includes *Vector Mean* and *Small Circle Pole*.
- Added circular confidence cones for bootstrap means.
- Added *Alpha* field and plotting of small circle data.
- Added option to plot hidden directed data, on opposing hemisphere, with an unfilled symbol.
- Added *Help Orient Home Page* command.
- Fixed NaN entry and polyline markers, that got broken in 3.1.0.
- Cleaned up Log file, added Fisher statistics.

3.1.0.27 (2015-12-14)
- Added *Sense* column for kinematic analysis to allow undirected (downward) lineation entry, previously it was necessary to input directed (upward or downward) fault lineations.
- Fixed weighting error in orientation field.
- Fixed orientation map page size setting.
- Added *Weight* column for data point weighting, 1 is the default value, 2 counts a data point twice, etc..
- Decreased non-splined points to 91 in spherical net small circles. Use *Restore defaults* to implement.
- Fixed duplicate drawing of spherical net small circles.
- Spherical net great circles in SVG are now computed as cubic Bezier paths.
- Added Windows system tray icon
- Added encapsulated PostScript (EPS) vector graphics export.
- Added AutoCAD drawing exchange format (DXF) vector graphics export.
- Added hexagon and pentagon symbols.
- Fixed arrowheads in kinematic analysis plots.
- Clarified directional versus orientation data definitions.
- Added *Rake* column for the rake of a line in the containing plane.
- Added *Error* column giving the angular error between a line and the containing plane. Read only.
- Fixed data entry to not delete invalid entry over existing value.
- Fixed several data entry display issues.
- Added *Calculate Line* command to calculate line in plane angles from projection, trend, plunge or rake.
- *Rotate Data* command now rotates only selected items.
- Modified status bar to display maximum and minimum eigenvectors for two or more data points.
- Fixed command clicking on plots to update multiple selections in the spreadsheet.
- Removed Yahoo! Maps linking, they shut down this service.
- Fixed bug setting X and Y fields when locating points.
- Added orthorectification option to *Calculate Line* command.
- Added bootstrapping analysis with elliptical confidence cones and polygon regions (hulls).
- Fixed Log Window Copy command.

3.0.2.1 (2015-09-28)
- Fixed Preferences Dialog list spacing.
- Optimized contour line segment joining for vector export.

- Optimized data grid scrolling.
- Fixed Linux About display.
- Optimized messaging.
- Fixed crash when non-Roman Unicode characters are in user name. A workaround is to run Orient from a thumb drive with only Roman characters in file and folder names.
- Work on User Manual.

3.0.1.0 (2015-05-30)
- Fixed bug importing dip direction.

3.0.0.77 (2015-05-01)
- First release of Orient 3. Complete rewrite with numerous new features. Compiled, tested, and debugged on Macintosh, Windows, and Linux.

2.1.2 (2012-10-31)
- Last release of Orient 2.

2.0.0.7 (2006-07-23)
- First release of Orient 2. Complete rewrite with Macintosh, Windows, and Linux versions.

1.6.1 (1995-02-28)
- Last release of Orient 1.

1.0.0 (1986)
- First release of Orient 1, Microsoft DOS. Introduced modified Kamb contouring, triangular fabric plots, and automated domain analysis (see Vollmer, 1985, 1988, 1990, 1993, 1995). Available by download (modem) from COGSnet, sponsored by the Computer Oriented Geological Society, Denver, CO.

This page intentionally left blank